Thermal Infrared Time Series Analysis for earthquake precursory detection

Nadira Aliyah Khan

March, 2010

Thermal Infrared Time Series Analysis for earthquake precursory detection

by

Nadira Aliyah Khan

Thesis submitted to the International Institute for Geo-information Science and Earth Observation in partial fulfilment of the requirements for the degree of Master of Science in Geo-information Science and Earth Observation, Specialisation: (Geo-Hazards)

Thesis Assessment Board

Prof. Dr. Freek. van der Meer	(Chairman)
Dr. E.A. Addink	(External Examiner)
Dr. Mark van der Meijde	(First Supervisor)
M.Sc. Chris Hecker	(Second Supervisor)
Drs. Tom Loran	(Course Director AES)

ITC

INTERNATIONAL INSTITUTE FOR GEO-INFORMATION SCIENCE AND EARTH OBSERVATION
ENSCHEDE, THE NETHERLANDS

Disclaimer

This document describes work undertaken as part of a programme of study at the International Institute for Geo-information Science and Earth Observation. All views and opinions expressed therein remain the sole responsibility of the author, and do not necessarily represent those of the institute.

Abstract

Thermal remote sensing has been used to indicate temperature increases prior-to major earthquakes in the vicinity of the future epicentre. These studies compared results of multi-temporal datasets which spanned only for days to weeks before an earthquake. Even though these results are promising, the scope of those studies did not allow for longer observations and it is unclear whether the temperature rise is unique, persistent and indeed earthquake-related. The purpose of this exploratory study is to verify whether significant thermal infrared anomalies were found in association with known earthquakes by systematically applying satellite data time series analysis to multi-year time series. An innovative multi-temporal satellite data approach was developed to investigate possible relations between thermal infrared fluctuations and the earthquake occurrence. The significance of the developed methodology was explored using a six year (1999- 2004) Meteosat-5 satellite dataset of the Bam earthquake which was later applied to a year (2009) of MSG2 dataset for the recent L'Aquila earthquake. Analysis of long time series of thermal imagery provides answers to whether significant anomalies appear prior to an earthquake event and are periodic in nature. A significant earthquake-related anomaly was detected for Bam's earthquake. Unlike Bam, there was no earthquake-related anomaly occurring in L'Aquila.

Keywords: *Earthquake; Thermal Anomaly; Meteosat-5; MSG2; Time series; Bam; L'Aquila*

Dedicated to my family

"The roots of education are bitter, but the fruit is sweet." Aristotle (384 BC- 322 BC)

Acknowledgements

I would firstly like to thank the Lord Almighty, for bestowing on me the strength, patience, guidance, knowledge and understanding because without Him, nothing would be possible.

To my supervisors, Dr. Mark van der Meijde and M.Sc. Chris Hecker, I express my deepest gratitude for your guidance, assistance, knowledge, effort, support, time and patience and for this; I am indebted to you always. This thesis would not have been possible without your continued encouragement, constructive criticism and valued suggestions throughout my entire research period. One simply could not wish for better or friendlier supervisors.

The assistance and scientific guidance received throughout the M.Sc. duration by the teaching staff of the Department of Applied Earth Sciences is duly acknowledged. Special thanks are expressed to my dear advisors M.Sc. Wim Bakker and Prof. Wouter Verhoef. I am grateful to all the ITC staff including those at the ITC Hotel who made my stay very eventful and comfortable.

This study could not have been accomplished without EUMETSAT's favourable data distribution policy for research and education. Special thanks go to this great organization.

I would also like to thank my colleagues, my classmates and my friends for their continued support, love, care and encouragement throughout the time spent at ITC.

In conclusion, I would like to thank my family, those present and those recently departed who have always supported and encouraged me, regardless of the task. Without your love, care and motivation this would not have materialized.

Nadira Khan
(2010)

Table of contents

List of figures

List of tables

List of abbreviations

ALICE	Absolutely Llocal Index of Change of the Environment
ASTER	Advanced Spaceborne Thermal Emission and Reflection Radiometer
AVHRR	Advanced Very High Resolution Radiometer
BT	Brightness Temperature
BUFR	Binary Universal Form for the Representation of meteorological data
CLA	Clouds Analysis
DMSP	Defense Meteorological Satellite Program
DN	Digital Numbers
ECMWF	European Centre for Medium-Range Weather Forecasts
ENVI	Environment for Visualizing Images
EUMETSAT	European Organisation for the Exploitation of Meteorological Satellites
FY	Feng Yun
GEOSS	Global Earth Observation System of Systems
GloVis	Global Visualisation Viewer
HANTS	Harmonic Analysis of Time Series
IDL	Interactive Data Language
IDV	Integrated Data Viewer
IODC	Indian Ocean Data Coverage
ISL	IDV Scripting Language
LST	Land Surface Temperature
MODIS	Moderate Resolution Imaging Spectroradiometer
MSG	Meteosat Second Generation
MSG-RSS	Meteosat Second Generation- Rapid Scanning Service
MVISR	Multi-spectral Visible and Infrared Scan Radiometer
NASA	National Aeronautics and Space Administration
NEIC	National Earthquake Information Center
NOAA	National Oceanic and Atmospheric Administration
PERL	Practical Extraction and Report Language
RETIRA	Robust Estimator of Thermal Infrared Anomalies
RST	Robust Satellite Techniques
SCE	Scenes Analysis
SEVIRI	Spinning Enhanced Visible and Infrared Imager
SSM/I	Special Sensor Microwave Imager
SST	Sea Surface Temperature
TIR	Thermal Infrared
U-MARF	Unified Meteorological Archive and Retrieval Facility
USGS	United States Geological Survey
UTC	Universal Coordinated Time
VNIR	Very Near Infrared
WIST	Warehouse Inventory Search Tool
WMO	World Meteorological Organization

1. Introduction

This introductory chapter of the research presents the overall framework of the study. It focuses on the background, problem definition, formulation of research objectives, research questions and hypotheses, and a brief overview of the outline of the research.

1.1. Background

Earthquakes are one of the most dangerous and destructive forms of natural hazards. They strike with sudden impact and very little warning. They may occur at any time of the day or on any day of the year. Earthquakes can devastate an entire city or a region of hundreds of square kilometres. The extent of damage from an earthquake is dependent on several factors, such as the magnitude of the earthquake, the geology of the area, distance from the epicentre, population concentration and structure design and construction [24]. Apart from direct losses in terms of property and lives, there are indirect losses such as disruption of transport networks, power supply, and communication or through the necessary evacuations of buildings, change in zonal plans and adverse effect on tourism. Society has a compelling strategic need to anticipate these earthquake events since large urban centres have expanded in tectonically active regions.

On December 26th, 2003 an earthquake of M_w 6.6 magnitude in the South-eastern region of Iran shook the city of Bam. This incident destroyed most of Bam city and the nearby villages where the official death toll exceeded 26,000 with more than 30,000 injuries and 75,000 left homeless. The fact that this earthquake occurred at 5:26am local time on a Friday morning during the Iranian weekend when most people were asleep in their homes provides one of the main reasons for the high death toll [28]. Another earthquake occurring on April 6th, 2009 of M_w 6.3 magnitude struck the province of L'Aquila located in Central Italy which caused extensive damage to the city and areas of the province just outside L'Aquila. The province is known for its medieval architecture and monuments of historic and artistic value which suffered damage and many of the modern buildings were subjects to the damage. Hundreds of people were killed, thousands were injured and tens of thousands were left homeless [63]. These two earthquakes will be studied in detail in this research.

Unfortunately up to date, there is no direct solution to determine when such a phenomena will occur. However, remote sensing applications are diverse and are widely used in earth observation research owing to its effective results, accessibility and time conserving methodologies. Its full capability is yet to be determined. Remote sensing has emerged as a potential tool in studying earthquake activities and may assist in providing a timely warning of the potentially damaging earthquakes in order to allow appropriate preparatory measures for the disaster, enabling people to minimize loss of life and reduce the economic losses of property and assets [47]. This research proposes a method to identify pre-earthquake activities for the Bam earthquake which will later be applied to L'Aquila. Indeed, this research may assist in reducing these effects caused by earthquake events.

1.2. Problem Definition

One area that may hold promise in advancing the science of short-term earthquake prediction is the study of earthquake precursors. The term earthquake precursor is used to describe a wide variety of physical phenomena that reportedly precede at least some earthquakes. During the last century, many precursors to the earthquake event were identified. These phenomena include induced electric and magnetic fields, groundwater level changes, gas emissions, temperature changes, surface deformations, and anomalous seismicity patterns. While each of these phenomena has been observed prior to certain earthquakes, such observations have been serendipitous in nature [6]. Thermal anomalies are one of the earthquake precursors that are gaining more attention from the scientific community.

Earlier studies have indicated that before major earthquakes satellite retrieved temperatures increase in the vicinity of the future epicentre [43]. Most of the studies compared results of multi-temporal datasets which spanned some days or weeks before and after the earthquake. These studies performed only visual assessments of the imagery. Even though these results are promising, the scope of those studies did not allow for longer observations and it is unclear in how far these anomalous temperatures also occur with no earthquake following (i.e. false positives).

In this study, long time series of thermal imagery will be used in order to provide answers to whether significant anomalies appear prior to an earthquake event and are periodic in nature. The research is being performed to understand normal patterns within the data thus defining the term "thermal anomaly" in the context of earthquake research. It is most suitable to conduct this research with high temporal resolution satellite like the Meteosat series of satellites since long time series is required. The occurrence of these anomalies will be evaluated for two major earthquakes. Subsequently the anomalies will be assessed as to whether they are directly related to the earthquake or caused by non-earthquake phenomena. The probability of the predicted earthquake to occur by chance and to match up with the precursory anomaly shall also be evaluated. The frequency of false positives (similar anomalies not followed by an earthquake) and false negatives (earthquakes not preceded by an anomaly) should be tested.

1.3. Research Objectives

1.3.1. Main Objective

To verify if significant thermal infrared anomalies can be found in association with known earthquakes by systematically applying satellite data time series analysis to multi-year time series.

1.3.2. Specific Objectives

i. To determine the average surface temperatures from the time series trends and the variance not related to earthquake activity.

ii. To develop a detection algorithm for anomalous surface temperatures related to earthquake activity by means of spatial and temporal surface temperature patterns using Meteosat-5 and MSG TIR imagery.

iii. To determine which anomalous temperatures are associated with large earthquakes and also those anomalies which are not directly earthquake-related.

1.4. Research Questions and Hypotheses

For Specific Objective 1

i. Can time series be used to predict normal variance in surface temperatures not related to earthquake activities?

Ho : Time series predict normal variance of land surface temperatures

For Specific Objective 2

i. Is it possible to detect a thermal anomaly prior-to large earthquakes using a time series of thermal images?

Ho: The thermal anomaly is detectable within a 0-4 week period prior-to the event

ii. How do spatial and temporal patterns of anomalous temperatures caused by earthquakes differ from those caused by other events (such as fires, weather-related, seasonal)?

Ho: Earthquake-related anomalies appear as a uniquely identifiable event in time series

For Specific Objective 3

i. Is there anomalous change in surface temperature in the vicinity of the located epicentre or fault zone?

Ho: The thermal anomaly appear closer to the epicentre or along a fault-line

ii. How do these anomalies appear over time?

Ho: Anomalies appear randomly in time

iii. Is it possible to use time series to detect anomalies for different conditions (for smaller magnitude earthquakes, other sensors and wet conditions)?

Ho: Time series is capable of detecting anomalies for different scenarios

1.5. Methodology

Data sources available include:

- ➢ Earthquake catalogue: generated from USGS website
- ➢ MSG and Meteosat imagery using GEONETCast Toolbox Plug-in and UMARF
- ➢ MODIS (as a base to assess whether anomaly was visible as suggested by other researchers)

Data processing includes:

- ➢ Conversion from DN to Radiant temperatures

- Cloud-Masking from data
- Detection of anomalies

Data analysis includes:

- Assessment of anomalies: earthquake- related versus false positives
- Comparison of several years of data
- Applied to L'Aquila

1.6. Outline of thesis

The reporting of the research is structured in five chapters. The structure of the thesis is as follows:
Chapter 1: *Introduction* provides an overview of the problem definition emphasizing the reason for research, research objectives, research questions, hypotheses, a general description of the methodology and an overall outline of the thesis.

Chapter 2: *Literature review* provides background information of earthquakes and thermal anomalies; the concepts of thermal remote sensing comprising satellite specifications; presents a background of the study area; includes the previous attempts made with regards to time series, as well as possible anomaly detection techniques.

Chapter 3: *Methodology* provides the overall methodology applied for the research and its implementation.

Chapter 4: *Data Analysis and Results* obtained from the methodology employed with respect to time series data and detection of thermal anomalies, and from statistical tests performed.

Chapter 5: *Discussion and Conclusion* addresses the main findings from the results obtained with brief explanations; and the major conclusions drawn from the research despite the limitations involved and several recommendations.

2. Literature Review

This chapter presents a review of literature on the concept and ideologies related to the present research. The review indicates the study areas for this research and highlights the previous studies performed by fellow researchers.

2.1. Earthquakes and Thermal Anomaly

Earthquakes are vibrations of a part of the earth's crust caused due to internal stresses acting on rocks in the crust. The increasing stress will result to some extent in subsurface heat production rather than to generate seismic waves. The total energy from an earthquake includes energy required to create new cracks in rock, energy dissipated as heat through friction, and energy elastically radiated through the earth. The heat or temperature rise resulting from the release of energy by the earthquake can provide interesting observations in earthquake studies which may offer clues about future earthquake activities. Figure 2-1 addresses two mechanisms that generate pre-earthquake thermal infrared (TIR) anomalies which can be detected from satellite thermal sensors.

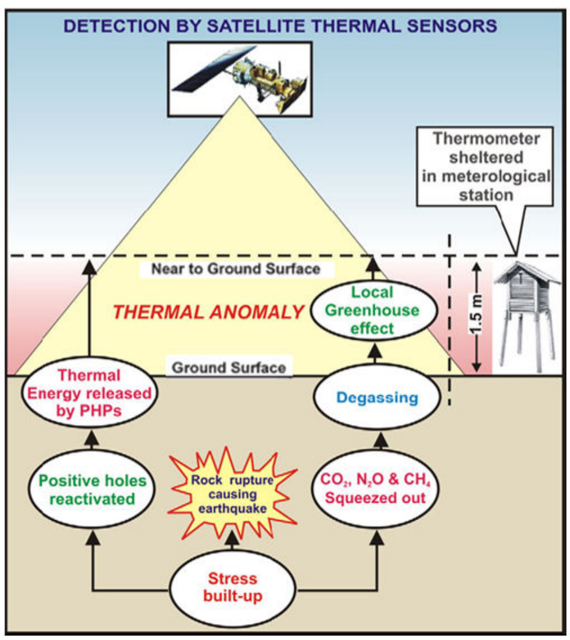

Figure 2-1: Schematic diagram showing two widely accepted theories of generation of pre-earthquake TIR anomaly that can be detected by satellite thermal sensors [44].

Thermal anomalies are the increase in emission of the earth's surface in TIR wavelengths. The enhanced emission gets recorded in the thermal sensors and can be separated from the surroundings with some uncertainty. It was shown that thermal anomalies appear before major earthquakes and can be traced through thermal sensors [35]. The mechanisms explaining the generation of thermal anomalies can be grouped into two categories, the first accounting atmospheric processes responsible for the appearance of thermal anomaly, and the second attributing rise in land surface temperature (LST) due to ground related processes. Several mechanisms which lead to the increment in outgoing infrared (IR) radiation ahead of an impending earthquake have been linked to:

- Gas emissions- stresses prior to these phenomena may also bring about sub-surface degassing. Upon their escape to the atmosphere, these gases like CO_2, CH_4, N_2, Rn may create a localized greenhouse effect and increase the temperature of the region, thus creating a thermal anomaly in the surrounding region. Such changes detected through thermal remote sensing can provide important clues about future earthquakes. An abnormality in the thermal properties of the Earth's surface, detected by thermal channels like Meteosat, can prove to be a valuable indicator of an impending earthquake [42, 44];
- Water level changes- wells have changed the water levels and water quality prior to the earthquake. Microfracturing prior to large earthquakes leads to increases in ion and gas concentrations in the groundwater (firstly it allows trapped gases to escape from the rock matrix and secondly, it produces fresh silicates, which are believed to increase the rate of reaction of groundwater) [6];
- Groundwater change- changes in the circulation patterns of groundwater bringing water of different temperature to the surface. The flow of water in the earth before an earthquake might allow that water to come into contact with hotter rock bodies at depth and raise the temperatures of near-surface groundwater [6];
- Activating positive-hole pairs (PHPs) during rock deformation- electronic charge carriers can be free electrons or sites of electron-deficiency in the rock/mineral structures (3-D array of oxygen, which has unstable radicals) [41, 44];
- Ground temperature change- frictional heating on fault surface could contribute to ground temperature changes. Because rocks have a relatively low thermal conductivity any such temperature –related changes that may occur at the depth in the earth would take a long time to reach the surface through the rock itself [6];
- Pore collapse- as stresses in the earth increase prior to an earthquake, the pore volume in the rocks collapses, thereby releasing chemical species into the groundwater, generating a geochemical anomaly [6].

Numerous observations of such thermal anomalies preceding several major earthquakes are reported from different parts of the world. These anomalies were almost always cited to be positive anomalies with the exception of the studies performed in Japan and China [55]. From research, short-lived anomalies:

- typically appear 6-24 days before and continued for about a week after an earthquake [35, 54, 55] ;
- affect regions of several to tens of thousands square km [5, 42, 53];
- display a deviation of 2-10 °C in the vicinity of the epicentres [35, 36, 42, 54];
- where the size of the anomaly is ~100km in length and ~10km in width [54];
- are sensitive to crustal earthquakes with magnitudes greater than 4.5 and are normally attached to large faults [54].

The rapidity with which these temperature excursions occur suggests that they cannot be due to thermal variations caused by a heat pulse rising from within the earth. Pre-earthquake thermal anomalies and their spatial and temporal variations are reportedly controlled by various factors which vary from earthquake to earthquake. These factors include magnitude, focal depth, geological setting, topography and vegetation cover, stress-buildup and degassing [55] as well as meteorological conditions [35, 54].

Thermal anomalies have been defined in different contexts regarding the researcher's task. For instance, Ouzounov (2006) was studying the relationship of the thermal anomaly in a spatial context. He defined a thermal anomaly as "*the difference between the spatial daily root mean square (RMS) LST value and the mean LST value of an area of M x N km^2 (i.e. the area of interest which is usually represented as 100x100 km) which is centred at the epicenter and located on the stress-released fault for the entire time interval of analysis"* [35]. Unlike the work that was conducted by Ouzounov (2006), another approach was addressed statistically by Tramutoli (1998). He defined a thermal anomaly only after assessing the datasets using the presence/absence of anomalous space-time TIR transients in the presence/absence of seismic activity [53]. Later in the research, the definition of an anomaly will be defined for the use of the required datasets.

2.2. Thermal Remote Sensing

Satellite thermal remote sensing can be used in the detection of anomalies in LST in and around epicentral regions. In 1988, Gornyi et al. [17] first analysed remotely sensed images of National Oceanic and Atmospheric Administration- Advanced Very High Resolution Radiometer (NOAA-AVHRR) of the earth's surface in the 10.5-11.3µm range who showed a stable increase of outgoing IR radiation over linear structures of a seismically active region in Central Asia as compared with adjacent areas. He indicated that outgoing IR radiation can be used as an indicator of seismic activity [27] and suggested that meteorological satellites be used to assess these indicators. It is first important to understand what the term thermal anomaly represents to know what these meteorological satellites actually observe.

The modern operational space-borne sensors in the IR spectrum allow monitoring of the Earth's thermal field with a spatial resolution of 0.5–5 km and with a temperature resolution of 0.12–0.5 °C. Temporal coverage is every 12 hours for the wide-swath, polar orbit satellites (for e.g. AVHRR and MODIS), and 15 minutes for geostationary satellites. Such sensors may closely monitor seismic prone regions and provide information about the changes in surface temperature associated with an impending earthquake. Thermal observations from satellites indicate the significant change of the Earth's surface temperature and near-surface atmosphere layers [54].

There are three principal laws within thermal remote sensing, namely

	Law	Equation	Parameters
1	Planck's Radiation Law- the amplitude of radiation emitted (i.e. spectral radiance) from a blackbody. It is generally provided in one of two forms; $L_\lambda(\lambda)$ is the radiance per unit wavelength as a function of wavelength λ and $L_v(v)$ is the radiance per unit frequency as a function of frequency v. By the Planck Law, all heated objects emit a characteristic spectrum of electromagnetic radiation, and this spectrum is concentrated in higher wavelengths for cooler bodies.	$L_\lambda(\lambda) = \frac{2hc^2}{\lambda^5}\left[exp\,\frac{hc}{\lambda kT} - 1\right]^{-1}$ Equation (1)	T- temperature (°K) c- speed of light ($2.99x10^{-8}\ ms^{-1}$) h- Planck's constant ($6.63x10^{-34}$ Js) k- Boltzmann's constant (1.38x10-23 J $°K^{-1}$) L_λ- spectral radiance ($Wm^{-3}sr^{-1}$)
2	Wien's Displacement Law- the wavelength (or frequency) where the spectral radiance has maximum value. This can be found by taking the derivative of L_λ with respect to wavelength and determining where the function is zero. Wien's Law explains the shift to shorter wavelengths with increasing temperature (i.e. as temperature increases the total amount of radiant energy peak shifts to shorter wavelengths). According to Wien's Displacement law, temperatures of 600°K and greater are associated with fire, lava flows which corresponds to bands around 3-to-5 μm in the SWIR, where the radiation maximum for those fires can be expected. On the contrary, the 8-to-14 μm band spans the radiant energy peak for a temperature of 300°K corresponding to the ambient temperature of the earth (LST).	$\gamma = \frac{hc}{kT\lambda_{max}}$ and in the more common form $\lambda_{max} = C_w/T$ Equation (2)	λ_{max}- peak wavelength (m) C_w –Wien's displacement constant ($2.898x10^{-3}$ m°K) T- temperature (°K)
3	Stefan-Boltzmann Law- the total blackbody irradiance as a function of the temperature T. This law can be derives by integrating the spectral radiance over the entire spectrum. Stefan-Boltzmann's Law is explained by the area under the Planck Law curve. It states that colder objects emit only small amounts of electromagnetic radiation.	$L = \int_0^\infty L_\lambda d\lambda = \frac{2\pi^5 k^4}{15c^2h^3}T^4$ and in the more common form $M = \pi L = \sigma T^4$ Equation (3)	M- radiant exitance (Wm^{-2}) L- radiance(brightness temperature) ($Wsr^{-1}m^{-2}$) σ- Stefan-Boltzmann's constant (5.67x10-8 $Wm^{-2}°K^{-4}$) T- temperature (°K)

Table 2-1: Radiation laws governing Thermal Remote Sensing [39].

Kinetic temperature is an “internal” manifestation of the average translational energy of the molecules constituting a body. In addition to this internal manifestation, objects radiate energy as a function of their temperature. This emitted energy is an “external” manifestation of an object’s energy state. It is this external manifestation of an object’s energy state that is remotely sensed using thermal scanning. The emitted energy is used to determine the radiant temperature of earth surface features , see Appendix A. The output from a thermal sensor is a measurement of the radiant temperature of an object, T_{rad} [26]. Radiance data and the inversion of Planck function provide the T_{rad} and the elimination of atmospheric effects leads to surface temperature [49]. Thermal sensors detect radiation from the surface (approximately the first 50 um) of ground objects. Temperature extremes, heating and cooling rates can often furnish significant information about the type and condition of an object. The extremes and rates of temperature variation of any earth surface material are determined, among other things, by the material’s thermal conductivity, capacity and inertia [26].

2.3. Satellite Specifications

NOAA-AVHRR have been used to observe past earthquakes in Bhuj (India), Boumerdes (Algeria), Xinjiang (China), Izmit/Kocaeli (Turkey), Hindukush (Afghanistan), Kalat (Pakistan), and also the devastating great mega-thrust Banda-Aceh (Sumatra, Indonesia) earthquake [41]. Other TIR sensors such as Multi-spectral Visible and Infrared Scan Radiometer (MVISR) on the Feng Yun (FY), Moderate Resolution Imaging Spectroradiometer (MODIS) on board satellites Terra and Aqua, Advanced Spaceborne Thermal Emission and Reflection Radiometer (ASTER) on board satellite Terra have been used to detect, short-term temporal pre-earthquake thermal anomalies around the epicentral region [41]. These polar orbiting satellites have relatively high spatial resolutions and better signal-to-noise ratios, but only acquire images twice during an evening thereby making trend analysis for monitoring diurnal LST change more difficult [35]. Depending on the latitude, NOAA-AVHRR has a revisit time of 2 to 14 times per day. ASTER has a temporal resolution of 5 days for the very near infrared (VNIR) channel. MODIS has a 1 ½ day revisit time.

Unlike polar orbiting satellites, geostationary satellites guarantee for each ground location, although at lower spatial resolution, constant view angles with the same ground resolution cell size [2]. It provides a much higher temporal coverage but owing to the low spatial resolution for land-based studies, it can be problematic. This high temporal resolution of geostationary satellites assists by reducing the chance for miscalculating trends due to weather front movement or local cloud/fog formation [35].

Geostationary satellites such as the Meteosat series of satellites are ideal for the time series analysis prior to an impending earthquake owing to its high temporal resolution. Meteosat’s first generation of satellites is equipped with three spectral channels: a broadband channel in the visible (VIS) spectral region, ranging from about 0.5 to 0.9 μm showing reflected light, a thermal infrared channel at approximately 6.4 μm in the water vapour (WV) absorption band, ranging from 5.7 to 7.1 μm, and a channel in the thermal infrared window region at approximately 11.5μm showing emitted radiation, ranging from 10.5 to 12.5 μm as seen in Appendix B part (i). The sampling distance of the channels at the subsatellite point is 2.5 x 2.5 km for the VIS and 4.5 x 4.5 km for TIR. The temporal resolution of observations amounts to 30 minutes, that is, in each of the three channels, an image of Meteosat's entire field of view is measured and sent to earth [40].

MSG is a significantly enhanced follow-on system to the previous generation of Meteosat. Meteosat had seven successful launches since the year 1977. MSG satellite series gives significantly increased information as it allows the acquisition of imagery at every 15 minutes for the MSG-2, also referred to as Meteosat-9 and 5 minutes over Europe (MSG-RSS) as a time series in order to assess the earthquakes. MSG consists of 12 spectral channels, quantization with 10 bits per pixel and image sampling distances of 3km at nadir for all channels except the high resolution visible with 1km [46] as seen in Appendix B part (ii). MSG-1 was launched on August 28th, 2002 whereas MSG-2 on December 21st, 2005. MSG is a geosynchronous weather satellite that has eight thermal bands.

Geostationary satellites as well as polar orbiting satellites used simultaneously assist in anomaly detection techniques. High temporal Meteosat imagery alongside with moderate spatial MODIS imagery can provide with a higher significance the anomalies that are related to earthquake events. Time series profiles can be constructed using TIR Meteosat imagery whilst any anomalous events or abnormal patterns within profiles can be analysed with visible imagery from MODIS.

2.4. Location of Study Area

The earthquakes that will be analysed are limited to (i) the coverage of the Meteosat series of satellites (i.e. Meteosat-5 and Meteosat-9), (ii) larger magnitudes, and (iii) earthquakes occurring on land (land-restricted and crustal earthquakes).

As aforementioned Meteosat-5 and MSG2 satellite imagery will be used. The coverage for these geostationary satellites can be seen in the Figure 2-2. This allows us to determine the spatial extent and the imagery which can be extracted for future applications.

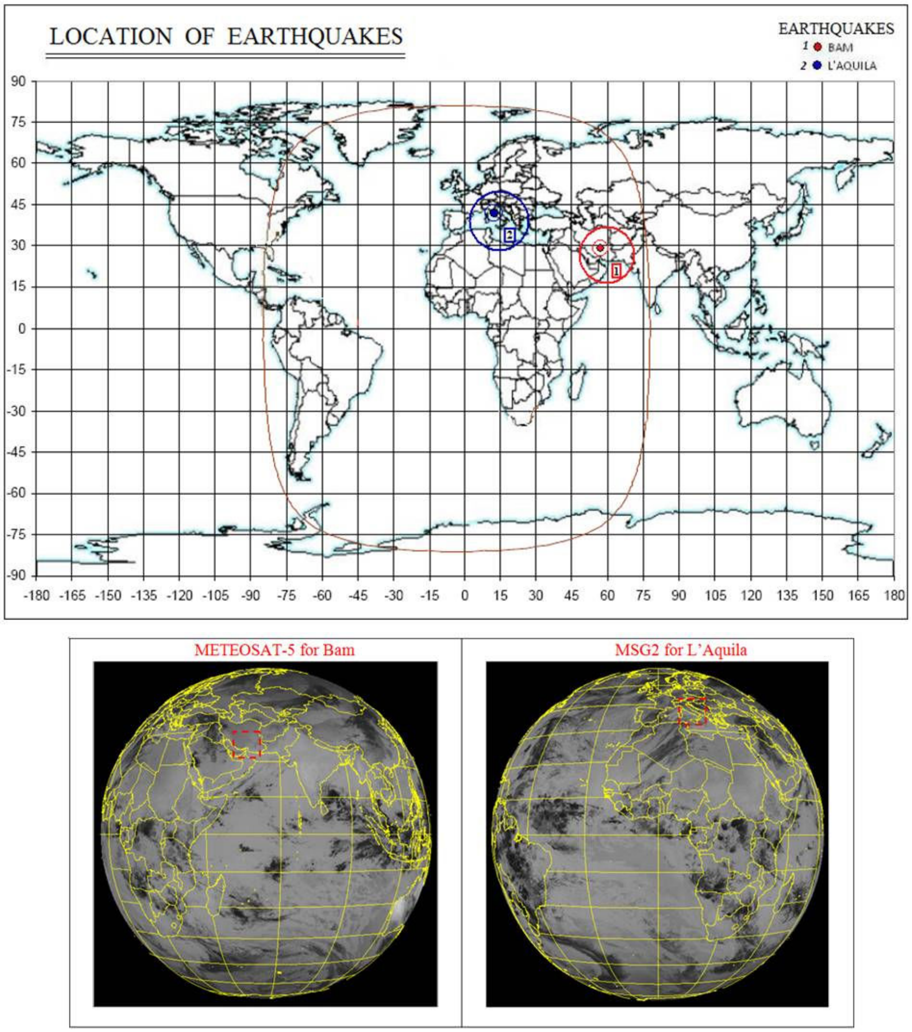

Figure 2-2: The approximate locations of the selected earthquakes [7] with their respective satellite geo-coverage.

2.4.1. Geological Settings

The coverage of the satellite is important since this enables the selected study areas and the acquisition of pre- and post- satellite imagery for our study. Table 2-2 is an earthquake catalogue of those earthquakes that will be studied and for each their respective geological/tectonic setting.

Earthquake Catalogue

Number	Earthquake	Origin		Location		Country	Magnitude (USGS) M_w	Focal depth (km)	Focal mechanism
		Date	Time (UTC)	Latitude N (°)	Longitude E (°)				
1	Bam	26-Dec-03	01:56	29.00	58.325	Iran (S.E.)	6.6	10	Reverse faulting, Strike-slip(Right-lateral)
2	L'Aquila	06-Apr-09	01:32	42.423	13.395	Italy (Central)	6.3	10	Normal Fault

Table 2-2: Earthquake Catalogue for analysis, extracted from USGS [58].

(1) Bam Earthquake

Saraf et al. [41] and Choudhury et al. [5] describes the tectonic and geological setting of the study area as having a tectonic belt of Iran which forms a linear NW–SE trending intra-continental fold and thrust belt between the Arabian shield and Central Iran. Furthermore, it was stated that this earthquake occurred as a result of stresses generated by the motion of the Arabian plate (which includes Saudi Arabia, Persian Gulf and the Zagros Ranges in Iran) northward against the Eurasian plate at a rate of approximately 3 cm/yr. Complex folding and fault movements in the Zagros Ranges have resulted due to the tectonic deformation by the collision of the two plates. However, in the interior parts of Iran in the north of the Zagros Ranges and in the south of the Alborz Ranges, deformation is mainly due to strike slip movements along complexly arranged intersecting faults. The Gowk fault is oriented along the west of the Bam fault in a similar north–south trend. Earthquakes in this region occur as the result of both reverse faulting and strike-slip faulting within the zone of deformation. Figure 2-3 provides an overview of these faults and how they are spatially related to each other where the star represents the approximate epicentre of the earthquake.

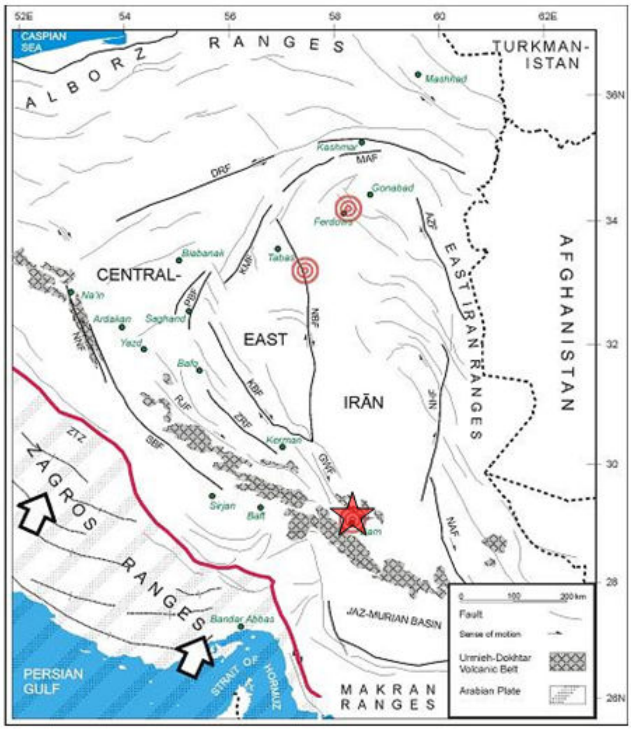

Figure 2-3: Main tectonics of Iran and active tectonic faults [38].

Besides its high seismicity, its relatively cloud-free and stable weather conditions during most parts of the year and its sparse vegetation cover make Iran a suitable study area [41]. Bam is a desert area. Extreme temperatures within this region can be found in Appendix C. Bam's earthquake is ideal as it is a large magnitude earthquake and is restricted to land thus for identifying thermal anomalies it is also suitable since they will be more pronounced.

(2) L'Aquila Earthquake

The earthquake in Central Italy occurred as a result of normal faulting on a NW-SE oriented structure in the central Apennines, a mountain belt that runs from the Gulf of Taranto in the south to the southern edge of the Po basin in northern Italy. Geologically, the Apennines are largely an accretionary wedge formed as a consequence of subduction. This region is tectonically and geologically complex, involving both subduction of the Adria micro-plate beneath the Apennines from east to west, continental collision between the Eurasia and Africa plates building the Alpine mountain belt further to the north and the opening of the Tyrrhenian basin to the west. Although Italy lies in a tectonically complex region, the central part of the Apennines has been characterised by extensional tectonics since the Pliocene epoch, with most of the active faults being normal in type and NW-SE trending. [58]

Occasionally parts of Italy experience very high temperatures in summer and even autumn when the sirocco blows. This warm humid wind originates over North Africa and acquires its humidity over the Mediterranean. Summer tends to be the rainiest season and thunderstorms are frequent in spring, summer, and autumn [4]. The earthquake corresponds to the month of April which is cool and is possibly rainy. Extreme conditions occurring within this region can be seen in Appendix D.

L'Aquila earthquake is being studied to test whether the developed methodological approach can be applied to an earthquake that is subjected to a lesser magnitude (< 6.5). As compared to the previous location, this study area is densely populated and has more vegetation cover. This earthquake is also restricted to land which can be used for identifying thermal anomalies.

Reports were made whereby a technician, Giampaolo Giuliani claimed that he was able to predict this earthquake owing to the high concentrations of radon gases that were produced prior to L'Aquila earthquake [15, 31]. Radon gas is one of the many earthquake precursors. To verify whether the reported radon gas anomalies produced a rise in temperature made L'Aquila earthquake an ideal study location.

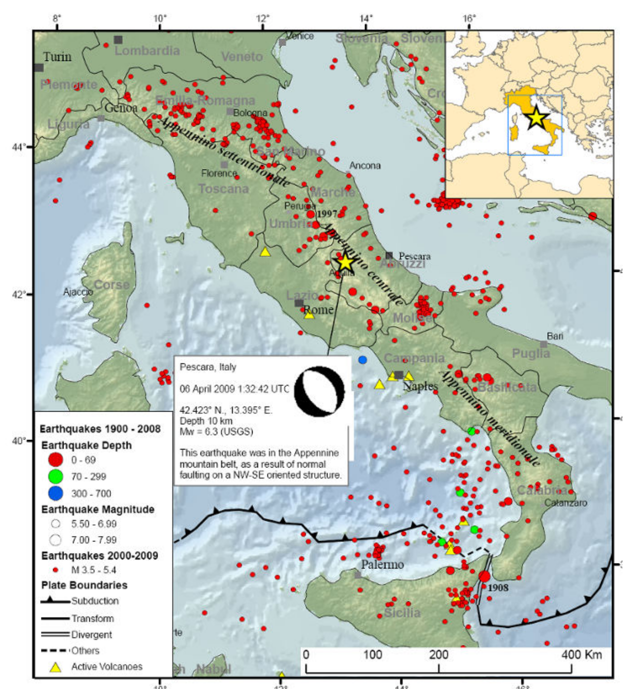

Figure 2-4:Location of the magnitude 6.3 L'Aquila earthquake, Italy on 06th April 2009 [60].

2.5. Time Series

Time series is a sequence of observations of well-defined data items measured typically at successive times, spaced at (often uniform) time intervals. The main features of many time series are trends and seasonal variations that can be modelled deterministically with mathematical functions of time. Time series analysis has been used in many application domains and for different purposes. The way the data is analysed also depends on the task. Anomalies in time series data are data points that significantly deviate from the normal pattern of the data sequence.

For earthquake research, time series of LST maps can be used to assess the temperature changes prior to the impending earthquake. Several studies have been performed which used short-term prediction techniques for these types of phenomena. *Short-term prediction* refers to the period of time in which changes in the surroundings and changes in temperatures are expected to occur which is often identified as 6 to 24 days, before the earthquake. Other characteristics such as the length of time before the earthquake when the precursor initiated, the duration of the precursor, the amplitude of the precursory signal, the signal-to-noise ratio of the anomalous relative to normal background noise and the distance from the observation point to the earthquake [6] are some factors which can be answered through time series analysis.

For instance, the night-time and daytime NOAA-AVHRR time series LST maps for the earthquake in Bam, Iran showed that there was a thermal anomaly appearing before the devastating earthquake of 26 December, 2003.

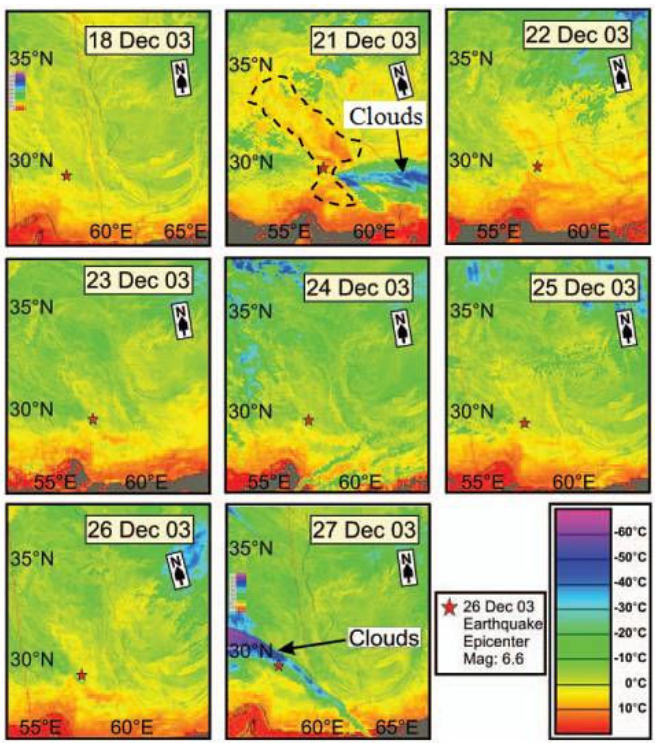

Figure 2-5: Nighttime NOAA-AVHRR LST time series map of Iran before and after the earthquake in Bam, Iran on 26 December 2003. The thermal anomaly in the night-time data was seen to be maximum on 21 December 2003 (5days before the earthquake) which is indicated as the black figure around the epicenter [41].

In the night-time maps as shown in Figure 2-5, it was seen that on 18th December 2003 there was no evidence of any anomalous activity. The appearance of an intense thermal anomaly was seen around the earthquake epicentre on the 21st December 2003 as indicted by the black figure. This anomaly shows a rise in temperature of approximately 10°C. The anomalous region in the night-time data on 21 December 2003 occupied an area of about 308,000km^2 [41]. However, data was unavailable for 19th and 20th December 2003 so there will be speculations as to the exact time the anomaly originated and its duration. Analysis and similar processing of night-time NOAA-AVHRR data of the year 2004 acquired at around the same time and on the same days as the 2003 data showed that there was no such abnormal behaviour of the LST on those days in that year. However, these results were not provided making this statement questionable.

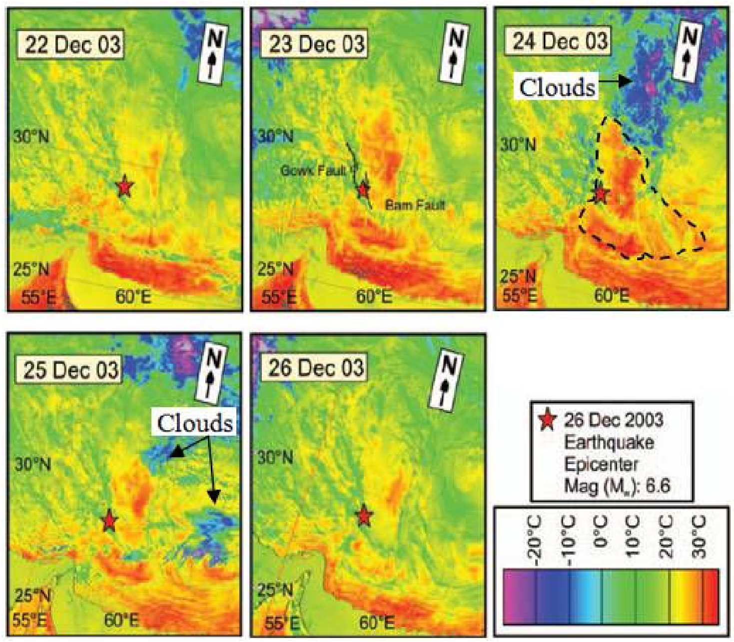

Figure 2-6: Daytime NOAA-AVHRR LST time series map of Iran before and after the earthquake in Bam, Iran on 26 December 2003. An intense thermal anomaly can be seen on 24 December 2003, 2 days before the earthquake, as indicated by the black figure. The Bam fault is placed on the map of 23 December 2003 is responsible for the Bam earthquake [41].

Daytime LST time series maps show that the rise in temperature started on 22 December 2003. The anomaly stayed on till 24 December 2003 (just two days before the earthquake), Figure 2-6. The anomalous region in the daytime LST map of 24 December 2003 covered an area of about 328200 km^2 [41].

If a short time series is used, it is difficult to define what are normal temperatures in a study area yet alone anomalous temperature. These anomalies as shown above can be caused by natural variations whereby some days are warmer than others. To ensure that these variations are not normal conditions, a short time series is useless thus requiring a long time series of TIR imagery.

2.6. Anomaly Detection Techniques

From Oxford dictionary, an *anomaly* is defined as an irregularity, deviation from the common order or an established trend. The anomaly can be found by detecting it. *Anomaly detection* refers to detecting these deviations or patterns in a given dataset that do not conform to an established normal behaviour.

When large data inputs are used, an automated detection mechanism is needed. A detection algorithm can be created to detect any anomalous behaviour within the large datasets which can show the time of the event. However, to differentiate events from non-events, a measure has to be developed. This detection algorithm can be based on temperature variations of a single pixel with time or on the comparison of pixel with its neighbouring pixels at a given time.

2.6.1. Variation per pixel in time series data

TIR signals measured from satellites depend on a number of natural and observational conditions: (e.g. atmospheric transmittance, surface temperature, spectral emissivity, topography as well as time of day/season, and satellite view angles, respectively. The contribution of those conditions to the measured signal can be so high as to completely mask the space–time fluctuations claimed as anomalous and connected with the seismic event under study. Space–time fluctuations of TIR signal cannot, therefore, be assumed as pre-seismic TIR anomaly without referring them to a normal TIR signal behaviour and without investigating whether or not similar space–time fluctuations can also be observed in the absence of seismic activity. This confutation process is difficult but a suitable definition of TIR anomaly (for validation purposes), are very hard to find [53].

The robust satellite techniques (RST) approach is a general satellite data analysis strategy which is based on a statistical definition of what “anomaly” of a signal measured from space actually means. The radiation, coming from Earth and measured by satellite sensors, is generally largely fluctuating due to many natural/environmental/observational causes, regardless of the phenomenon we are dealing with [37]. The RST based on the approach proposed by Tramutoli (1998) seems to offer both, a statistically well-founded definition of TIR anomaly and a suitable tool for assessing the actual potential of satellite TIR surveys in seismically active regions. He proposed a statistically-based method that, using only satellite data that is capable of identifying a (statistically significant) signal anomaly, comparing the signal at hand with previously defined and computed, expected value and natural level of fluctuation [37, 52].

The approach has been implemented by using a validation/confutation approach, devoted to verifying the presence/absence of anomalous space-time TIR transients in the presence/absence of seismic activity [37]. In some of these test cases , for instance in Kocaeli (İzmit) in Turkey [53], Irpinia-Basilicata in Italy, Gujarat in India and Umbria-Marche in Italy [3] to identify anomalous TIR patterns, a specific index, RETIRA was computed on the image at hand using the following equation:

$$\otimes\Delta T(r,t) = \frac{[\Delta T(r,t) - \mu_{\Delta T}(r)]}{\sigma_{\Delta T}(r)} \quad \text{....Equation(4)}$$

where $r \equiv (x,y)$ represents location coordinates on a satellite image,

t is the time of image acquisition with $t \in \tau$ where τ defines the homogeneous domain of satellite imagery collected in the same time-slot of the day and period of the year,

$\Delta T(\boldsymbol{r},t)$ refers to the difference between the punctual value of the brightness temperature $T(\boldsymbol{r},t)$ at the location $\boldsymbol{r}$ and at the acquisition time t and its spatial average T(t) (i.e. $\Delta T(\boldsymbol{r},t) = T(\boldsymbol{r},t) - T(t)$ computed on the investigated area considering only cloud-free pixels locations, all belonging to the same, land or sea class,

$\mu_{\Delta T}(\mathbf{r})$ is the time average value of $\Delta T(\mathbf{r},t)$ at the location $\mathbf{r}$ computed on cloud-free record belonging to the selected dataset ($t \, \varepsilon \, \tau$),

$\sigma_{\Delta T}(\mathbf{r})$ is the standard deviation of $\Delta T(\mathbf{r},t)$ at the location $\mathbf{r}$ computed on cloud-free record belonging to the selected dataset ($t \, \varepsilon \, \tau$) [3, 37, 53].

A ‘‘standardized” local variation index named ALICE is then defined reporting, at pixel level, the relative amplitude of deviations of the measured signal with respect to the reference values, expected for the specific considered period (temporal domain) and the selected region of interest (spatial domain). RETIRA belongs to the ALICE indexes [37]. ALICE assists in estimating the TIR anomalies in terms of signal-to-noise (S/N) ratio. The local excess $[\Delta T(\mathbf{r},t) - \mu_{\Delta T}(\mathbf{r})]$ represents the signal to be investigated for its possible relation with seismic activity and is evaluated by comparison with the corresponding observational/natural noise represented by $\sigma_{\Delta T}(\mathbf{r})$. This way the relative importance of the measured TIR signal (or the intensity of anomalous TIR transients) can naturally be evaluated in terms of S/N ratio by the ALICE indexes. Generally, the higher (in modulus) the value of ALICE, the stronger (in terms of intensity) and/or larger (in terms of size) is the detected anomaly.

The amplitude of a detected anomaly is given in ‘‘number of sigma’s”, to be interpreted in the classical statistical way. The ‘‘background reference fields” (i.e., the expected value of satellite signal for a specific site and time period and its natural variability, $\mu_{\Delta T}$ and $\sigma_{\Delta T}$ in the above equation are obtained, pixel by pixel, by a multi-temporal analysis of multi-year satellite records, stratified according to homogeneity criteria [3, 37, 52].

However, there are two main drawbacks of such an anomaly detection approach making it inapplicable to the research being conducted. One reason that questions the work set out by Tramutoli (1998, 2005) and Aliano (2008) was the proximity of the anomaly to the epicentre or fault location. For instance, the outputs of the algorithm obtained for the İzmit (Kocaeli) M_w 7.4 earthquake in Turkey on August 17th, 1999 at 3:02AM local time [57] is seen below.

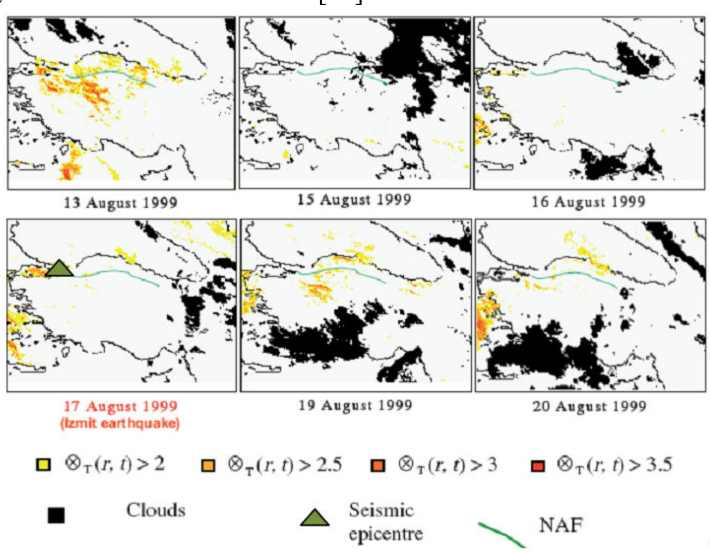

Figure 2-7: The RST approach applied to Meteosat satellite data. Results of the analysis of the daily index $\otimes_{\Delta T}(r,t)$computation on the epicentral area of the day of İzmit's earthquake [2].

There were no geographical coordinates on these time series map layouts. Thus, in a Google map, these anomalies that were detected were beyond a 5° geographical coordinate radius (approximately 700km away) from the epicentre as shown in Figure 2-8. For a magnitude 7.4 earthquake, the fault length is approximately 150km [61] on which the epicentre occurs. It is highly unlikely for thermal anomalies to be related or directly linked to an earthquake when it is occurring at this distance away from the epicentre. Even the author stated that problems remain in interpreting thermal signals in a seismogenetic region: understanding whether the observed anomalous TIR signals are in statistical significant relation with time and place of incoming earthquakes or they are on the contrary related to other natural phenomena [2].

Figure 2-8: Spatial extent of the study area on a Google map with reference to the work performed by Tramutoli and Aliano.

The second drawback is the high number of environmental factors (independent from any seismic activity) which could affect the (possible) precursor signal up to completely mask it. In order to be interpreted, the data should be preliminarily corrected, at least for the effects of atmospheric absorption (mainly due to the water vapour) superficial emissivity (highly variable over land) and observational conditions (mainly satellite zenithal angle) [52]. Meteosat does not have any split-window spectral channels and hence did not permit us to reduce the natural noise related to the variability of atmospheric water vapour so a different index is needed [2]. It is also important to note here that within this six day period, a few days can be warmer than the surrounding area making a short time series be of no use.

2.6.2. Variation of pixel to neighbouring pixels in time series data

Kuenzer et al. (2007) uses TIR satellite imagery to detect thermal anomalies which are influenced from sub-surface coal fires and cause extremely weak anomalies, which can by no means be compared with thermal applications like forest fire detection, lava flow detection or the spotting of large industrial heat islands. In general, in remote sensing-related coal fire research, the greatest challenge is the fact that the temperature difference between a coal fire-influenced pixel and a normal background pixel is usually very low, so thermal anomalies to be extracted are usually subtle [22]. Like sub-surface coal fire thermal anomalies, earthquake-related thermal anomalies are very subtle.

Like Tramutoli (1998), Kuenzer et al. (2007) also used a split-window approach but his method in determining thermal anomalies was different. This automatic approach calculates the ratio images between two different bands, where pixels with similar emission in the bands will show values of around 1, while pixels containing thermal anomalous areas with relatively greater temperatures will yield values greater than 1. Thus, the ratio of the two leads to a ratio image enhancing strong hotspots [22].

The algorithm facilitates raw satellite data as inputs for a sub-image statistical analysis which is based on a moving window concept where each centre pixels within the window matrix is sampled multiple times. These pixels are compared to the surrounding background which then provides a probability of being represented as a thermal anomaly. This means that pixels of very different temperature and within a different temperature background can be declared thermally anomalous. [22].

Certain criteria were set to remove false alarms that do not stem from coal fires. Anomalies were assessed spatially and if it appears within a certain cluster (based on an eight-pixel neighbourhood), it will be regarded as a thermal anomaly. However, it was furthermore investigated how many false alarms from the existing cluster can be rejected through coal fire (risk) area delineation. A clipping process with the delineated risk area (one time with a 500m buffer, one time with a 1000m buffer), and how large the resulting thermally anomalous area is [23] conducted. Any anomalies outside these buffer zones are regarded as false alarms. Unfortunately, it is not that simple to delineate an earthquake risk area and many other criteria needs to be set to overcome this difficulty.

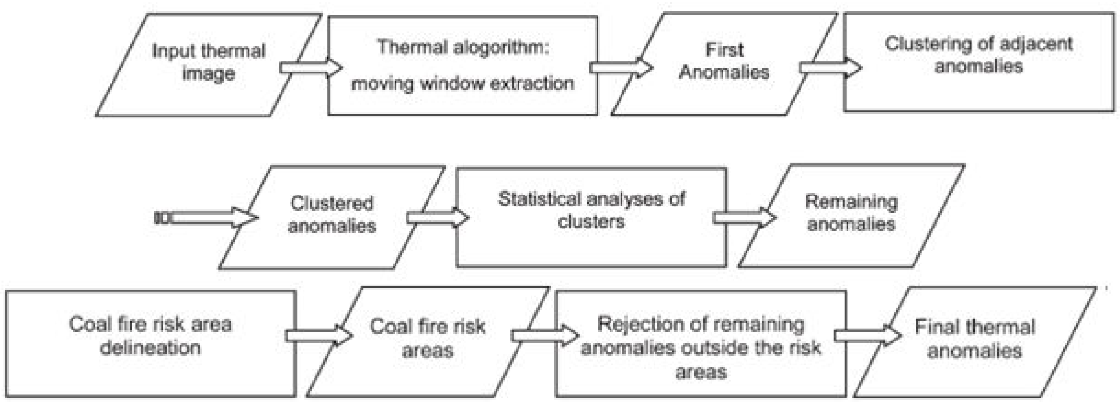

Figure 2-9: Sequence of the algorithm for automated thermal anomaly extraction [23].

A similar approach will be attempted for the detection of earthquake related anomalies. However, several alterations need to be made to this approach. Likewise, the criteria set for coal fire detection will be different to that of an earthquake.

3. Methodology

This chapter describes the methods employed to achieve the objectives of the study. The results of the methodology are explained in the following chapter.

3.1. Framework of Methodology

The following is an overview of the steps taken to obtain results which are seen in the following chapter

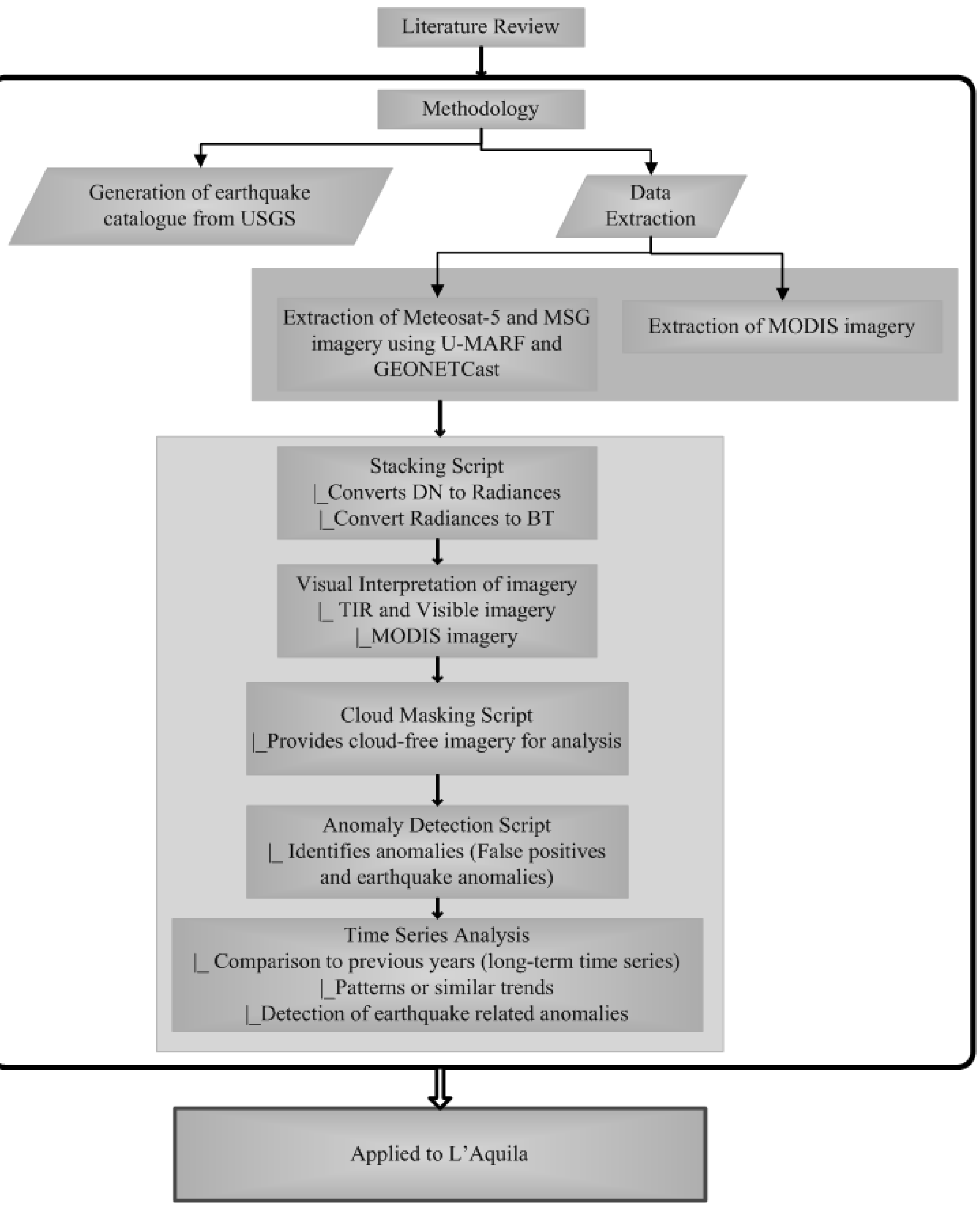

3.2. Data Acquisition

The study attempted to use Meteosat-5 and MSG imagery to assess anomalous behaviour for two earthquakes, namely Bam and L'Aquila. The earthquake catalogue consisted of basic information regarding the date, time, location of epicentre and magnitude of these earthquakes which were extracted from USGS. The images for these phenomena were obtained from different data archives called U-MARF [10] which can be accessed from the following link, http://archive.eumetsat.org/umarf/ and GEONETCast [11] which is an extension for Ilwis 3.6 user interface.

3.2.1. Meteosat-5 Satellite Data for the Bam region

Meteosat-5 imagery was used. This satellite was launched on March 02, 1991 which provides timely imagery for the designated period of acquisition. It is located over 63°E longitude in support of the Indian Ocean Data Coverage and provides good coverage of Iran as seen in Figure 2-2.

Meteosat-5 has a single channel in the TIR window which is centred at 11.5µm wavelength band. Due to the fact that the Meteosat visible channel only gives information at daytime and due to the fact that the Meteosat water vapour channel is not situated in the thermal infrared window and insofar not able to provide information of the lower atmosphere, this study uses the Meteosat channel in the thermal infrared window. In respect to diurnal cycles, this enables a more uniform detection quality without discontinuities between day and night [40].

Six years of Meteosat-5 TIR observations have been acquired for Bam, Iran using the U-MARF facility. The six years of imagery ranges from January 01, 1999 to December 31, 2004 for a time interval of every 30 minutes which takes into account the earthquake occurring on December 26, 2003.

U-MARF provides EUMETSAT with the capability of offering users access to the Meteosat archive, comprising historical data from all Meteosat satellites [10]. It provides a comprehensive range of products to the user community to facilitate access to, and exploitation of, the > 20 year archive of data for which it is responsible. It is important to know what product and what sensor from Meteosat should be used in data retrieval [10].

Level 1.5 images is rectified in order to remove the effects of spacecraft induced perturbations due to orbit and attitude of the spacecraft; instrument induced perturbations (for instance, detector mis-registration); and correction of any radiometric or geometric instrument anomalies [9, 14]. This product is not corrected for atmospheric absorption.

Image data is thought to be of most important, but the metadata (or "ancillary" data) describing the data gives details of the instrument that collected the image, including calibration information, and also include information date and time that the image was collected, the geographical location of the image corners and centre, the size of the image in terms of rows, columns and bands and other information such as solar azimuth and zenith angles [30]. The U-MARF facility has several output formats. However, still this posed a tremendous problem since the output file is a TIFF. This format only provides image data.

A two degree geographical coordinate in every direction from the epicentre was used as the coordinates for the area of interest. This facility uses the line/pixel as well as lat/long coordinates for the selection of the area. The coordinates used range from 27.000°N to 31.000°N latitude and 56.325°E to 60.325°E longitude with a corresponding line/pixel (Upper Left: 1957, 1388 while Lower Right: 1828, 1316). On retrieving these large datasets, storage capacity within the computer and transferring of such large files to an external storage device was very time consuming.

Visible imagery was also obtained from Meteosat-5 Level 1.5 for a five week period (i.e. one month prior to the earthquake and one week after) only for the year of the earthquake occurrence, with the same area of interest.

3.2.2. MSG Satellite Data for the L'Aquila region

Four years of MSG2 (i.e. Meteosat-9) TIR observations have been acquired for L'Aquila, Italy using the GEONETCast Toolbox [11]. The thermal band selected for this sensor was the 10.8µm channel. Of the two TIR window channels in MSG2, the 10.8 µm wavelength was selected rather than 12.0µm to conform to similar specifications as the 11.5µm single channel in Meteosat-5.

The four years of imagery ranges from December 21, 2005 (the launch date) to December 31, 2009 for a time interval of every 15 minutes. Even though this satellite was recording imagery before, reliable imagery was assumed to be provided only on the said date. The earthquake occurred on April 06, 2009.

GEONETCast is a low-cost global environmental information delivery system that transmits satellite and in-situ data, products and services from GEOSS to users through communication satellites using a multi-cast, access-controlled broadband capability. It provides near-global coverage for data dissemination and will contribute to revolutionising the way policy- and decision-makers will be making decisions on the basis of the best available scientific data [11].

GEONETCast Toolbox offers flexibility to choose multiple channels in one file or multiple times in one file. The former allows the timestamp to be recorded on each image whilst the latter this is not the case. Also, original digital count (that is DN) results in 16 bits image of which only 10 bits are used whereas Reflectance/Temperature (K) converts these raw DN to reflectance for the visual band and temperature for all other bands at sensor (this results in 32 bits floating point numbers). This facility also has several output formats. The Reflectance/Temperature (K) were selected and the outputs chosen were in a GeoTIFF format and contained a lat/long projection. This output produces a brightness temperature of surface and cloud top temperatures. Likewise, a two degree geographical coordinate in every direction from the epicentre was used as the coordinates for the area of interest. The coordinates used range from 40.423°N to 44.423°N latitude and 11.395°E to 15.395°E longitude.

Visible imagery was also obtained from MSG2 VIS 0.06µm channel for a five week period (i.e. one month prior to the earthquake and one week after) only for the year of the earthquake occurrence, with the same area of interest.

3.2.3. MODIS Satellite Data

MODIS imagery was obtained from an ftp website which was provided by the data administrator of ITC. The following is the link provided ftp://e4ftl01u.ecs.nasa.gov/MOLT/ . USGS GloVis [56] which is a quick and easy online search and order tool for selected and aerial data was used alongside with this link to search for the tile coordinates corresponding to the study areas. However, raw MODIS imagery can also be obtained through WIST which was used to determine the UTC times for the overpass of the sensor at the study area. This was neither provided by the link nor the GloVis site. WIST [32] is a client for searching and ordering Earth science data from various NASA and affiliated centres.

MODIS has a higher spatial resolution as compared to the Meteosat series of satellites. Visible images were acquired from MODIS Aqua for the five week period as was done for the visible imagery for both earthquake events to assess the anomalous patterns appearing in the time series. This satellite has a local equatorial crossing time at approximately 1:30 pm UTC in an ascending node with a sun-synchronous, near polar, circular orbit whereas MODIS Terra crosses at approximately 10:30 am in a descending node [34]. MODIS Terra imagery was not available for several days for Bam, therefore MODIS Aqua imagery was obtained.

3.3. Data Processing

On retrieving these large datasets, storage capacity within the computer and transferring of such large files to an external storage device was very time consuming. Image processing software such as ENVI encountered software memory management issues, owing to the vast amount of data. IDL within ENVI also could not handle the datasets. Programming and script writing within Python 2.6 and Perl was essential for data processing.

3.3.1. Stacking

A python script was created and ran on an Ubuntu Linux system in order to stack the thermal images as well as the visible images; Appendix E. Imagery was still missing within the datasets which can affect the analysis of time series. These missing images were not obtained from these facilities probably owing to sensor malfunctions at that time. Furthermore, from these two facilities, different file formats were obtained one as a GeoTIFF and one as a TIFF containing no spatial information. These two formats are of different data types and each type was processed and evaluated differently within the python script to produce a stack or a data cube of equally spaced time imagery. Another python script was created to view the values of one pixel within the datacube as seen in Appendix E.

3.3.2. Conversion from Digital Counts to Radiances to Brightness temperatures

After stacking the imagery, only the Meteosat-5 data for Bam needs to be converted into temperature values. The MSG2 imagery for L'Aquila was already calibrated and provided brightness temperature values.

3.3.2.1. Calibration for Meteosat-5

Image calibration converts Level1.5 raw image counts to geophysical parameters. A raw image does not have any scientific or quantitative meaning value per se if not calibrated, since the calibration function describes the relationship between the digital count and the actual geophysical value of the object seen. Scientists and any other persons working with satellite images are usually dealing with calibrated images. Further, when dealing with time-series of images, comparisons are made between images acquired at very different instants. These images should be well-calibrated with respect to each other, in order to ensure that any variation in time is due to change in the signal coming from the observed target, and not from a change in calibration of the observing system [25].

For quantitative exploitation, Meteosat-5 TIR data have to be calibrated in BT and cloud-screened. The calibration of the available raw data was performed using the calibration coefficients that were online obtainable from EUMETSAT website for Meteosat-5 (IODC Service) [8] and used to convert to radiances with the formula[18]: $R = \alpha(C_{nt} - C_o)$ .....Equation (5)

Where R= Radiance,

α= Calibration Coefficient (W/m2/sr/count)

C_{nt} = Digital Meteosat Count,

C_o=Space Count (radiometric offset of the instrument).

The following calculation of the brightness temperature images from the calibrated radiance images was done by using the inverse Planck radiance formula in consideration of the different sensor response functions. For the derivation of BTs from Meteosat-5 radiances, the following regression equation is used: $R(T) = \exp\ (A+B/T)$....Equation (6)

Where T= temperature (°K),

A= 6.7348,

B= -1272.2 (°K)

The equation fits the relationship between BTs and radiances with and root mean square error of less than 0.2°K in the range between 200°K and 330°K [18].

A python script was written to automate this process, see Appendix E. A small python program called PyENVI was created and needed to run on the Linux operating system.

3.3.3. Cloud Masking

Good cloud detection is extremely important since clouds obscure the surface view in all solar and thermal channels. Surface-related products, such as SST and LST, vegetation cover, snow cover, and wildfire detection, can only be inferred for pixels where the surface is not obscured by clouds [21]. Cloud cover usually denies the generation of LST time series over large areas from TIR data sensed by satellites.

Depending on sensor properties, clouds can especially be discriminated from cloud-free regions due to their spectral features (e.g. clouds are often white and bright), spatial features (e.g. clouds often increase the spatial variance) or characteristics in time series (e.g. clouds can introduce discontinuities in radiance or brightness temperature time series) [40]. An efficient cloud mask is needed to remove clouds from the data.

3.3.3.1. Unsuccessful Attempts for Cloud Masking

- Using a Cloud Sky Product from U-MARF called *Clear Sky Radiance*

This product provides mean brightness temperatures and radiances for cloud-free conditions. It is based on histogram analysis schemes [12]. However, pixels of this product are of a resolution of 80x80 km^2 at sub-satellite point, which suggests that the information of an individual pixel is not retained. It is too coarse for time series analysis. This product is disseminated hourly in a BUFR format. This format is the World Meteorological Organization (WMO) standard binary code for the representation and exchange of meteorological data. The BUFR representation is not suitable for data visualization without computer interpretation [50]. In other words, a detailed description is contained in lookup tables which need to be decoded to get the desired parameters out.

Furthermore, observing the data of this product, BT values of 236K were regarded to be cloud-free temperatures whilst in the Meteosat-5 TIR data these values appeared to be that of a cloud.

- Using HANTS Algorithm

Harmonic Analysis of Time Series (HANTS) [33] calculates a Fourier series which models a time series of pixel-wise observations. It simultaneously identifies outliers within the time series. When an outlier is found, HANTS replaces these values with values from the Fourier series. In HANTS, options of a negative outlier or a positive outlier can be removed. In my case, negative outliers represent clouds and these are the values needed to be removed. To help identify errors, user can specify thresholds. It uses a curve fitting which is applied iteratively. Any value falling under this curve will be removed and a new time series cure is plotted. Once again, values that fall under the curve will be removed. This is repeated until a smooth curve is formulated [33]. For the use of HANTS, certain requirements are needed as seen in Table 3-1.

	Requirements of HANTS
1	Input images are in a so-called binary format with no header information included
2	Images must be in an 8 or 16 bits/integer data type
3	Maximum of 1200 images can be processed
4	There must be no missing mages within the time series
5	Processing of time series in HANTS is executed on a single-interleaves image file (BIL).

Table 3-1: Requirements for HANTS algorithm.

Cloud free images are the outputs from HANTS as seen in Figure 3-1. The steps taken to obtain cloud free images for the Bam dataset, from the HANTS algorithm is found in Appendix F. However, the time series profiles corresponding to these images cannot be used. When observing these profiles, it was found that for a certain period (365 days), there was a pattern repeating as seen in Figure 3-2.

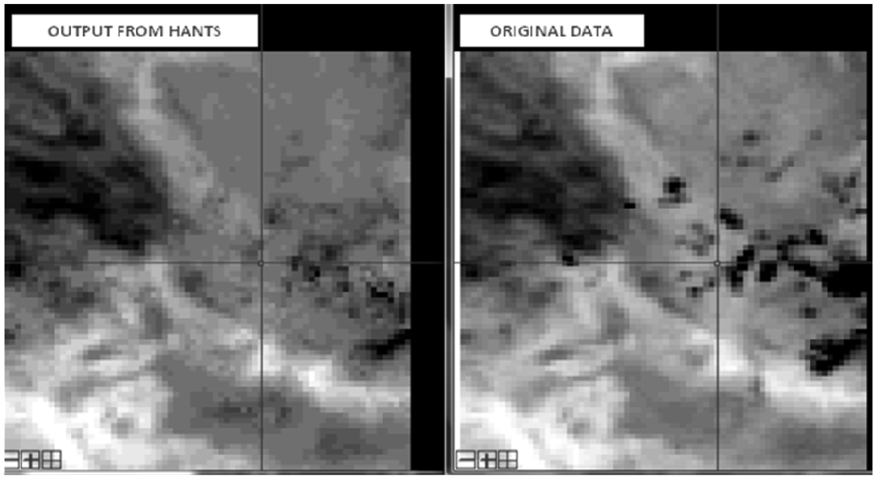

Figure 3-1: Comparison of the original cloud-contaminated image to the cloud-free output image from HANTS.

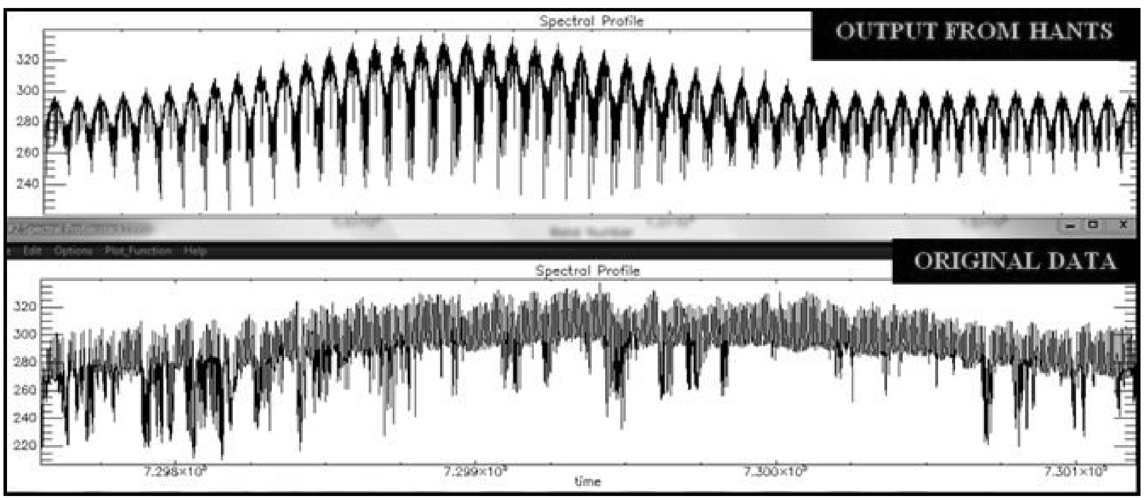

Figure 3-2: Comparison of the time series profiles (per pixel) of an original image to that of a HANTS cloud-free image.

3.3.3.2. Cloud Masking Method Chosen

- Thresholding within TIR scenes

Several cloud masking algorithms were created by other researchers and described by Masika (2007) [29]. Reuter et al (2009) stated that these techniques can be divided by (simple) radiance threshold methods, spatial variance methods, temporal variance methods and methods using an independent dataset to estimate clear sky radiances [40]. These algorithms use multispectral thresholding techniques, histogram-based scene analysis with multiple bands [29]. This suggests that data for more than one wavelength band should be available. Reuter (2009) developed a cloud detection algorithm for a single band, however this method requires additional datasets such as forecast data and a radiative transfer model to predict clear sky temperatures [40]. As mentioned earlier, only one band was acquired from the data archives. Therefore, a simple cloud masking algorithm based on scenes analysis will be developed for the study areas.

The developed cloud masking algorithm should take into account the extreme conditions as well as natural temperature variations in the study area. Extreme temperatures are derived from historical data concerning temperatures in Bam and were acquired from the Bam Meteorological Organization which states that the lowest temperature recorded was -9 °C (264°K) and temperatures between 38-44 °C (311-317°K) was said to be common for summer [1]. From exploring the data, temperatures of 260°K were recorded in December for a clear sky period. The lowest value that will be assigned as cloud-free is 260°K. This is a static threshold, a hard value in the algorithm: all temperatures below are masked as containing clouds. A dynamic threshold was also used, depending on the natural variation in a scene. The natural variation is estimated from the acquired data based on histogram analysis of differing forms (i.e. clear-sky hot summer days versus clear-sky cold winter nights). This natural variation is taken into consideration because a relatively large area is chosen (73x80pixels ~ 329x360km) and climatological variations and weather patterns can influence the thresholds to be chosen. The observed variation within an image ranged between ~15°K to ~25°K so 20°K, which is the average was selected. This dynamic range is subtracted from the maximum observed temperature in the image. However, positive outliers could possibly influence the threshold for clouds (lift it to undesired high values resulting in masking of non-cloud covered pixels). To reduce the effect of possible outliers appearing in the dataset, for calculations only 95% of the maximum observed temperatures were used. So the dynamic cut-off value for the removal of clouds was to set a temperature threshold, where every temperature of that value and lower in a scene would be removed. This cut-off value is calculated using the following formula:

*Cut-off = (0.95*Maximum temperature) – Natural Variation in the study area.*

If temperatures are < = 260°K, these values are always removed as clouds. Temperatures above this hard, static threshold are matched against the dynamic threshold. If the observed temperature is below the dynamic threshold, the pixel is masked as cloud. Computational aspects have to be considered in algorithm design because of the large number of scenes each day, the process is therefore automated by a PERL script as seen in Appendix E. The outputs of the cloud masking algorithm were compared to a cloud-masked scene created manually within ENVI to confirm the accuracy of the algorithm.

3.3.4. Creation of Algorithm for Anomaly Detection

3.3.4.1. Definition of anomaly

Researchers have often defined what an anomaly or anomalous behaviour can be with regard to their purpose, often with respect to what is considered a "normal condition". It is important to understand and observe patterns in the data, as this makes it easier to differentiate normal and abnormal conditions.

The underlying assumption is that the normal behaviour of a time-series follows a predefined pattern. A subsequence within the long sequence which does not conform to this pattern is regarded as an anomaly. However, any deviation from the normal pattern is an anomaly so additional criteria are used to distinguish between thermal earthquake-related anomalies and those not related to any earthquake activities (i.e. "false positives"). Any sudden, unusual temperature rise within a region as compared to the surrounding area which appears within a month of the earthquake and lasts for at least six hours can be defined as a "thermal earthquake-related anomaly". Figure 3-3 describes the framework used to assess anomalies and their relation to earthquake events.

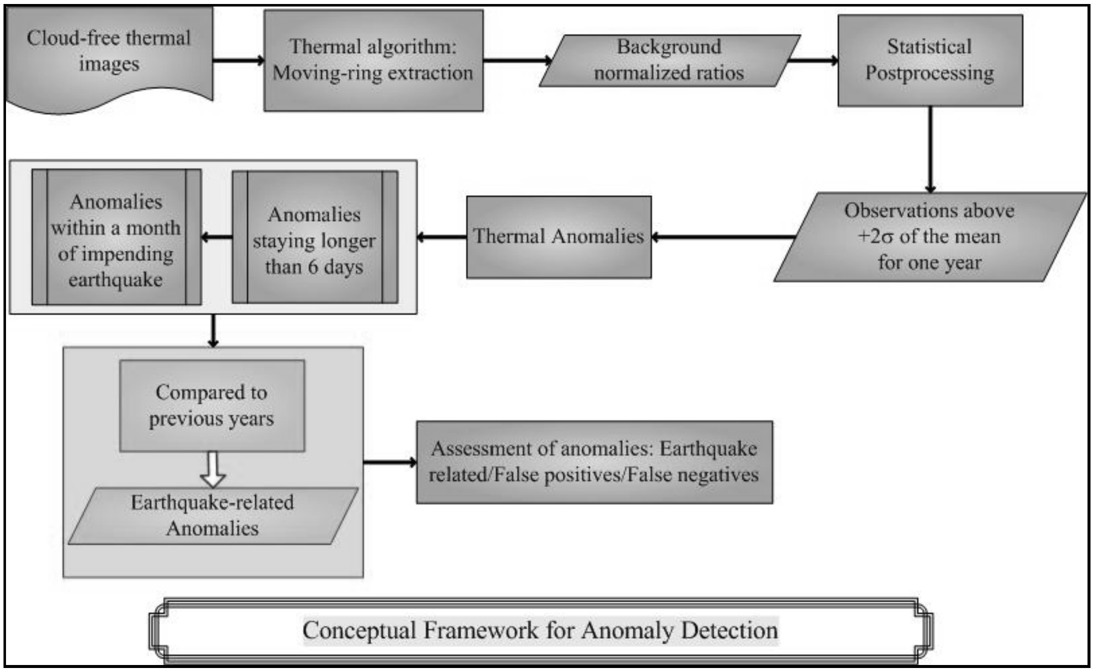

Figure 3-3: Conceptual Framework for earthquake-related anomalies.

3.3.4.2. Method for normalizing pixel values for diurnal and seasonal variations

Earthquake related temperature increases are weak anomalies. To enhance the anomaly and reduce the effect of temporal variation not related to the occurrence of earthquakes a normalization approach is sought. A moving ring approach has been chosen. One of the main reasons for selecting a moving ring approach as shown in Figure 3-4, is to avoid anomalous temperature values from neighbouring pixels that may influence a normal background temperature. It is assumed that if the central pixel is an anomalous pixel, the adjacent pixels are possibly influenced by the anomaly and have similar temperatures. A 10 pixel buffer around the central pixel will be excluded from background temperature determination. This 10 pixel radius (~ 50 km) was selected to remove any diurnal and annual patterns which may contribute to meteorological and weather patterns occurring between these locations.

The ratio between the anomalous pixel and the normalized background temperature is calculated. In this way, strongly contrary to an overall threshold, the thermal anomalies extracted represent variation of the pixel with respect to the surrounding area. This means that pixels of very different temperature and within a different temperature background can be declared thermally anomalous [23]. An automatic algorithm was written in PERL can be seen in Appendix E. It is applied over the time series stack of cloud-free images.

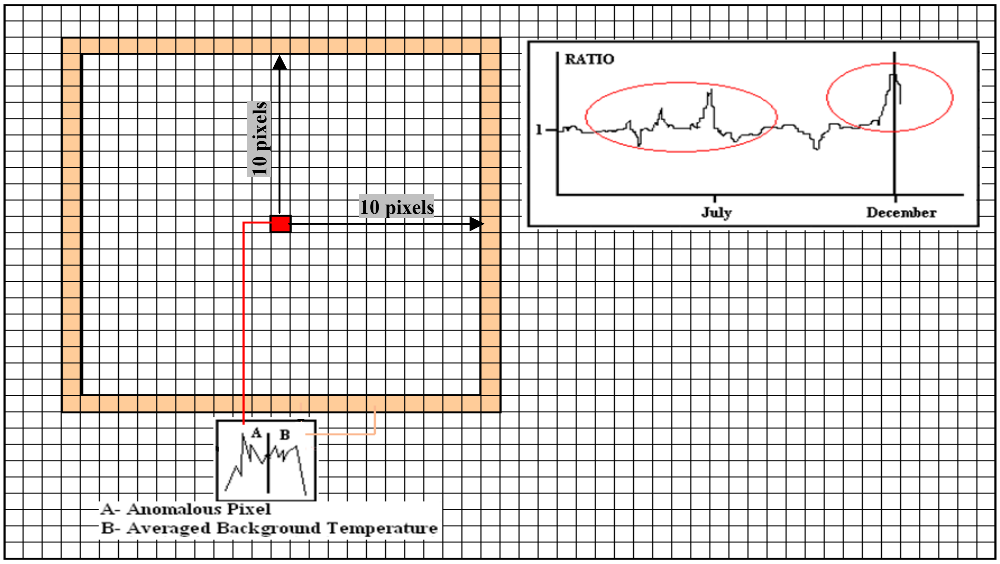

Figure 3-4: Moving ring concept applied over the entire stack of cloud-free images.

Figure 3-4 illustrates the normalization process when using a moving-ring approach over an image. A 10 pixel radius from the central pixel is used as the ring to obtain an averaged background temperature, *B*. The temperature of the central pixel is regarded as the anomalous pixel, *A*. A ratio is then calculated between *A* and *B* producing a time series plot which is used for anomaly detection.

3.3.4.3. Identifying Earthquake-related Anomaly

As mentioned in Section 2.1, anomalies were mainly positive with the exception of negative anomalies in Japan and China. Even though this paper identified negative anomalies, there was no valid or credible explanation to describe what mechanism caused a negative anomaly within their study. Based on the findings of other researchers, and only positive anomalies will be addressed throughout this research.

Statistical post-processing on the background normalized ratios was performed for a time series stack of images, per year. Observations above standard deviations of $\pm1\sigma$, $\pm2\sigma$, and $\pm3\sigma$ from the mean ratio of one year were calculated. The $\pm2\sigma$ of the mean was used as 95% of the observations are assumed normal and any anomalous values that fall outside are significant values not fitting, with 95% confidence, the average value for that pixel. All observations in the time series that appeared above a $+2\sigma$ of the mean were flagged as anomalies. The anomalies that have a duration of a week within the time series are counted. For an earthquake-related anomaly, the flagged anomalies should appear within a six day period and occur within a month before the earthquake phenomena. However, the exact location of the epicentre as well as the time of the impending earthquake is unknown.

To ensure that the anomalies detected are indeed related to an earthquake event, previous years (that followed the same method as aforementioned) were examined. This is important to assess whether and how often the anomalies caused are earthquake-related, false positives and/or false negatives.

4. Data Analysis and Results

Analysis of time series in tectonically active regions for the detection of earthquake anomalies is one of the objectives of this study. This chapter analyses two study areas with different conditions: large versus moderate magnitude earthquakes, climatic conditions, and population density. Moreover, this chapter includes the attempts made to differentiate earthquake-related anomalies from false positives and to quantify these anomalies including false negatives.[62]

4.1. Results from Anomaly Detection for Bam

Each step in the conceptual framework of the developed methodology produced its own output which will be assessed in a sequential manner. Figure 4-1 (a) shows a raw unprocessed Meteosat-5 TIR image obtained from the U-MARF data archive. These images are converted into brightness temperatures (BTs) and used as inputs for the cloud masking algorithm. Figure 4-1 (b) provides an output of the same scene after the algorithm was applied. As compared to the raw image of the same scene, this result proved efficient as cloud cover was removed. In the raw unprocessed image, the yellow feature represents thick clouds, whereas the pink feature represents thin clouds and cloud shadow. In the cloud free image, the green area represents clouds that were masked.

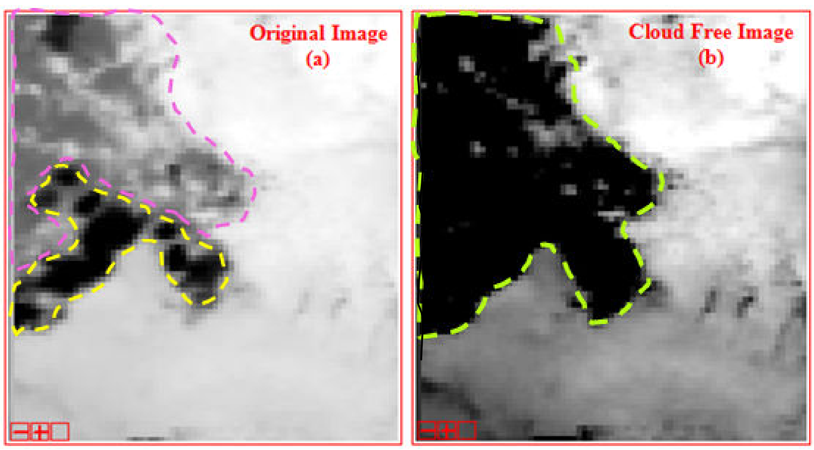

Figure 4-1: A comparison between the same scene recorded in July 20th 2003 for (a) which show a raw, unprocessed Meteosat-5 TIR image; and (b) which shows the output from the cloud detection algorithm for the same scene.

Time series of Meteosat-5 cloud-free images were then created per pixel. In the time series profile, there were regions with large dropouts. These dropouts correspond to the time when clouds appeared, and were masked out by the cloud detection algorithm. Figure 4-2 represents a time series profile for Pixel 35,44 in the year 2003. This pixel is in close proximity to the epicentre of the earthquake. Even though the epicentre was analysed, this pixel was selected based on the theory that the epicentre is not the region where the most stress is emanating, the fault trace is the point where the maximum stress is being released and the highest temperature is recorded, Appendix G. The time series profile showed a normal trend whereby warmer temperatures occur in the summer period whereas colder temperatures appear in winter seasons. However, this is another reason why a long time series is needed to assess fully if the trend appears to be normal in other years or deviated.

The normalization algorithm generates background normalized temperature ratios for a certain pixel as seen in (Figure 4-3). From observing the output of this algorithm in its pure form, not much can be said about the anomaly and its relation to the impending earthquake event thus further analysis is required. In order to detect anomalies, the sample mean of the ratios was used over the entire series to assess the normal conditions of Pixel 35,44. In this case, the average ratio for one year was calculated as 0.977. In science, researchers commonly report the standard deviation of experimental data, and only the effects that fall far outside the range of standard deviation are considered statistically significant- normal random error /variation on the measurements is in this way distinguished from causal variation. Standard deviations from the calculated mean of $\pm1\sigma$, $\pm2\sigma$ and $\pm3\sigma$ were observed. If the data distribution is approximately normal then about 68% of the values are within $\pm1\sigma$ of the mean of the temperature ratios (mathematically, $\mu\pm\sigma$, where μ is the arithmetic mean), about 95% are within 2σ ($\mu\pm2\sigma$), and about 99.7% lie within 3σ ($\mu\pm3\sigma$) [62].

As one can see, there are several ratios occurring that are above a $\pm1\sigma$ standard deviation as indicated by the orange lines in Figure 4-3. However, normalized background temperature ratios above a $\pm2\sigma$ (green lines) and $\pm3\sigma$ (pink lines) standard deviation were taken as extreme conditions within the time series. A $\pm1\sigma$ deviation introduces noise within the data and alters the extreme anomalous values from being highlighted giving a false interpretation. Likewise the ratios appearing above a $+3\sigma$ deviation, are for very extreme anomalies in which only a 0.3% chance of the observations to be statistically significant (anomalous). As mentioned in Section 3.3.4.3, ratios appearing above a $+2\sigma$ deviation are flagged as anomalies.

The anomalies lasting within a seven day time window were counted. This fits one criterion for an earthquake-related anomaly. The output of this count provides the percentage of images being significantly different within that week in the time series, for a certain pixel. Figure 4-4 shows the counts of anomalous images for pixel 35,44 for each of the three calculated standard deviations indicating the appearance and duration of the anomaly for the year 2003. The number of anomalies counted within a week was most prevalent for a $+1\sigma$. However, for a $+1\sigma$, 32% of the observations are regarded statistically significant thus increasing the number of anomalies within the counts. Even though $+3\sigma$ shows a smaller number of anomalies counted within a week, it is more significant to very extreme anomalies occurring in the ratios. If a 3σ deviation is used, some anomalies that may be related to an earthquake event are excluded. Further in this paper only the $+2\sigma$ deviation will be used. The counts showed that prior to the earthquake, for all standard deviations there was a distinct anomaly in December as compared to other months in the time series profile.

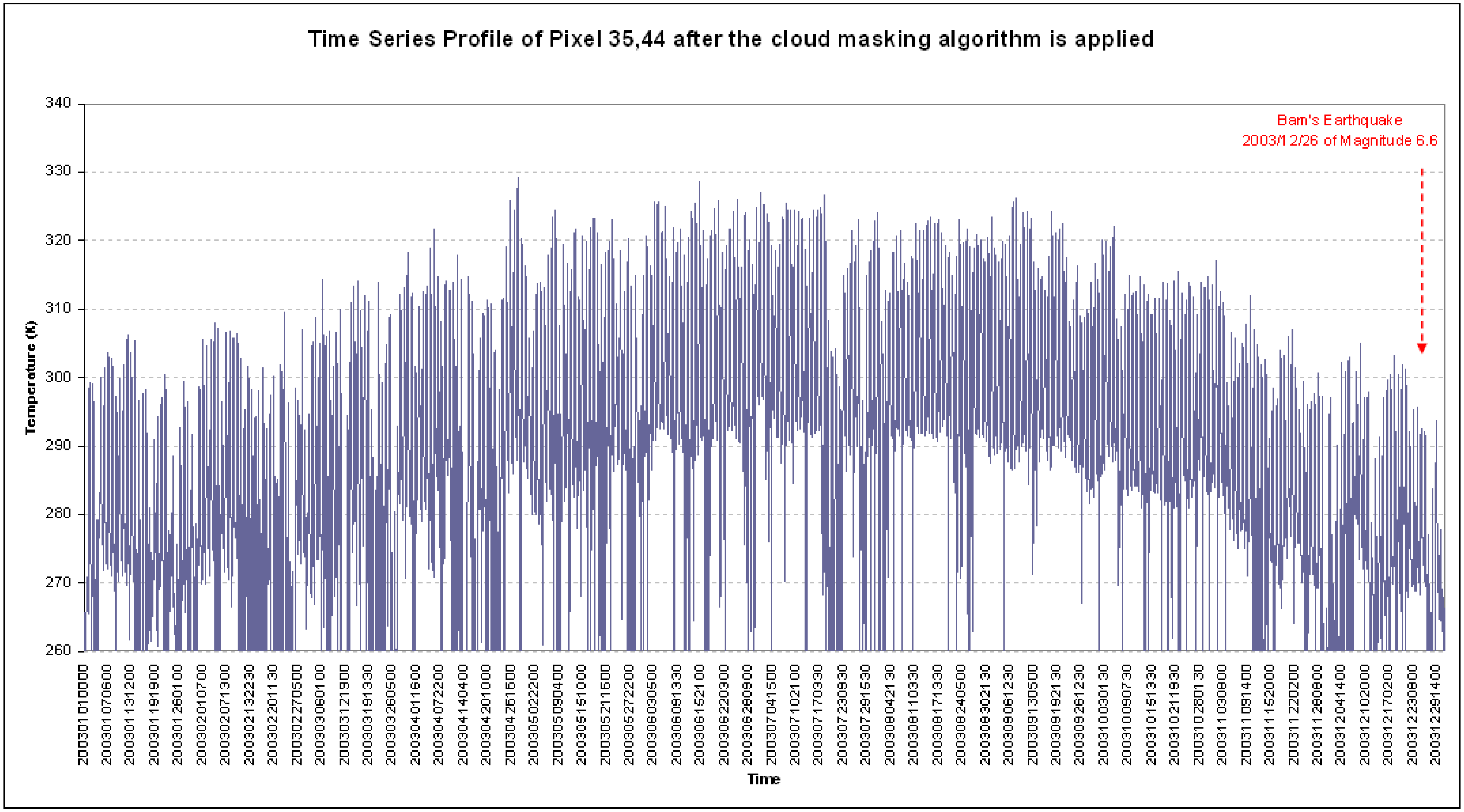

Figure 4-2: Time Series profile of Pixel 35,44 obtained as an output of the cloud masking algorithm for the year of the earthquake occurrence, 2003. All temperatures below the cutoff values will be removed as clouds. Cloud contaminated pixels are represented as dropouts within the time series.

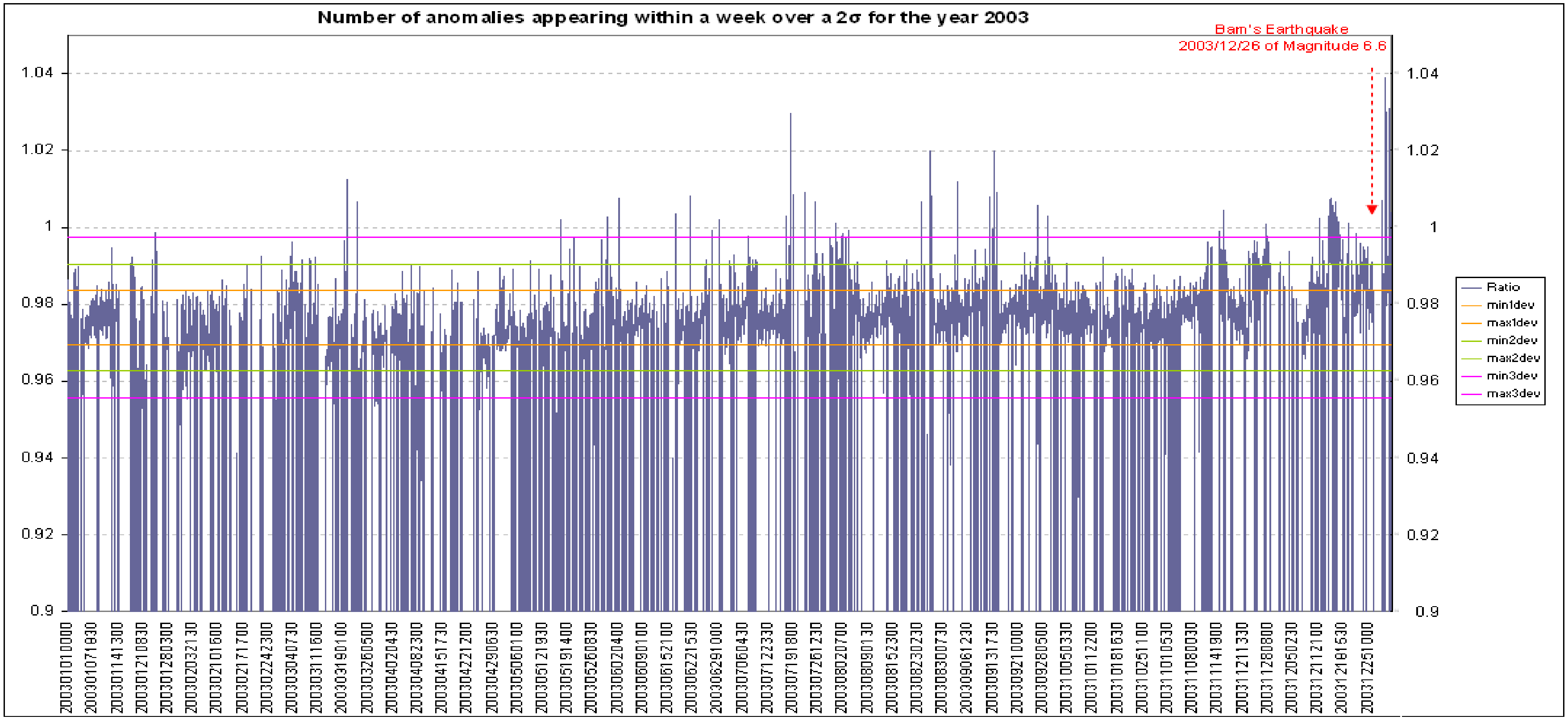

Figure 4-3: Time series profile for Pixel 35,44 obtained as an output of the normalization algorithm for the year of the earthquake occurrence, 2003. Orange lines represent a ±1σ of the average temperature ratio over an entire year, green lines represent a ±2σ of the average temperature ratio over an entire year, and pink lines represent a ±3σ of the average temperature ratio over an entire year. Temperature ratios appearing above a +2σ and +3σ standard deviations were regarded as statistically significant. Applying a +3σ deviation allows only a 0.3% chance that observations are anomalous owing to very extreme conditions. Ratios appearing above a +2σ deviation from the mean allow 5% of observations to be regarded as statistically significant and flagged as anomalies.

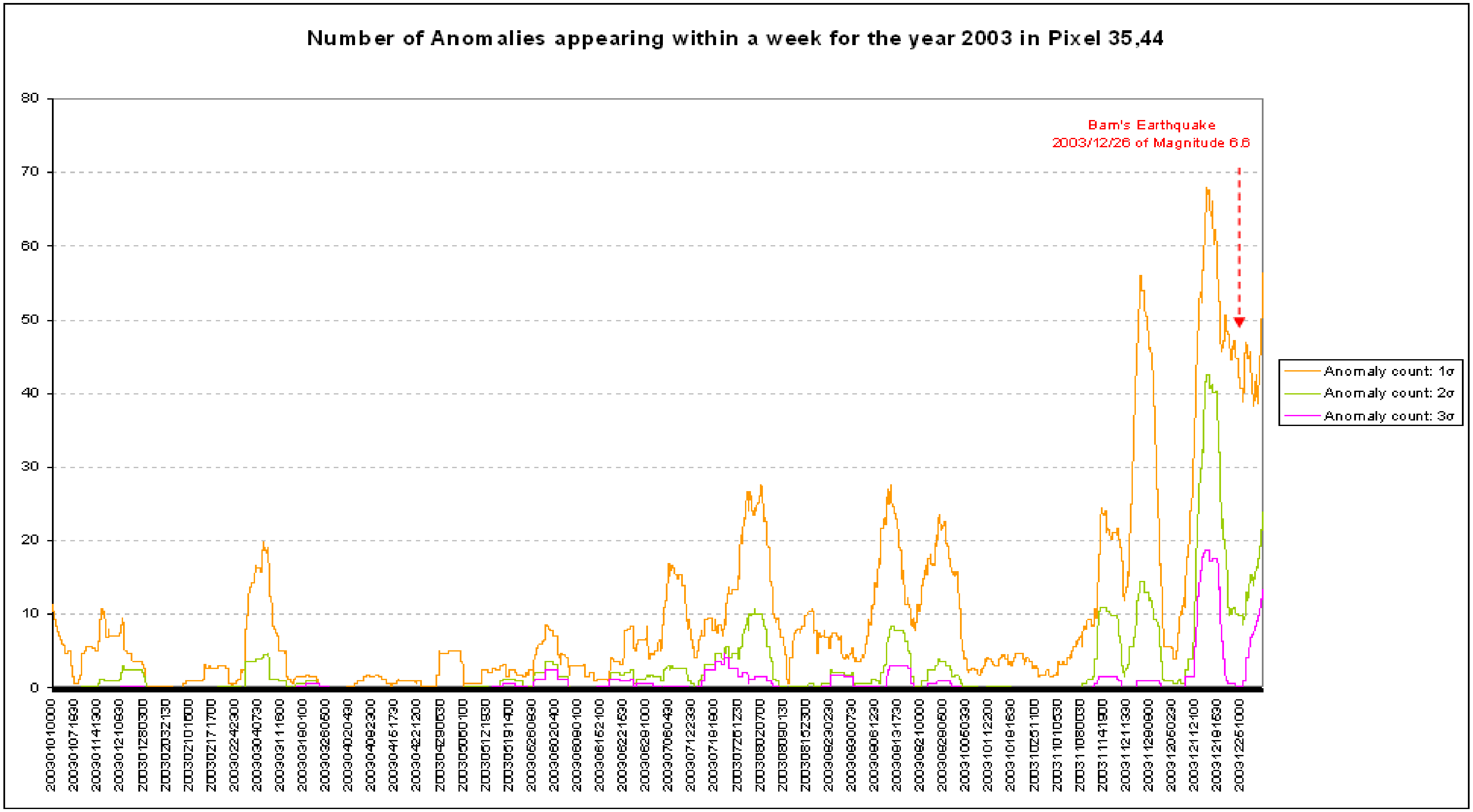

Figure 4-4: Time series profile showing the counts of anomalous images for pixel 35,44 for each of the three calculated standard deviations indicating the appearance appearance and duration of the anomaly for the year 2003. The number of anomalies counted within a week was most prevalent for a 1σ. However for a 1σ, 32% of the observations are regarded statistically significant thus increasing the number of anomalies within the counts. Even though 3σ shows a smaller number of anomalies counted within a week, it is more significant to very extreme anomalies occurring in the ratios. The counts were highest in December periods prior to the earthquake event for all degrees of standard deviations.

4.1.1. Time Series Analysis for earthquake precursory detection in Bam

Six years of data were investigated and compared to draw conclusions of the multi-temporal dynamics of the study area. These profiles whereby anomalies were counted above a +2σ deviation will be compared to several years of data to ensure that the anomaly that were claimed to be detected is indeed an earthquake-related anomaly and not a false positive within the dataset. To assist in determining false positives and false negatives in the dataset, the National Earthquake Information Centre (NEIC) disseminates information regarding the magnitude and location which is compiled in a global seismic database for earth science research. The following link provides access to the NEIC archive: http://earthquake.usgs.gov/earthquakes/eqarchives/epic/. This information for the Bam area assists in determining where false positives as well as false negatives are within the profiles, Appendix H. The NEIC earthquake catalogue provides the user with the distance and magnitudes of earthquakes occurring in a certain study area. The NEIC search results in Appendix H provide the proximity of other earthquakes in relation to the Pixel 35,44.

On observing the year of earthquake occurrence for Bam, Figure 4-6, a smaller magnitude earthquake of 5.9 was identified in the summer period on August 21, 2003. This earthquake called Kerman's earthquake was located 141km away from the Bam's earthquake epicentre. It was seen that a significant anomalous signal lasting for a week period appeared in December. Approximately 45% of the images contained anomalies. This anomaly showed a distinct peak which lasted for almost a 10 day period (2003/12/11 at 05:30 UTC to 2003/12/21 at 22:00 UTC). This significant anomalous pixel appeared during a month prior-to an earthquake and lasted for a week, which fit the criteria for an earthquake-related anomaly. However, during the year there were signs where anomalies lasting for a week were also detected. Dual peaks in November showed that only 10% of the images within the series were shown to have anomalies with duration of one week, which are insignificant and were avoided. If 10% or less of the images showed anomalous activity within a week were regarded insignificant and excluded for relating to an earthquake-related anomaly.

Central Pixel		Background Temperature		RESULT
Anomaly	No Anomaly	Anomaly	No Anomaly	
Y		Y		Not Detectable
Y			Y	Increase in Ratio (Detectable)
	Y	Y		Decrease in Ratio (Detectable
	Y		Y	False Positive within Ratio
Where Y- Yes				

Table 4-1: The effects of anomaly detection in a time series.

Table 4-1 describes the effects of how anomalies can be detected within a time series. False positives and false negatives are judged on the distance of a pixel to the epicentre as well as the magnitude of the earthquake event. A false negative can be defined as earthquakes of magnitude >= 5.0 that do not show any anomalous activity within a duration of 1 week and do not appear 1 month prior to the phenomena. A false positive is defined then as the anomalous signals that last a week and is not influenced by any earthquake. Another criteria set for false positives and false negatives within the data is the relationship between the magnitude and the fault length. For a magnitude 6.6

earthquake, the fault length is roughly 50-70 km on which the epicentre occurs. It is around this region that anomalous activity should appear, so if a signal is recorded 200km away, it is likely that it is not an earthquake-related anomaly but a false positive within the dataset. For an earthquake-related anomaly of magnitude 6.6, anomalies appearing within a 70km distance from the fault or epicentre that appear within one month of the earthquake, and the number of images appearing with a duration of 1 week that show anomalous activity of at least 15% is ideal.

In order to draw conclusions other years were compared. Figure 4-5 to Figure 4-10 shows the profiles for the six years of data. For instance, in Figure 4-8, a magnitude 5.0 event occurring on November 25th 2001, with a distance of 110km away from pixel 35,44 showed anomalies lasting for a week prior to the event. This explains 30% of the number of images in the series being anomalous. This is significant but still it is not regarded as an earthquake-related anomaly since it falls outside a 70 km range. All other anomalies appearing within the time series were insignificant and regarded as false positives.

Similarly, for Figure 4-5 there was an earthquake of the same magnitude occurring on December 8th 2004, but it is also regarded as a false positive as described for Figure 4-8. However, a false negative appeared in Figure 4-5 for the magnitude 5.2 earthquake occurring October 6th 2004 which was 30km away from the studied site. In Figure 4-7, there was a false positive also occurring in the same region in December that was relatively insignificant. In January 2002, a sudden anomalous signal appeared, this peak was also regarded as a false positive. Figure 4-9 and Figure 4-10 had false positives as the number of images within a week which are influenced by anomalies are relatively insignificant.

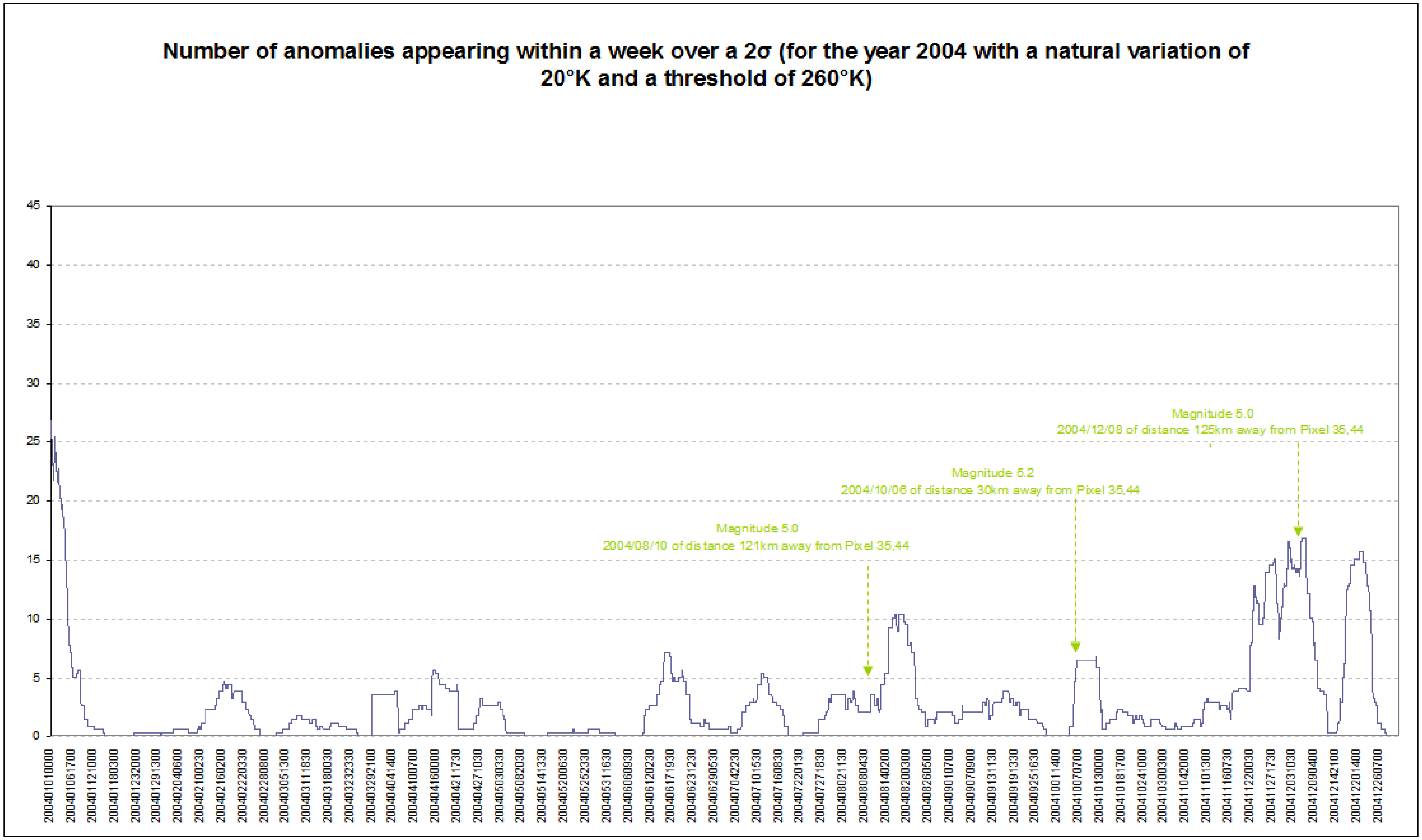

Figure 4-5: Number of anomalies appearing within a week period for Pixel 35,44 in the year 2004. A false negative was evident for the magnitude 5.2 earthquake in October 6th 2004 whilst other anomalies were caused by false positives in the profile.

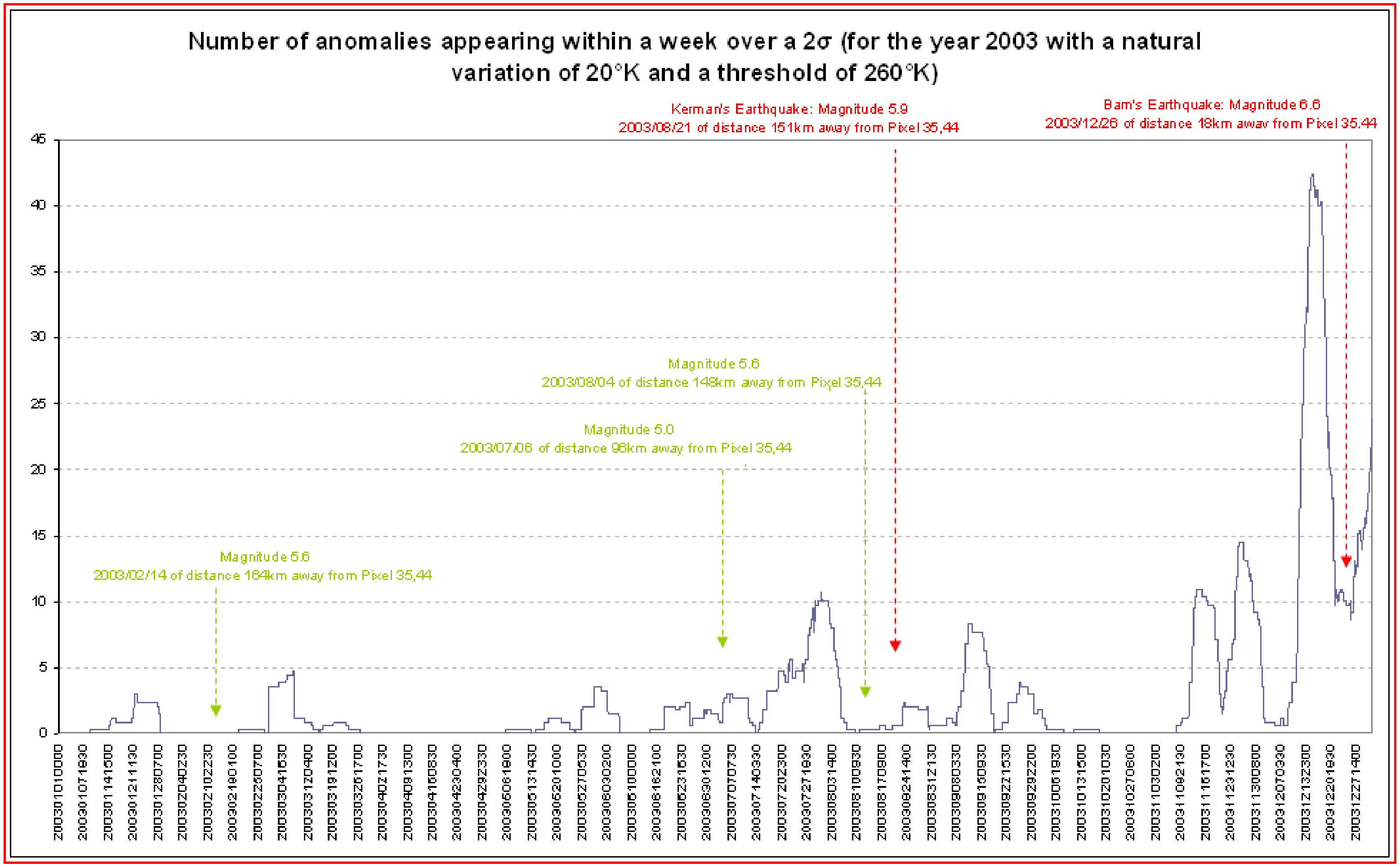

Figure 4-6: Number of anomalies appearing within a week period for Pixel 35,44 in the year 2003. A significant earthquake related anomaly appeared in December prior to Bam's earthquake. All other anomalies were regarded as false positives.

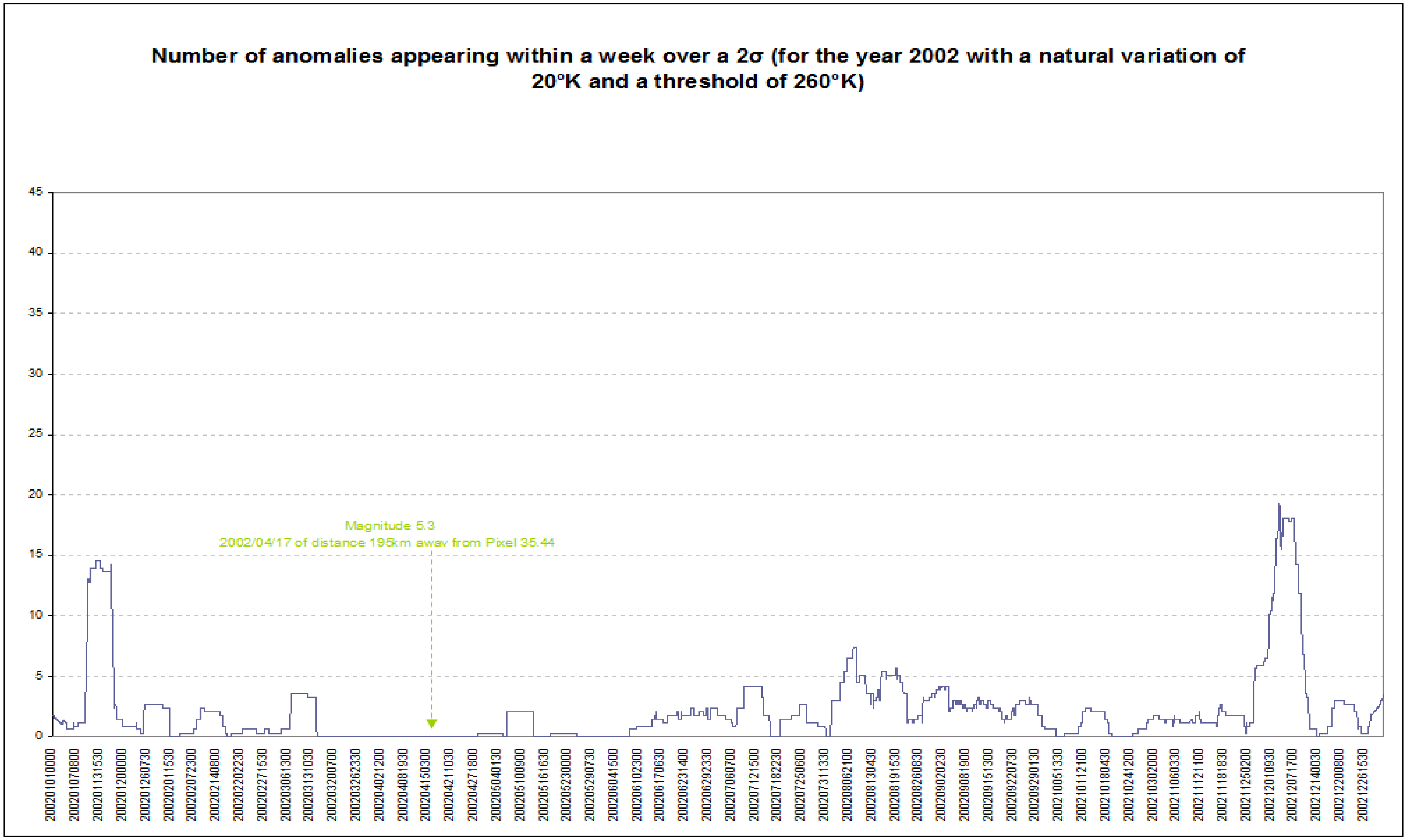

Figure 4-7: Number of anomalies appearing within a week period for Pixel 35,44 in the year 2002. There were no significant anomalous signals appearing. These small anomalous effects are false positives within the profiles.

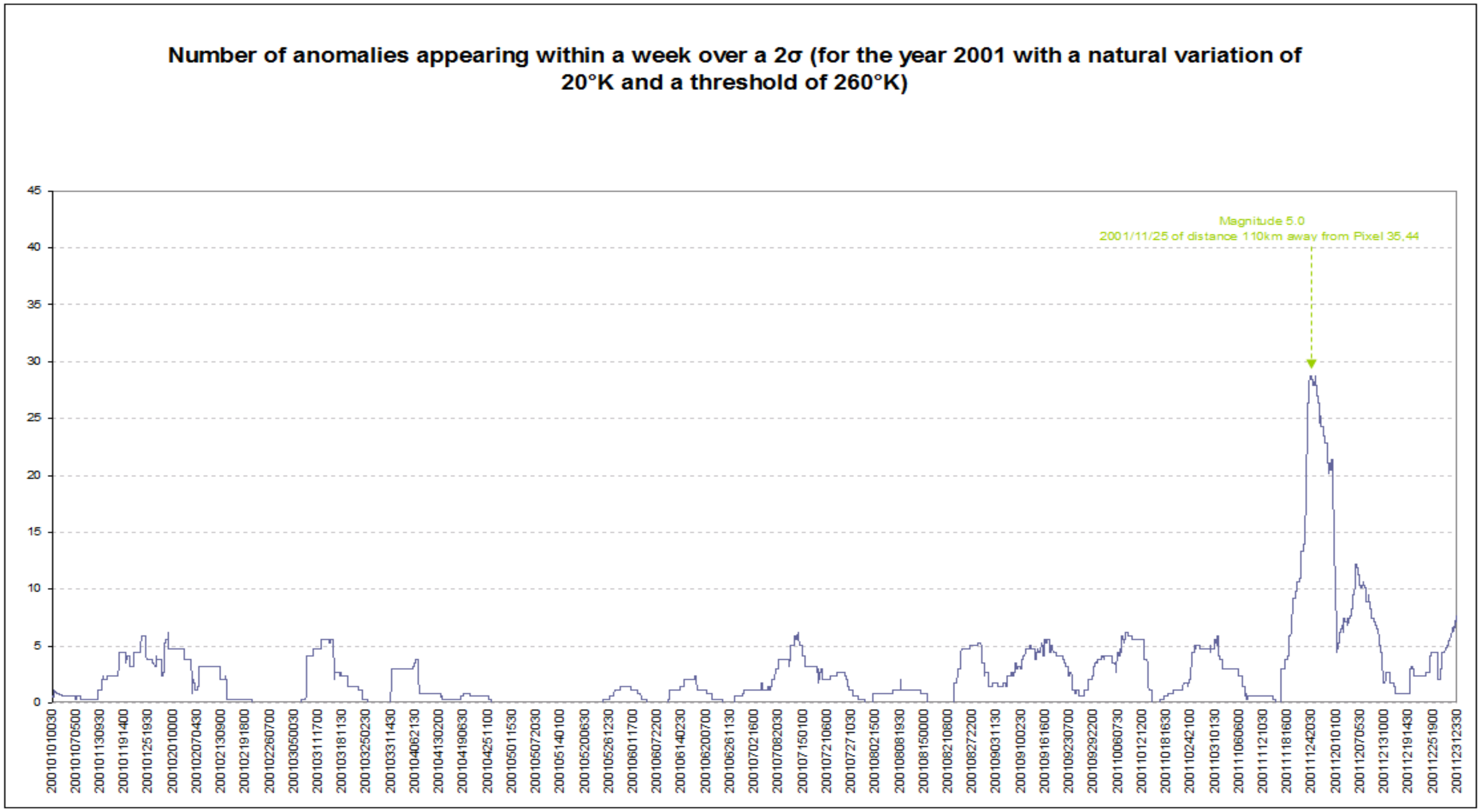

Figure 4-8: Number of anomalies appearing within a week period for Pixel 35,44 in the year 2001. Initially this peak would suggest that it is an earthquake-related anomaly as it lasts for one week, appears within a one month prior to the earthquake event and the number of images recorded within the time series is significant (roughly 30%). However, this peak is also a false positive as the detected number of anomalies is within a large spatial difference from the pixel which is being studied.

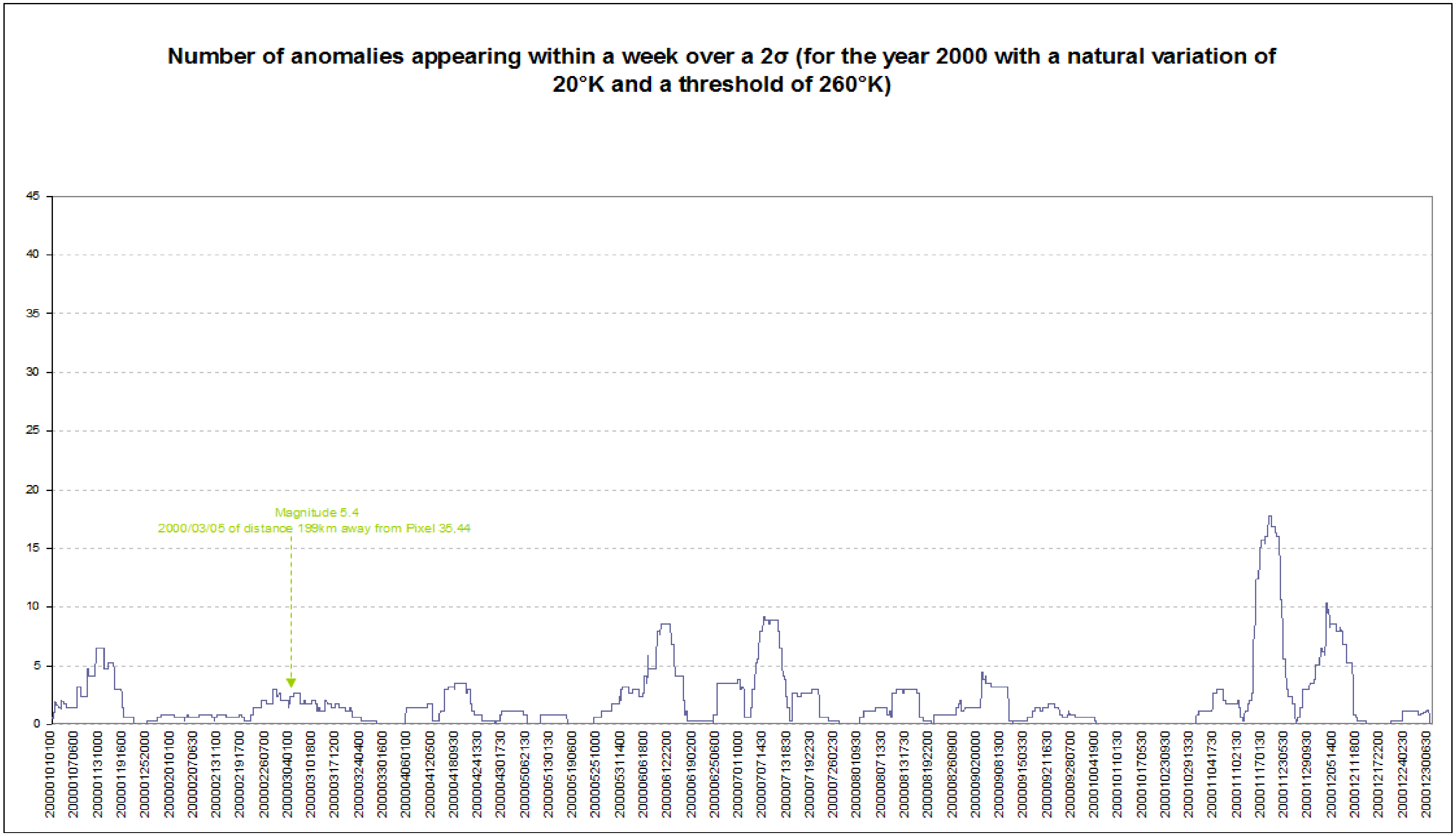

Figure 4-9: Number of anomalies appearing within a week period for Pixel 35,44 in the year 2000. Insignificant false positives appear within the profile except for the peak in November.

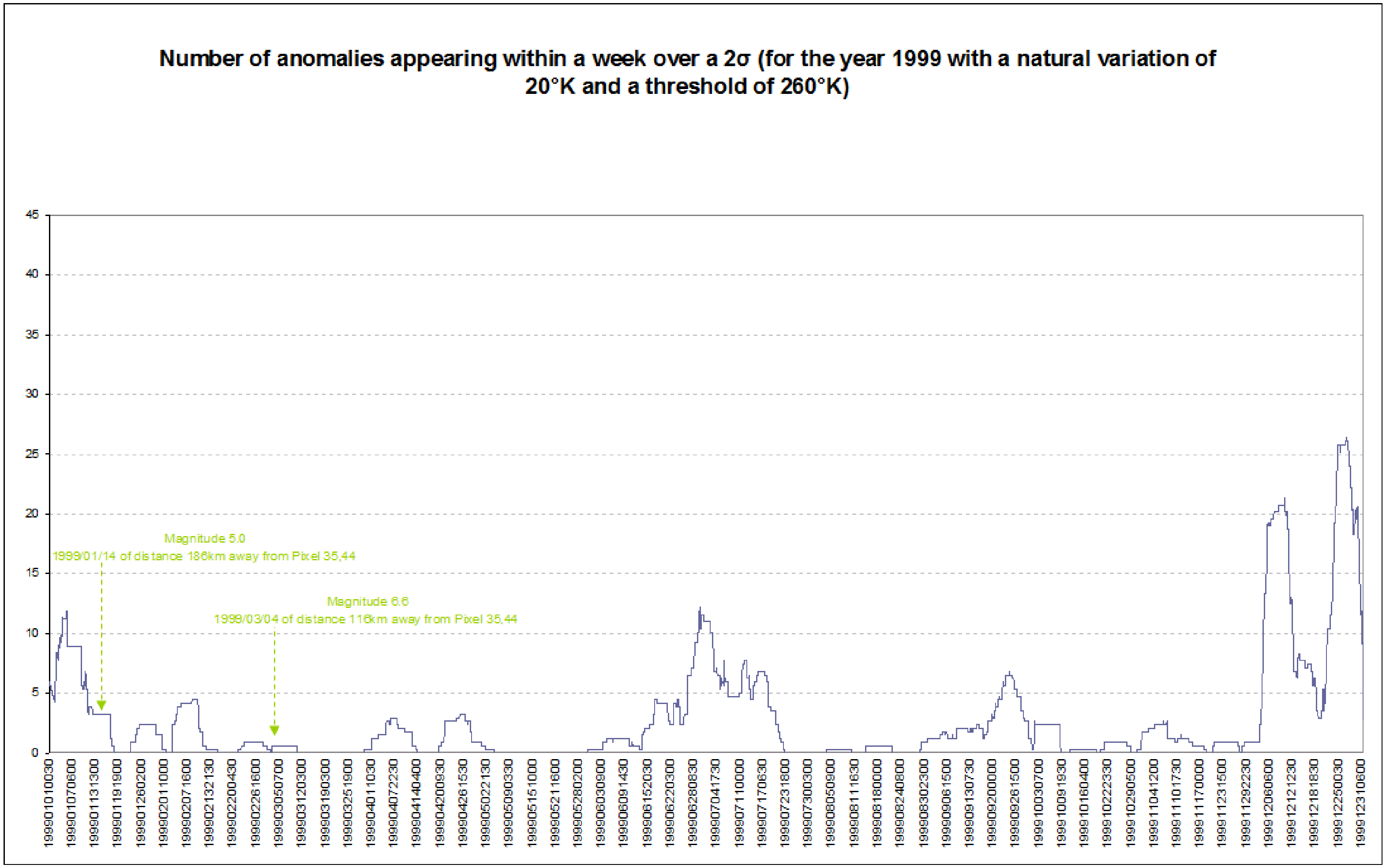

Figure 4-10: Number of anomalies appearing within a week period for Pixel 35,44 in the year 1999. Initially this peak would suggest that it is an earthquake-related anomaly as it lasts for one week but there were no earthquakes occurring in December 1999 which indicates that this peak is also a false positive.

In almost all the years studied, false positives appeared and a trend in the winter period (November-December months) was seen either with a distinct peak or dual peak of lower chance of being earthquake-related. There were similar trends for the summer period (July-August months). The anomaly appearing in Figure 4-6 seems to be 15% stronger as compared to the other years within the same time frame, but relatively throughout the year it is at least 50 % and in some cases even 100% stronger. It is then safe to assume that this occurrence in Figure 4-6 is an earthquake-related anomaly.

4.1.2. Spatial Extent Analysis on earthquake precursory detection in Bam

In order to validate the theory which describes a pixel in close proximity of the epicentre as having the highest temperature rise, a pixel located far from the epicentral distance is analysed. As suggested, pixels occurring far from the epicentre should not be influenced by the thermal anomalies and have a greater chance of not being related to the impending earthquake event. Pixel 20,15 which is located on the periphery of the study area was used in this case (see Figure 4-11), other profiles can be seen in Appendix I .

The proximity of Pixel 20,15 to the epicenter is 232 km away. The approximate fault length for a 6.6 magnitude earthquake event is 50 -70 km [61]. The highest temperatures are recorded near the epicentre and around the fault zones so to relate an anomaly, occurring at this pixel to Bam's earthquake is unjustifiable. An assessment of the time series was performed for the year of the earthquake occurrence, 2003. Figure 4-11 confirmed that anomalous signals within a pixel located far from the epicentral region are not influenced by any earthquake-related anomaly. As mentioned earlier, only significant anomalous signals appearing within a week are assessed suggesting that if 10% or less of the images showed anomalous activity the signal will be regarded as insignificant and excluded for relating to an earthquake-related anomaly. All the anomalies within this year were relatively insignificant as the number of images within that week were all under 5%, suggesting false positives within the time series. These false positives were a result of the large distance away from the selected pixel.

Figure 4-12 describes the spatial extent to which anomalous values were found by using the normalized background temperature ratio profiles. These anomalous values were based on the observations above a +2σ, only for 2003. Owing to the lack of time, other years were not assessed. It may be valuable though to analyse those anomalies appearing in a 7 day period spatially. The Google map was shown to provide some knowledge about the proximity between data points being studied.

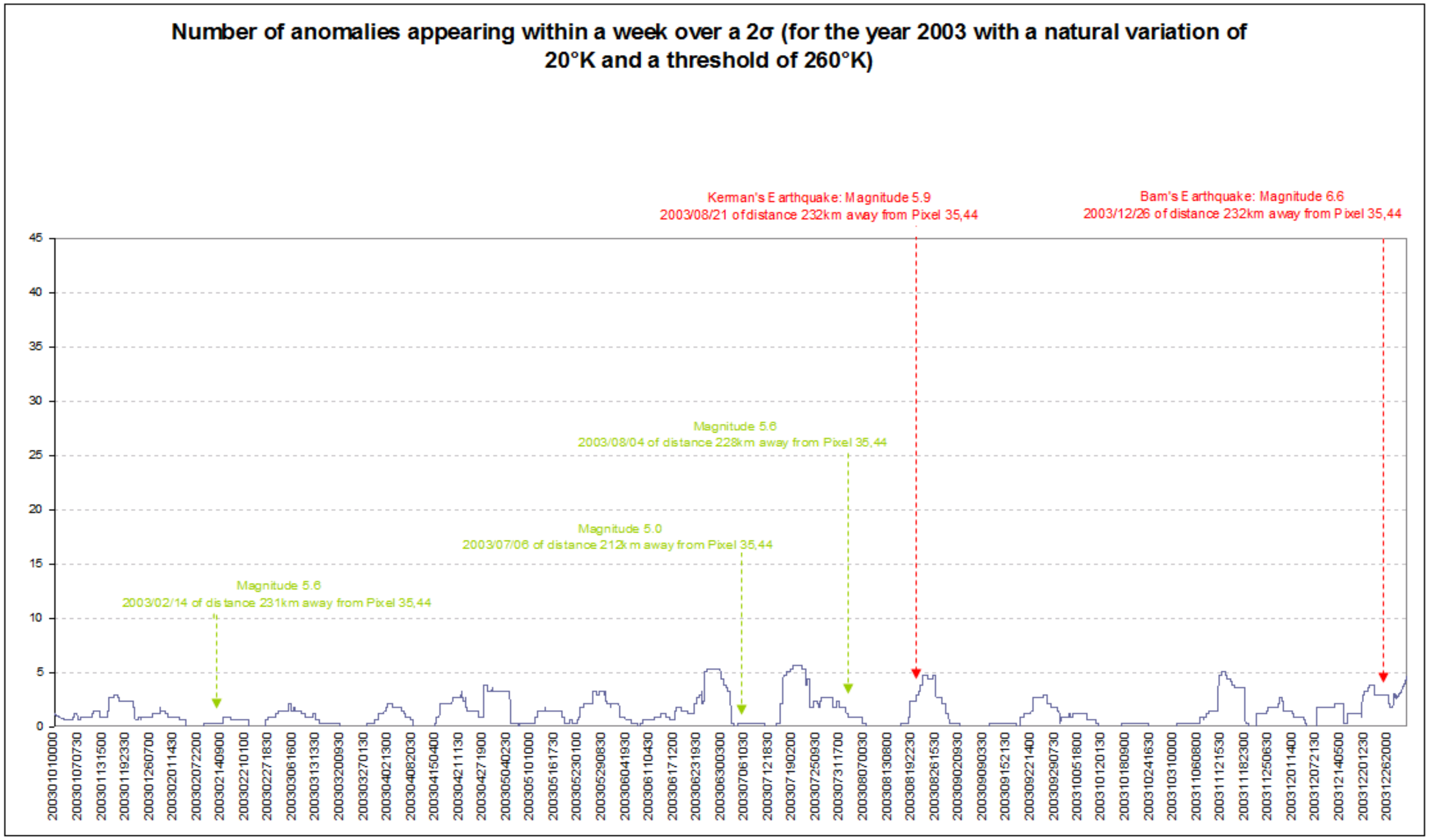

Figure 4-11: Illustrates the number of anomalies appearing in a Pixel 20,15 which is located far from the epicenter. These anomalous signals appearing within a week were regarded insignificant as all earthquakes occurred a distance > 200km away from the pixel under study. These pixels are regarded as false positives within the time series profile.

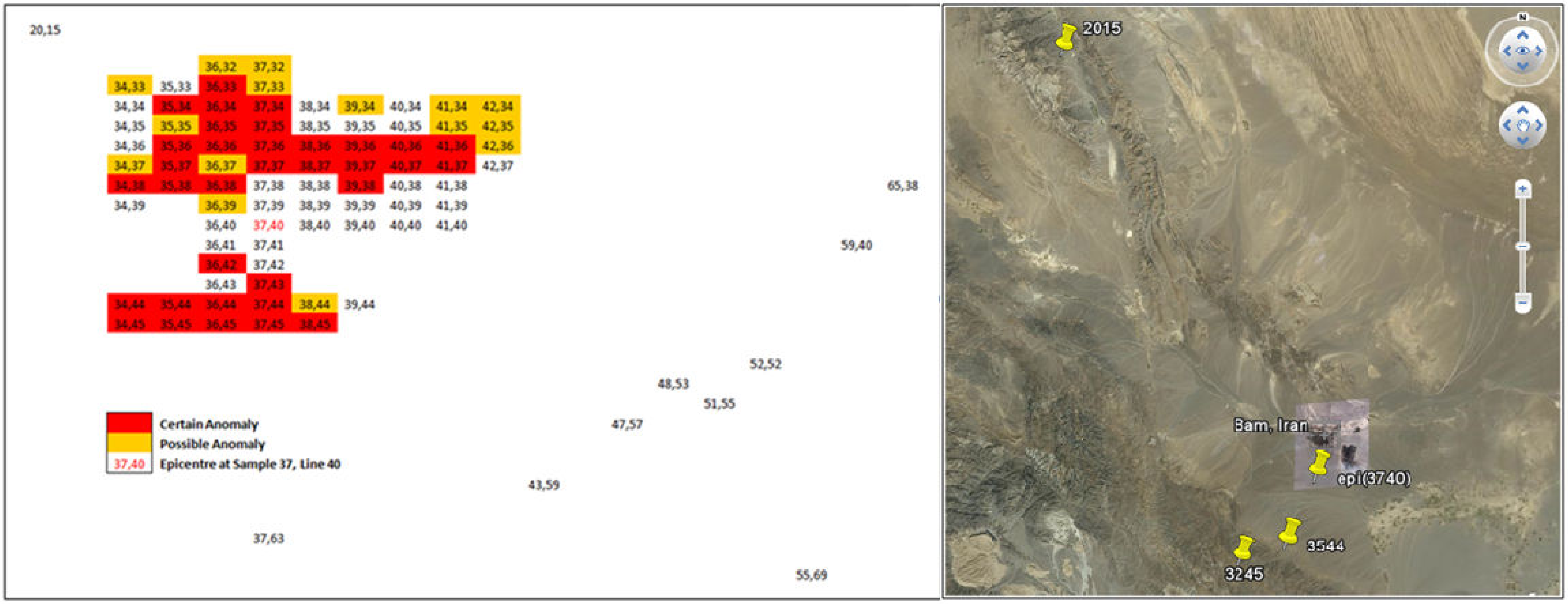

Figure 4-12: All the pixels that were analysed from the approximate epicenter and provided the spatial extent to which anomalous values were found by using the normalized background temperature ratio profiles. These anomalous values were based on the observations above a +2σ, only for 2003. It should be noted that these numbers such as 37,40 represents sample number 37 and line number 40 within the image.

4.1.3. Robustness Testing of Detection Algorithm

Several tests were performed on the profiles for Pixel 35,44, namely:

(i) Adjusting the size of the time window: Initially the profiles used was for a week period (i.e. 3.5 days before and 3.5 days after) which counted the number of anomalies present in images for one week. Shifting this time window might have an impact on the number of anomalies appearing and can either have a stronger relation to earthquakes or not. This parameter has been shifted from a week period to a two week period (i.e. 7 days before and 7 days after) and compared.

On increasing the time window as seen in Figure 4-13, it was seen that the number of anomalies has decreased from a 45% to an approximate 25%. The large peak that appeared in November has decreased to about 12%. The outcome of this action was similar to applying a smoothing filter over the data, which enhanced the significant anomalies and reduced the noise. However, from observing the 2003 profile alone, the 25% anomaly in December provides reason to believe that this can be caused by the Bam's earthquake.

(ii) Altering the threshold and the natural variation: The variables are changed within the cloud-masking algorithm and owing to the long processing time, it was attempted only once. The threshold value for cloud masking was originally set to 260°K and is changed to 265°K. The original natural variation used was 20°K which was also changed to 15°K. It was observed that by decreasing the natural variability within the study area, the temperature cut-off value for the removal of clouds was increased. This increase removed many observations which took into account clouds that remained in the dataset. On increasing the threshold, even fewer observations will be analysed.

From Figure 4-14, it was seen that the number of anomalies counted within a week were increased. These anomalies increased almost by 5% with minor reductions. However, two extreme conditions in the winter period which showed the existing anomaly almost doubled, for a period in November and in late December. However, it is more certain that these anomalies are not related or impacted upon by clouds within the background, when ratios are calculated (i.e. the anomaly detection algorithm). Owing to the lack of time, the original profiles with a threshold value of 260°K and a natural variation of 20°K were used; even though the new conditions provide outputs that are more justifiable.

Table 4-2 provides an overview of the anomalies detected within each pixel that was analysed. The table illustrates whether anomalies are detected within each profile.

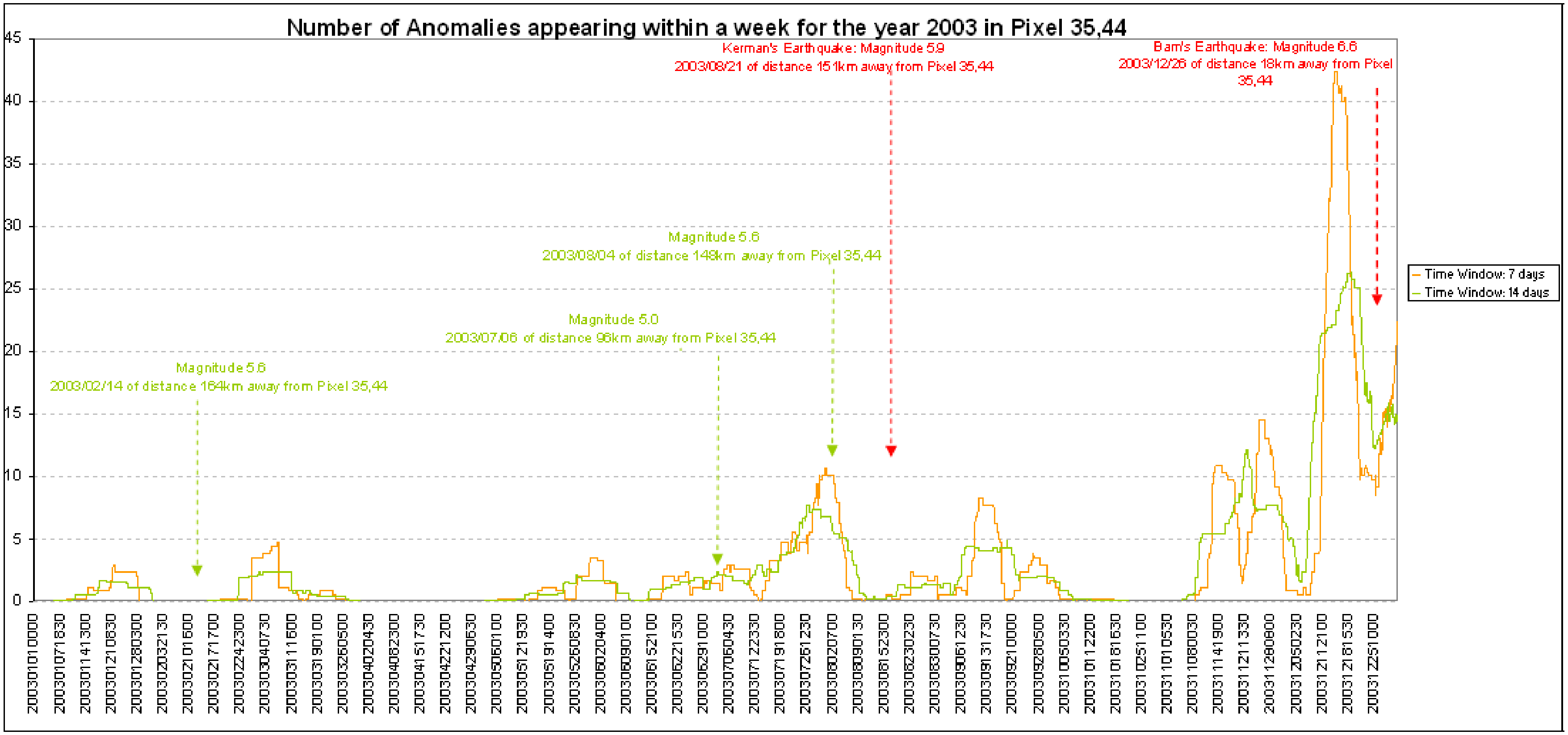

Figure 4-13: The effect of changing the time window for counting the number of anomalies appearing above a 2σ, in 2003. On increasing the time window it was seen that the number of anomalies has decreased from a 45% to an approximate 25%. Green represents the number of images where anomalies appear within two weeks whilst orange represents the number of images where anomalies appear within one week. From observing the 2003 profile alone, the 25% anomaly in December provides reason to believe that this can be caused by the Bam's earthquake.

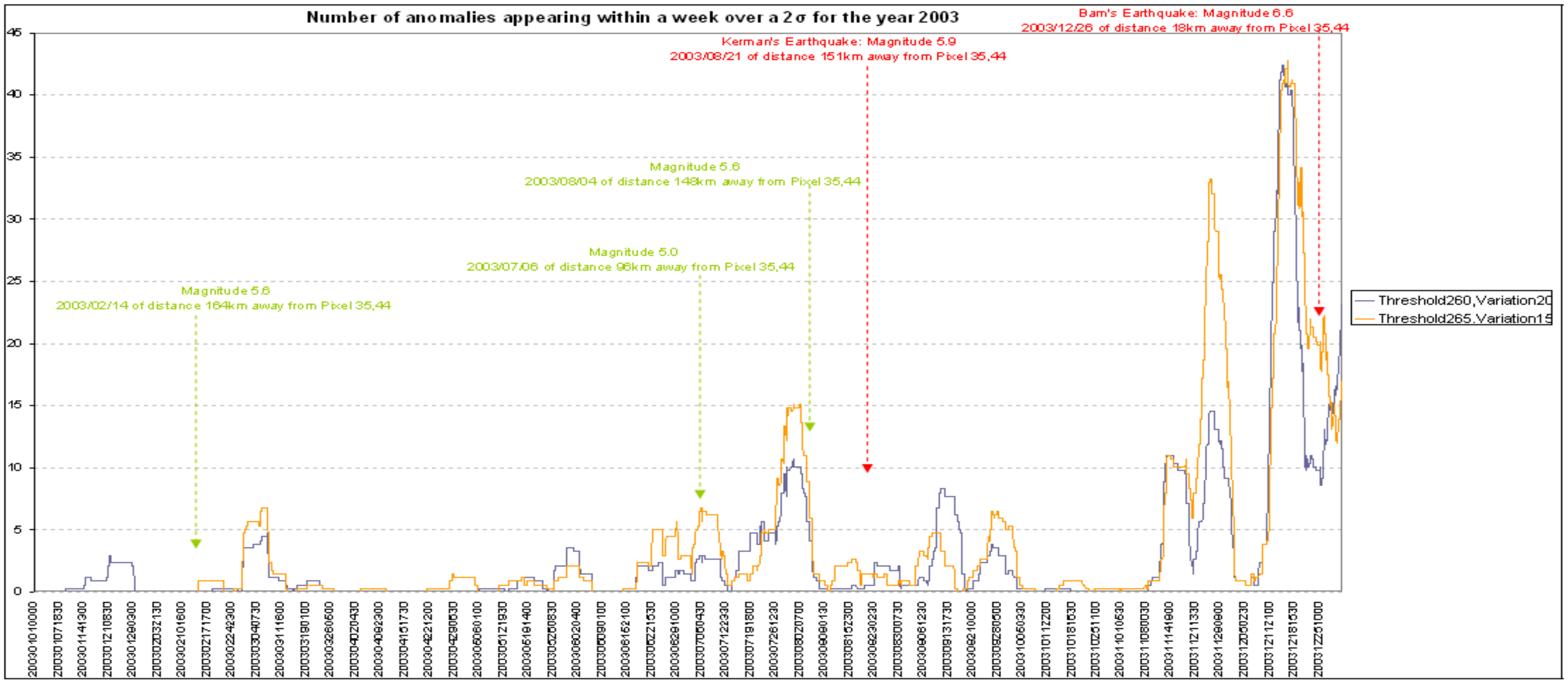

Figure 4-14: The effect of altering the threshold and the natural variation within the cloud masking algorithm for Pixel 35,44 in 2003. The blue line which represents the threshold 260°K and natural variation 20°Kwas the original parameters used in the algorithm. However on increasing the threshold and decreasing the natural variability in the area, it was found that the majority of images appearing within a week had significantly more anomalies appearing.

PIXEL	YEAR																	
	2004			2003			2002			2001			2000			1999		
	EQ Relate	False Positive	False Negative	EQ Related	False Positive	False Negative	EQ Related	False Positive	False Negative	EQ Related	False Positive	False Negative	EQ Related	False Positive	False Negative	EQ Related	False Positive	False Negative
35,44	N	Y	Y	Y	Y	N	N	Y	N	N	Y	N	N	Y	N	N	Y	N
20,15				N	Y	N												

Table 4-2: Assessment of anomalies detected within certain pixels of the study area for a six year period.

4.2. Results from Anomaly Detection for L'Aquila

Time series analysis of MSG2 thermal images have been analysed also using the developed methodology. As described in Section 3.3.3.2, the natural variability in a study area as well as extreme climatic conditions is needed for a good cloud removal. The natural temperature variation occurring in L'Aquila ranged from~10°K to ~18°K. The estimated variation chosen was 15°K. Also, the threshold set for cloud masking was 255°K from the extreme temperatures occurring in close proximity to L'Aquila, as shown in Appendix D. All anomalies detected over a 2σ of the mean will be used and if these anomalies last for a week period only then they are analysed for L'Aquila. Owing to the lack of time and the processing speed to run the scripts for L'Aquila only one year will be analysed owing to a higher spatial resolution as well as temporal resolution is doubled. Within the NEIC earthquake results for L'Aquila as seen in Appendix H, only in 2009 there were significant earthquakes. Slope aspects will be studied in detail in this section.

4.2.1. Spatial Extent Analysis on earthquake precursory detection in L'Aquila

Pixel 60,49 as well as Pixel 15,59 were analysed in detail. Other profile observed were placed in Appendix I. Figure 4-15 (b) and (c) which show the distribution of the points. Pixel 60,49 was roughly 23 km away from the epicentre and oriented on a north-eastern slope whereas Pixel 15,59 was located in a water body approximately 124km away from the epicentre. As seen in Figure 4-16, Pixel 60,49 which is land restricted shows a very weak anomaly lasting for 7 days and within a month prior to L'Aquila earthquake. It is regarded as a false positive. Even though this pixel is within a 23km radius of the epicentre the anomalous signal in the profiles are insignificant.

As seen in Figure 4-17, for Pixel 15,59 which is located in a waterbody there were no earthquake related anomaly. This pixel is 124km away from the epicentre and can be considered as a background pixel. This pixel will have different climatic conditions owing to the extent from the epicentre.

4.2.2. False Positives versus Earthquake-related anomalies

Table 4-3 provides an overview of the anomalies detected within Pixels 60,49 and Pixel 15,59. It gives an idea of how anomalies appear within the time series profile and whether they can be regarded as earthquake-related, false positives or false negatives. The NEIC result for L'Aquila as seen in Appendix H, provided two smaller magnitude earthquakes occurring around the epicentre. To assess fully whether these anomalies are false negatives, the distance from the pixel studied within a specified radius to the epicentre is observed.

PIXEL	YEAR			
	2009			
	Feature	Earthquake Related	False Positive	False Negative
60,49	North-east slope	N	Y	N
15,59	Waterbody	N	Y	N

Table 4-3: Assessment of slope aspect and a water body and their relation to anomalies detected within certain pixels of the study area.

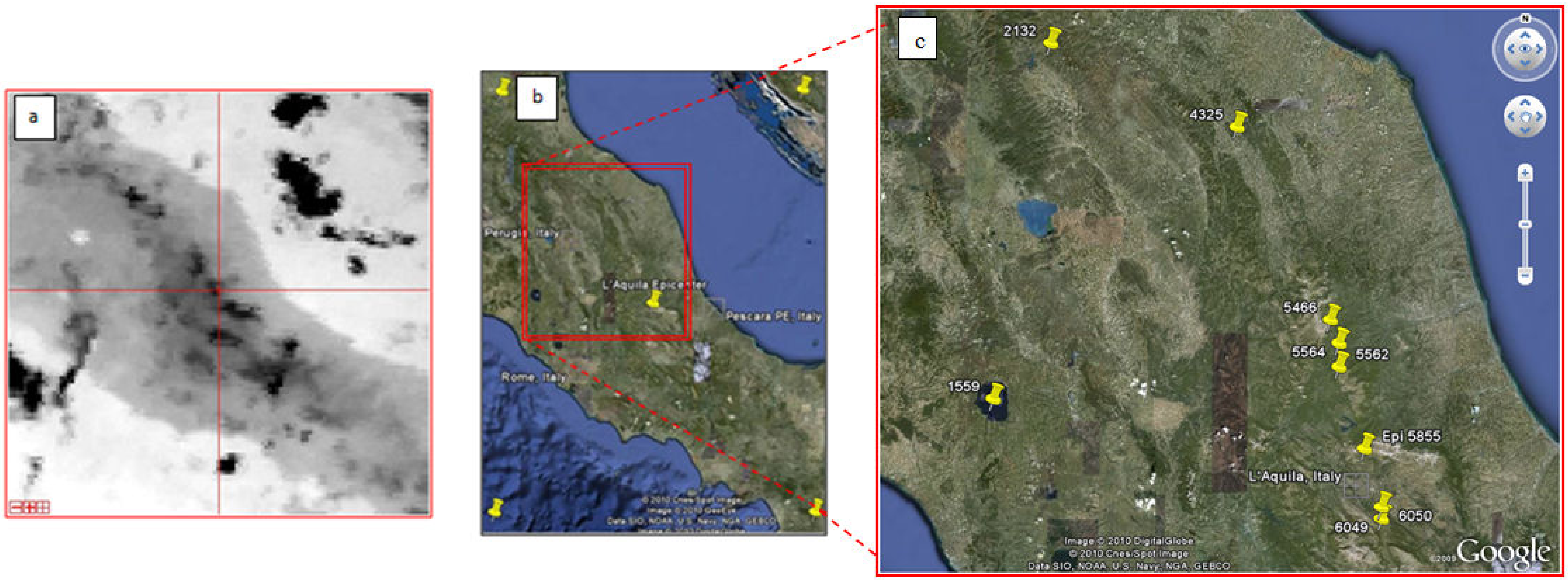

Figure 4-15: Comprised of three parts: (a) A MSG2 image showing the extent of the study area; (b) The study area in a Google map where the red bounding box illustrates the distribution of points; and (c) Detailed view of the points selected and analysed as seen in a Google map where the bounding box illustrates the distribution of points; and (c) Detailed view of the points selected and analysed as seen in a Google map.

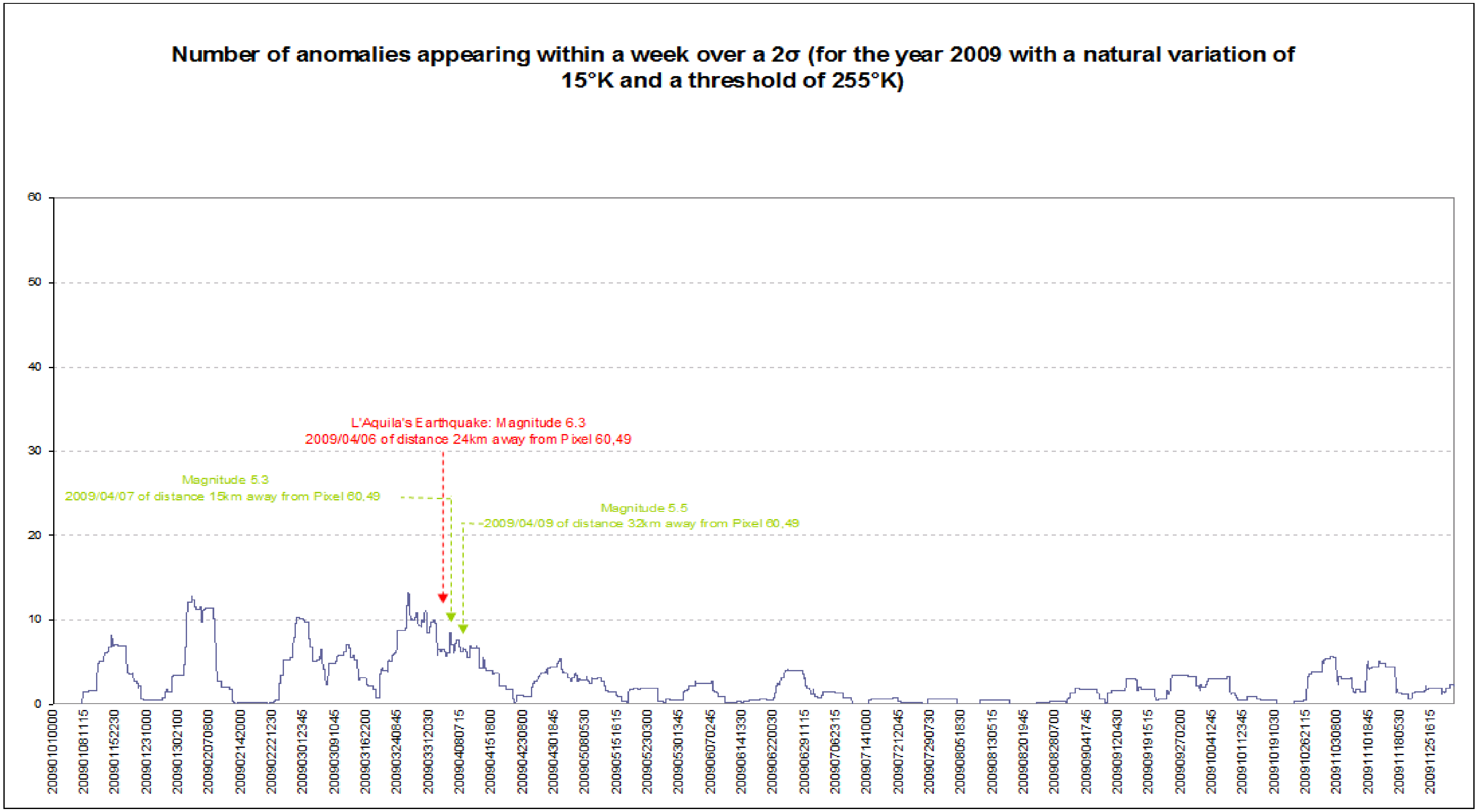

Figure 4-16: Number of anomalies appearing within a week period for Pixel 60, 49 in the year 2009. This anomalous signal lasting within a week is insignificant and regarded as a false positive within the profile. These anomalies were regarded insignificant because for an earthquake-related anomaly, the assumption was that at least 15% of the number of images contained anomalies with a duration of one week.

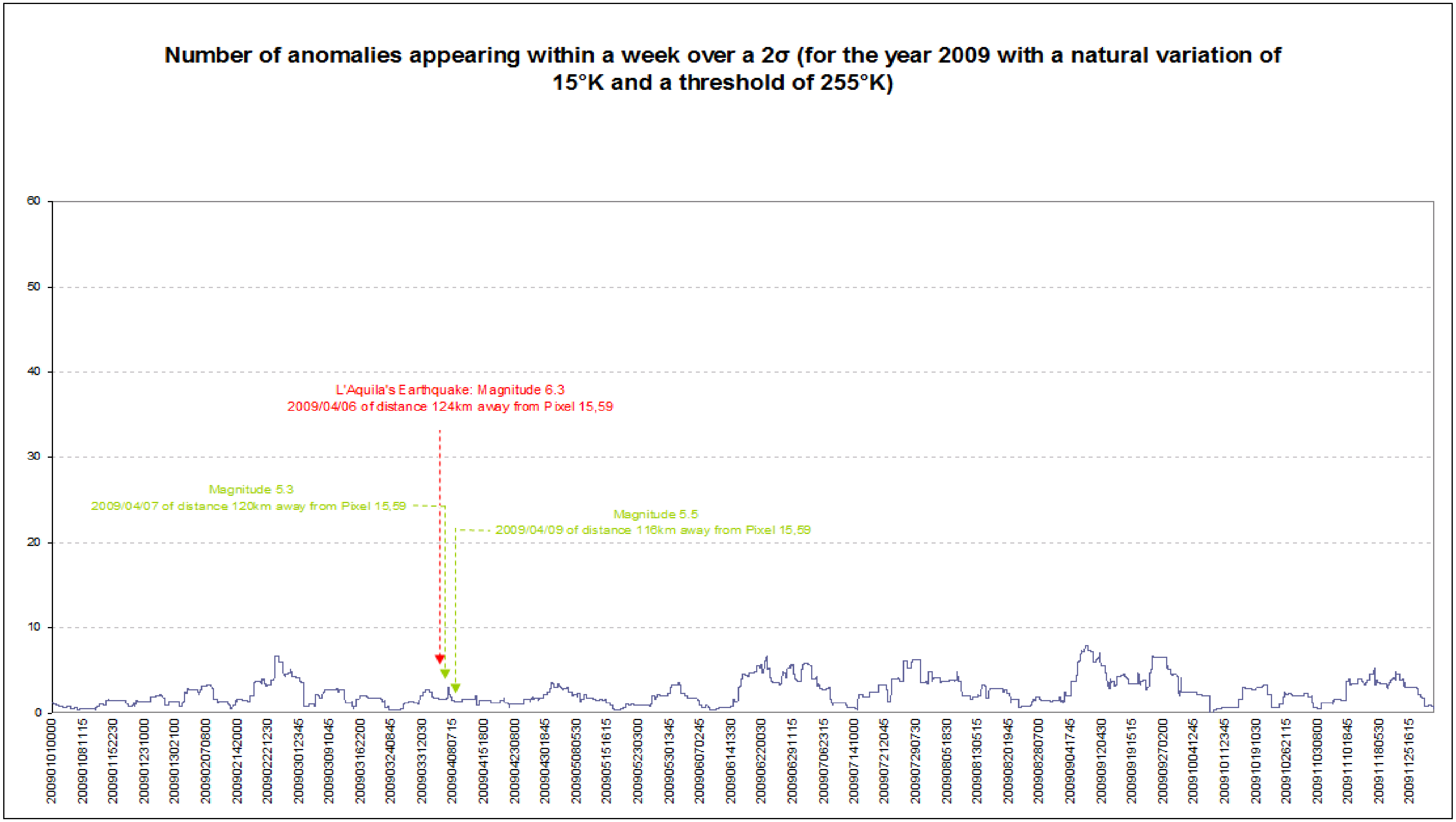

Figure 4-17: Number of anomalies appearing within a week period for Pixel 15,59 in the year 2009. As suggested, there is so significant anomaly appearing in this pixel owing to its proximity to the earthquake epicenter.

.

4.3. Anomaly Detection Reliability

Bam and L'Aquila have totally different conditions and need to be analysed separately. Bam is a relatively dry, desert-like region with little vegetation and regarded as being cloud free. The images were obtained by the Meteosat-5 satellite which has a different orientation than the sensor being used for L'Aquila. The sensor has a much coarser spatial resolution and the temporal resolution is 30 minutes. Unlike Bam, L'Aquila is densely populated, vegetated, and topography-driven and has a stronger influence by clouds. MSG2 images were acquired for the L'Aquila study area.

Both study areas show that thermal anomalies can be detected; however relating it to an earthquake phenomenon is very challenging. To assess whether it is an earthquake-related anomaly, the year of the earthquake is studied after which the anomaly findings will be compared to other years. If a significant anomaly is detected within a month before the earthquake, lasts for a week and is in close proximity to the epicentre or fault zone, only then anomalies can be compared as earthquake-related. Many false positives appeared within the profiles.

5. Discussion and Conclusion

One of the objectives of this study is to verify whether significant thermal infrared anomalies can be found in association with known earthquake events by systematically applying satellite data time series analysis to multi-year time series. The framework for this was applied to Bam and L'Aquila by developing a method to detect anomalies. The goal of this chapter is to interpret and assess potential reasons for the findings obtained from this study.

5.1. Discussion

A rather straightforward but simple cloud removal algorithm was developed based on recurring temperatures in the images. Clouds act as powerful reflectors to solar radiation, sending much energy straight back into space. Thin high clouds absorb thermal radiation from the surface and radiate much of it back down , contributing to the natural greenhouse effect which makes global cloud cover a major factor in the distribution of thermal energy in the atmosphere [51]. In order to remove the clouds, selection of parameters is based on the extreme temperatures as well as the natural variation over a study area. The main problem is that thresholds for cloud masking are functions of many variables such as; surface type (land, ocean, ice), surface conditions (vegetation, soil moisture), recent weather (which changes surface temperature and reflectance significantly), atmospheric conditions (temperature inversions, haze, fog), season, time of day and even satellite-earth-sun geometry (hence bidirectional reflectance and sun glint). These factors may play a role in the simplified cloud masking algorithm. Further studies are needed to fully assess the impact of these factors on the derived anomalies. It is believed that the impact is rather small and only in very specific cases might result on false positive anomalies. This is based on the rather stable and constant normalized time series that was found for each pixel over multiple years indicating a proper removal of clouds throughout the images.

For the normalization, a window size was set based on common knowledge rather than scientifically proven facts. A moving ring approach was applied over a time series stack in the normalization algorithm where a 10 pixel buffer radius around the pixel under investigation was selected as described in Section 3.3.4.2. This size was based on the fact that if a too small ring size (of less than 10 pixels) is used adjacent anomalous pixels can influence the background temperatures. A too large ring size would make the variation between pixels possibly too large; it is well possible that over a distance of > 200km varying meteorological conditions occurring in different region can impact on the temperature ratios. The smaller the area, the more likely it is that weather conditions in the normalizing ring are similar to those in the pixel under investigation. This ~ 50km ring size provided suitable results but a more thorough analysis should be performed to study the most optimal ring size.

In the anomaly detection process, any ratio appearing above a ±2σ was flagged as anomalous. To assess how many anomalous images are actually occurring within a certain time frame (i.e. an indication for the strength and persistence of an anomalous feature), a running cumulative moving window of one week length was applied as this was the period stated in literature where an earthquake-related anomaly could probably last. The higher the percentage of anomalous images, the stronger is the anomaly. As seen in Figure 4-6, a significant earthquake anomaly (45%) occurred prior to Bam. A long time series was then used to assess the chance of this earthquake-related anomaly appearing in the year of the earthquake occurrence to indeed be caused by the earthquake or another phenomenon. On comparing Figures 4-5 to Figure 4-10, this anomaly occurring in Figure 4-6 is 50-200% stronger than any other anomaly appearing in 6 years time and therefore significantly earthquake-related. There is, however, a trend of occurring anomalies in December. The source of these anomalies is unclear but might be related to snow cover in mountainous regions covered by the normalization ring. This is only speculative till now and needs further investigation of individual pixels in the normalization ring.

For L'Aquila the anomaly is less strong (it was also a less strong earthquake) and only one year of data is available for analysis. Similar analysis as done for Bam is therefore not possible for now but should be done in future work.

5.1.1. Significant Findings Associated with Earthquakes

5.1.1.1. Earthquake Cloud

There was an unusual cloud emerging exactly from the epicentre of the December 26th Bam earthquake. This was likely because its hot vapour condensed into a cloud immediately due to very cold surroundings at night during the winter. However, in many cases the vapour released at the epicentre does not immediately encounter atmospheric conditions suitable for condensation into a cloud. Since the cloud's travel time and direction are not well known, this greatly reduces the precision, or specificity of a prediction. First, an earthquake cloud appearing in satellite images can pinpoint an impending epicentre from an earthquake cloud only when it condenses at the epicentre in cold surroundings, as it did in Bam [48].

5.2. Limitations/Challenges

Several limitations were encountered within this research as described below:

- U-MARF facility for data acquisition of Meteosat-5 TIR images:

The outputs required for this research, from this facility provided only image data thus no georeferencing was applied. Even though there are options for subsetting an area of interest from a full disc image preview, outputs after retrieval tends to be shifted. In other words, it provides you with an inaccurate study area. Owing to the projection of an ellipsoidal earth on a two dimensional image, the spatial resolution is not constant for all Meteosat image pixels. At sub-satellite point, the pixel distance amounts to 4.5 km in both directions for Meteosat-5. At high latitudes, the pixel distances can exceed the grid sizes [40] and spatial resolution at these distances tends to be too coarse. By trial and error, the correct coordinates were provided, to get the epicentral location in the centre of the image. This is important since there is no spatial information attached to the image the epicentre can be located much simpler.

- Atmospheric corrections were not applied:

Meteosat has a single channel in the TIR window, which implies that split-window techniques cannot be used. This channel is slightly influenced by absorption of gaseous atmospheric constituents. Neglecting atmospheric effects, the measured BTs of a target is equal to the target temperature. In order to determine LST, the influence of the atmosphere on measured BTs has to be accounted for. This can be achieved by using split window techniques[40, 45] .

In order to atmospherically correct its historically valuable time series of BTs, Schädlich et al. (2001) used a previous version of the model of the diurnal temperature cycle proposed by Reuter (1994) to temporally interpolate atmospheric corrections for Meteosat single channel [45]. Additional data is required such as forecast data based on humidity and temperature profiles to temporally interpolate atmospheric corrections for Meteosat.

Brightness temperature is an alternate measure of intensity which gives the temperature of a black body with the specified radiance, at that wavelength. It is used because it has linear correlations with atmospheric temperature parameters, easing statistical analysis [51]. Due to computational limitations associated with the single channel method, the results presented in the research are based on BTs and not LST.

- Uncertainties within time series:

It is important to note that there were uncertainties within the datasets that can influence the anomalies. These uncertainties were not corrected for and thus some anomalies were even increased owing to this. Such uncertainties include shifts in the sensor, a wobble effect of the sensor (at least one pixel off), line striping, and missing data (either for entire image or part of an image) as seen in Figure 5-1. These uncertainties will produce inaccurate normalized background temperature ratios and may appear as a peak above a +2σ as a different study area is observed, for a shift in the sensor. Wobbling effects appear as a sudden spike within the normalization process as a different pixel will be analysed.

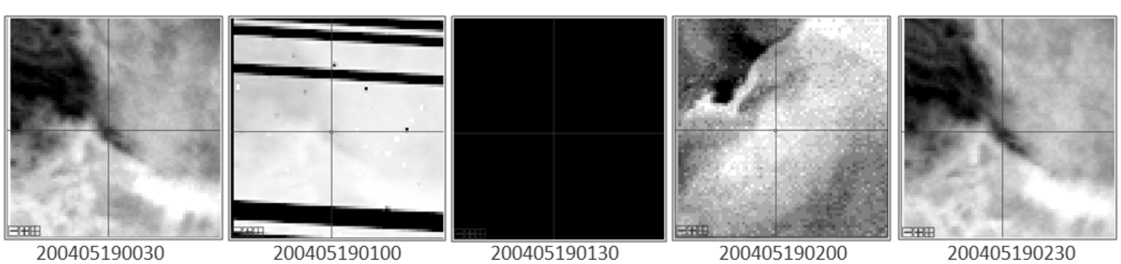

Figure 5-1: Errors appearing in time series profiles for the year 2004, in the study area of Bam. Similar errors were seen in the L'Aquila region.

5.3. Conclusion

Based on the results, it was found that the developed methodology in terms of its applicability for detecting significant thermal infrared anomalies in relation to earthquakes by systematically applying satellite data time series analysis to multi-year time series was reasonable. The study confirms that time series is an important component in any earthquake anomaly detection study. The main conclusion drawn from this study is a short time series is not justifiable for detection of earthquake anomalies.

Even though anomalies were detected in order to relate to an earthquake event, a shortened time series cannot be used. Long time series has shown that thermal anomalies are influenced by topography, and seasonality and defining a normal condition which encompasses every possible normal behaviour is very difficult. Often the data contains noise which tends to be similar to the actual anomalies and hence is difficult to be distinguished. A long time series can assist in overcoming these difficulties to identify earthquake-related anomalies. The answers of the research questions will be addressed and discussed in order to fulfil the objectives set forth within this research.

5.4. Recommendations

Recommendations for future work are as follows:

- Determining how accurate and with what degree of error this method achieves by testing other earthquake. An attempt for earthquake anomaly detection should be made for higher magnitude earthquakes such as the recent Chile and Haiti earthquakes.
- Incorporate in the methodology, atmospheric correction to obtain LSTs instead of using BTs.
- Aid of ancillary datasets such as a DEM, to assess the impact of elevation on earthquake-related anomalies.
- Assessment of earthquake-related anomalies in a spatial context.
- Apply methodology to non-crustal earthquakes (i.e. earthquakes originating in the ocean).

REFERENCES

1. Ahmadi, M., *Official report on Bam Climate by Bam Meteorological Center*. 2004: Iran.
2. Aliano, C., R. Corrado, C. Filizzola, N. Genzano, N. Pergola, and V. Tramutoli, *Robust TIR satellite techniques for monitoring earthquake active regions: limits, main achievements and perspectives.* Annals of Geophysics, 2008. **51**(1): p. 303-317.
3. Aliano, C., R. Corrado, C. Filizzola, N. Pergola, and V. Tramutoli, *Robust satellite techniques (RST) for the thermal monitoring of earthquake prone areas: the case of Umbria-Marche October, 1997 seismic events.* Annals of Geophysics, 2008.
4. BBC, B.B.C. *Country Climate Guide*. 2009 August 2009 [cited 2009 July]; Available from: http://www.bbc.co.uk/weather/world/country_guides/.
5. Choudhury, S., S. Dasgupta, A.K. Saraf, and S. Panda, *Remote sensing observations of pre-earthquake thermal anomalies in Iran.* International Journal of Remote Sensing, 2006. **27**(20): p. 4381-4396.
6. Cicerone, R.D., J.E. Ebel, and J. Britton, *A systematic compilation of earthquake precursors.* Tectonophysics, 2009. **In Press, Corrected Proof**.
7. Cospas-Sarsat, I.S.S.f.S.a.R., *Cospas-Sarsat METEOSAT Second Generation (MSG) GEOSAR Performance Evaluation Report*. 2006: Montreal (Quebec), Canada. p. 1-12.
8. European Organisation for the Exploitation of Meteorological Satellites, E. *Meteosat First Generation: Calibration Coefficients*. [cited 2009 December]; Available from: http://www.eumetsat.int/Home/Main/Access_to_Data/Meteosat_Meteorological_Products/Calibration/SP_1119512203627.
9. European Organisation for the Exploitation of Meteorological Satellites, E., *MTP Operations Services Specification*. 2000: Darmstadt, Germany.
10. European Organisation for the Exploitation of Meteorological Satellites, E., *The Meteosat Archive User Handbook*. 2001: Darmstadt, Germany.
11. European Organisation for the Exploitation of Meteorological Satellites, E., *GEONETCast Implementation Plan*. 2006: Darmstadt, Germany.
12. European Organisation for the Exploitation of Meteorological Satellites, E., *Cloud Detection for MSG-Algorithm Theoretical Basis Document* 2007: Darmstadt, Germany.
13. European Organisation for the Exploitation of Meteorological Satellites, E., *MSG Level 1.5 Image Data Format Description*. 2007: Darmstadt, Germany.
14. European Organisation for the Exploitation of Meteorological Satellites, E., *Operational Services Specification* 2009: Darmstadt, Germany.
15. Fox, S., *Did a Technician Accurately Forecast the L'Aquila Earthquake--Or Was It a Lucky Guess?*, in *Scientific American*. 2009, Nature America Inc.
16. Gommes, R. *Mountain Climates*. 2002 [cited 2010 March]; Available from: http://www.fao.org/nr/climpag/pub/EN0701_en.asp.
17. Gornyi, V.I., A.G. Sal'Man, A.A. Tronin, and B.V. Shilin, *Outgoing infrared radiation of the earth as an indicator of seismic activity.* Akademiia Nauk SSSR, 1988. **301**(1): p. 67-69.
18. Göttsche, F.-M. and F.S. Olesen, *Modelling of diurnal cycles of brightness temperature extracted from METEOSAT data.* Remote Sensing of Environment, 2001. **76**(3): p. 337-348.
19. Herrera, M. *Extreme Temperatures around the world*. 2005 [cited 2009 December]; Available from: http://www.mherrera.org/temp.htm
webmaster@mherrera.org.
20. Kanamori, H., *Magnitude scale and quantification of earthquakes.* Tectonophysics, 1983. **93**(3-4): p. 185-199.
21. König, M. *Creating Meteorological Products from Satellite Data*. 2008; Available from: http://www.eumetsat.int/metprods_webcast/print.htm#z4.1.

22. Kuenzer, C., C. Hecker, J. Zhang, S. Wessling, and W. Wagner, *The potential of multidiurnal MODIS thermal band data for coal fire detection.* International Journal of Remote Sensing, 2008. **29**(3): p. 923-944.
23. Kuenzer, C., J. Zhang, J. Li, S. Voigt, H. Mehl, and W. Wagner, *Detecting unknown coal fires: synergy of automated coal fire risk area delineation and improved thermal anomaly extraction.* International Journal of Remote Sensing, 2007. **28**(20): p. 4561 - 4585.
24. Labov, S.L. *United States Search and Rescue Task Force - Earthquakes*. 2000 Monday, January 25, 2010 [cited 2010 February]; Available from: http://www.ussartf.org/earthquakes.htm
ussartf@ussartf.org.
25. Lefevre, M., O. Bauer, A. Iehle, and L. Wald, *An automatic method for the calibration of time-series of Meteosat images.* International Journal of Remote Sensing, 2000. **21**(5): p. 1025-1045.
26. Lillesand, T.M., R.W. Kiefer, and J.W. Chipman, *Remote Sensing and Image Interpretation*. Sixth Edition ed. 2008: John Wiley & Sons, Inc.
27. Liu, S. and L. Wu. *Study on mechanism of satellite IR anomaly before tectonic earthquake*. in *Geoscience and Remote Sensing Symposium, 2005. IGARSS '05. Proceedings. 2005 IEEE International*. 2005.
28. Manafpour, A.R., *The Bam, Iran Earthquake of 26 December 2003*. 2004, Institution of Structural Engineers: London.
29. Masika, P.S., *Meteosat Second Generation (MSG) Cloud Mask, Cloud Property Determination and Rainfall Comparison with In-situ Observations*, in *Water Resources and Environmental Management Programme*. 2007, International Institute for Geo-Information Sciecnce and Earth Observation: Enschede.
30. Mather, P.M., *Computer Processing of Remotely-Sensed Images: An Introduction*. 3rd ed. 2004, Chinchester: John Wiley & Sons Ltd. 324.
31. Moseman, A. and S. Rao, *Scientist Smackdown: Did a Seismologist Accurately Predict the Italian Quake?* , in *Discover Magazine*, E. Strickland, Editor. 2009.
32. Naranjo, L. *Finding Data Introduction*. 2010 22 February 2010 [cited 2010 March]; Available from: http://nasadaacs.eos.nasa.gov/search.html.
33. Nationaal Lucht-en Ruimtevaartlaboratorium, N.A.L.-N., *HANTS: Harmonic Analysis of Time Series*.
34. National Snow and Ice Data Center. *MODIS Data*. unknown; Available from: http://nsidc.org/data/modis/terra_aqua_differences/index.html.
35. Ouzounov, D., N. Bryant, T. Logan, S. Pulinets, and P. Taylor, *Satellite thermal IR phenomena associated with some of the major earthquakes in 1999-2003.* Physics and Chemistry of the Earth, Parts A/B/C, 2006. **31**(4-9): p. 154-163.
36. Panda, S.K., S. Choudhury, A.K. Saraf, and J.D. Das, *MODIS land surface temperature data detects thermal anomaly preceding 8 October 2005 Kashmir earthquake.* International Journal of Remote Sensing, 2007. **28**(20): p. 4587-4596.
37. Pergola, N., G. D'Angelo, M. Lisi, F. Marchese, G. Mazzeo, and V. Tramutoli, *Time domain analysis of robust satellite techniques (RST) for near real-time monitoring of active volcanoes and thermal precursor identification.* Physics and Chemistry of the Earth, Parts A/B/C, 2009. **34**(6-7): p. 380-385.
38. Ramezani, J. *Earthquakes in Iran: A Geological Perspective*. 2004 [cited 2010 March]; Available from: http://payvand.com/news/04/jan/1109.html.
39. Rees, W.G., *Physical Principles of Remote Sensing*. Second ed. 2001, United Kingdom: Cambridge University Press.
40. Reuter, M. and J. Fischer, *A comparison of satellite-retrieved and simulated cloud coverage in the Baltic Sea area as part of the BALTIMOS project.* Theoretical and Applied Climatology, 2009.

41. Saraf, A., V. Rawat, P. Banerjee, S. Choudhury, S. Panda, S. Dasgupta, and J. Das, *Satellite detection of earthquake thermal infrared precursors in Iran.* Natural Hazards, 2008. **47**(1): p. 119-135.
42. Saraf, A.K. and S. Choudhury, *Satellite detects surface thermal anomalies associated with the Algerian earthquakes of May 2003.* International Journal of Remote Sensing, 2005. **26**(13): p. 2705 - 2713.
43. Saraf, A.K. and S. Choudhury, *Thermal Remote Sensing Technique in the Study of Pre-Earthquake Thermal Anomalies.* Journal of Indian Geophysical Union, 2005. **9**(3): p. 197-207.
44. Saraf, A.K., V. Rawat, S. Choudhury, S. Dasgupta, and J. Das, *Advances in understanding of the mechanism for generation of earthquake thermal precursors detected by satellites.* International Journal of Applied Earth Observation and Geoinformation. **In Press, Corrected Proof**.
45. Schädlich, S., F.M. Göttsche, and F.S. Olesen, *Influence of Land Surface Parameters and Atmosphere on METEOSAT Brightness Temperatures and Generation of Land Surface Temperature Maps by Temporally and Spatially Interpolating Atmospheric Correction.* Remote Sensing of Environment, 2001. **75**(1): p. 39-46.
46. Schmetz, J., P. Pili, S. Tjemkes, D. Just, J. Kerkmann, S. Rota, and A. Ratier, *SEVIRI Calibration*. 2002, American Meteorological Society (AMS).
47. SEVGİ, L., *A Critical Review on Electromagnetic Precursors and Earthquake Prediction.* Turk. J. Elec. Eng. & Comp. Sci., 2007. **15**(1): p. 1-15.
48. Shou, Z. and D. Harrington. *Bam Earthquake Prediction & Space Technology*. in *United Nations /Islamic Republic of Iran Regional Workshop on theUse of Space Technology for Environmental Security, Disaster Rehabilitation and Sustainable Development*. 2004. Tehran, Islamic Republic of Iran: UN Workshop.
49. Souza, J.D.D., B.B.D. Silva, and J.C. Ceballos, *Efficiency of a simple split-window for land surface temperature estimation using MODIS products*, in *23rd Conference on Hydrology*. 2009, American Meteorological Society (AMS): Camp Springs, MD.
50. Stackpole, J.D., *A Guide To The Code Form FM-94 BUFR*. 2003, World Meteorological Organization.
51. Tendel, J., *Multispectral Radiative Transfer Simulations in the Thermal Infrared in Comparison with Satellite Measurements*. 2007, Institut für Weltraumwissenschaften,
Meteorologisches Institut,
Freie Universität Berlin. p. 87.
52. Tramutoli, V. *Robust AVHRR techniques (RAT) for environmental monitoring: theory and applications*. in *Earth Surface Remote Sensing II*. 1998. Barcelona, Spain: SPIE.
53. Tramutoli, V., V. Cuomo, C. Filizzola, N. Pergola, and C. Pietrapertosa, *Assessing the potential of thermal infrared satellite surveys for monitoring seismically active areas: The case of Kocaeli (Izmit) earthquake, August 17, 1999.* Remote Sensing of Environment, 2005. **96**(3-4): p. 409-426.
54. Tronin, A.A., *Remote sensing and earthquakes: A review.* Physics and Chemistry of the Earth, Parts A/B/C, 2006. **31**(4-9): p. 138-142.
55. Tronin, A.A., M. Hayakawa, and O.A. Molchanov, *Thermal IR satellite data application for earthquake research in Japan and China.* 2002: p. 519-534.
56. U.S. Geological Survey, U. *USGS Global Visualization Viewer: Help*. 2010 8th March 2010 [cited 2010 March]; Available from: http://glovis.usgs.gov/ImgViewerHelp.html.
57. USGS- U.S. Geological Survey, E.H.P. *Implications for Earthquake Risk Reduction in the United States from the Kocaeli, Turkey, Earthquake of August 17, 1999*
2000 Monday 19th December, 2005; Available from: http://pubs.usgs.gov/circ/2000/c1193/.
58. USGS- U.S. Geological Survey, E.H.P. *Earthquake Archives*. 2009 May 27 2009 [cited 2009 June]; Available from: http://earthquake.usgs.gov/eqcenter/eqinthenews/.

59. USGS- U.S. Geological Survey, E.H.P. *Earthquake Glossary*. 2009 November 03, 2009 [cited 2010 March]; Available from: http://earthquake.usgs.gov/learn/glossary/?term=fault plane.

60. USGS- U.S. Geological Survey, E.H.P. *Magnitude 6.3- L'Aquila, Italy Earthquake of 06 April 2009* 2009 October 15, 2009 [cited 2009 July]; Available from: http://earthquake.usgs.gov/earthquakes/eqinthenews/2003/uscvad/ http://earthquake.usgs.gov/earthquakes/eqarchives/poster/2009/20090406.php.

61. Wald, L. *Earthquakes 101 (EQ 101)*. unknown October 27, 2009 [cited 2009 December]; Available from: http://earthquake.usgs.gov/learn/classroom.php.

62. Weisstein, E.W. *Standard Deviation*. 2010 3 March 2010; Available from: http://mathworld.wolfram.com/StandardDeviation.html.

63. Wikipedia. *2009 L'Aquila Earthquake*. 2009 26th June 2009 [cited 2009 June]; Available from: http://en.wikipedia.org/wiki/2009_L'Aquila_earthquake.

64. Wikipedia. *Aspect (geography)*. 2009 21 December 2009 [cited 2010 January]; Available from: <http://en.wikipedia.org/wiki/Aspect_(geography)>.

65. Wikipedia. *Empirical*. 2010 February 2010 [cited 2010 March]; Available from: http://en.wikipedia.org/wiki/Empirical.

66. Wikipedia. *L'Aquila*. 2010 9 February 2010 [cited 2010 February]; Available from: http://en.wikipedia.org/wiki/L%27Aquila.

Appendix A: Radiation Definitions

Definitions and relationship associated with radiation measurements, extracted from Lillesand (2008) [26]:

Terms & Definition	Symbol	Unit
Radiant energy- the energy carried by an electromagnetic wave and a measure of the capacity of the wave to do work	Q	J
Radiant flux- the amount of radiant energy emitted, transmitted, or received per unit time	φ	W (=Js^{-1})
Radiant flux density- the radiant flux at a surface divided by the area of the surface. Irradiance- the density for flux incident upon a surface Radiant exitance- the density for flux leaving a surface	 E M	Wm^{-2}
Radiant spectral flux density- the radiant flux density per unit wavelength interval Spectral irradiance Spectral radiant exitance	 E_λ M_λ	Wm^{-2}µm^{-1}
Radiant intensity-t he flux emanating from a point source per unit solid angle in the direction considered	I	Wsr^{-1}
Radiance- the radiant flux per unit solid angle emanating from a surface in a given direction per unit of projected surface in the direction considered	L	Wm^{-2}sr^{-1}
Spectral radiance per wavelength interval	L_λ	Wm^{-2}sr^{-1} µm^{-1}

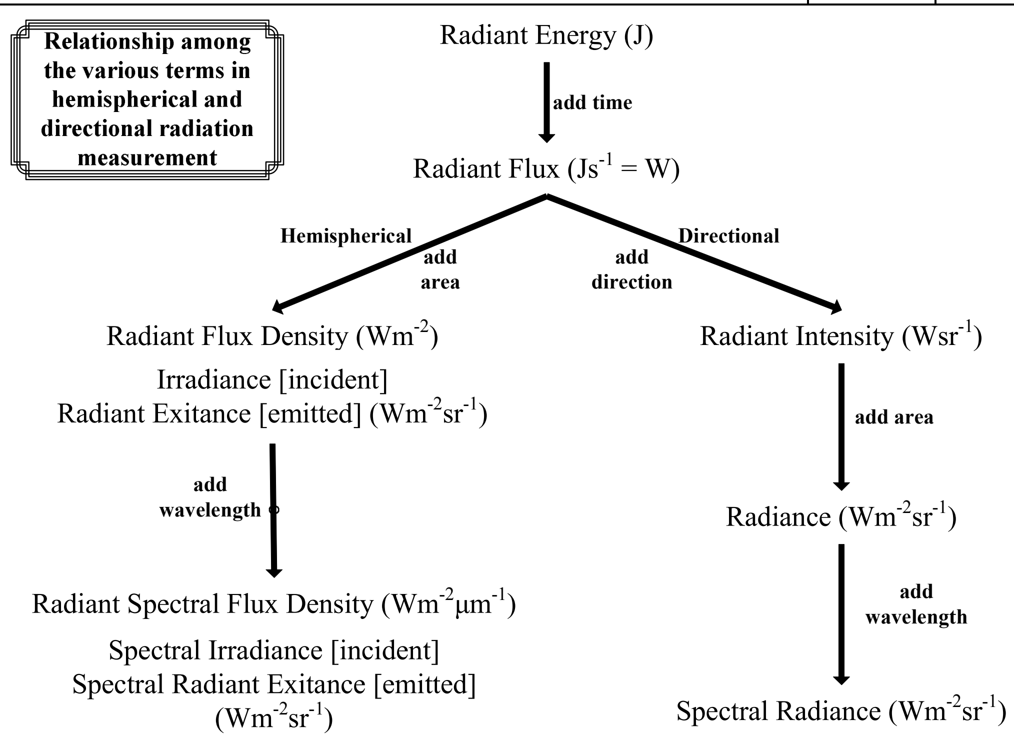

Appendix B- Satellite Specifications

Part (i)

Satellite Specifications (i)

Channel ID	Absorption Band Channel Type	Spectral Band width (µm)	Central Wavelength (µm)	Sub-satellite sampling (km)
VIS 0.7	High Visible Resolution	0.50 to 0.90	0.700	2.5
IR 6.4	Water Vapor Absorption	5.70 to 7.10	6.40	4.5
IR 11.5	IR/ Window Imager	10.50 to 12.50	11.500	4.5
Radiometric Resolution: 8 bits			Temporal Resolution: 30 minutes	
Launch Date: 2nd March 1991			Orbital Longitude: 63°E	
End of Launch: 26th April 2007				

Table 5-1: Meteosat-5 Spectral Channels [10, 40].

Part (ii)

Satellite Specifications (ii)

Channel ID	Absorption Band Channel Type	Spectral Band width (µm)	Central Wavelength (µm)	Sub-satellite sampling (km)	Noise
HRV	High Visible Resolution	0.60 to 0.90	0.750	1	S/N > 4.3 for target of 1% of max dynamic range
VIS 0.6	VNIR Core Imager	0.56 to 0.71	0.635	3	S/N > 10.1 for target of 1% of max dynamic range
VIS 0.8	VNIR Core Imager	0.74 to 0.87	0.810	3	S/N > 7.28 for target of 1% of max dynamic range
IR 1.6	VNIR Core Imager	1.50 to 1.78	1.640	3	S/N > 3 for target of 1% of max dynamic range
IR 3.9	IR/ Window Core Imager	3.48 to 4.36	3.920	3	0.35 K @ 300 K
IR 6.2	Water Vapor Core Imager	5.35 to 7.15	6.250	3	0.75 K @ 250 K
IR 7.3	Water Vapor Pseudo-Sounding	6.85 to 7.85	7.350	3	0.75 K @ 250 K
IR 8.7	IR/ Window Core Imager	8.30 to 9.10	8.700	3	0.28 K @ 300 K
IR 9.7	IR/Ozone Pseudo-Sounding	9.38 to 9.94	9.660	3	1.50 K @ 255 K
IR 10.8	IR/ Window Core Imager	9.80 to 11.80	10.800	3	0.25 K @ 300 K
IR 12.0	IR/ Window Core Imager	11.00 to 13.00	12.000	3	0.37 K @ 300 K
IR 13.4	IR/Carbon Dioxide Pseudo-Sounding	12.40 to 14.40	13.400	3	1.80 K @ 270 K
Radiometric Resolution: 10 bits			Temporal Resolution: 15 minutes		
Launch Date (Meteosat-8): 28th August 2002			Orbital Longitude: 0°E		
Launch Date (Meteosat-9): 21th December 2005					

Table 5-2: MSG SEVIRI (Spinning Enhanced Visible and Infrared Imager) Spectral Channel [13].

Appendix C: Weather conditions in Bam

Weather Conditions for Bam

World Health Organization / Iran-Bam

Official report on Bam Climate by Bam Meteorological Center

Desert Climate; Altitude: 1067 m

Temperature information:
Absolute highest temperature recorded in the past 30 years: 47 °C
Absolute lowest temperature recorded in the past 30 years: -9 °C
Increase in temperature is usually from February and temperatures between 38-44 °C is common in summer

Wind:
Approximately all through the year; max recorded: 133 km/hr; less severe storms are common more at the end of winters and beginning of spring.

Humidity:
Low because of the desert climate

Rain:
Low; average annual precipitation is 61 mm. Some years 10-20 mm has also been recorded. Max recorded: 147 mm

Mr. Massoud Ahmadi
Bam Meteorological Center
13th January 2004

Note: Especial report and forecasts of weather (8 days and 16 days) for Bam can be found at:
- www.accuweather.com (Select “World” then search “Bam”) [1]

Appendix D: Weather conditions in L'Aquila

Weather Conditions for Italy

```
ITALY
Rome City            -8.2  42
Rome Ciampino Air.   -11   40.6
Rome Fiumicino Air.-7.8   38.6
Milan City         -17.3  41.1
Turin City           -21  41.6
Turin Airport      -21.8  37.4
Florence City      -12.9  42
Florence Airport   -23.2  42.6
Venice             -13.5* 36.6     * -17.5C was also recorded in January 1709
Genoa                 -8  37.8
Bologna            -18.8  39.8
Perugia              -17  40
Naples                -5* 40       * a dubious -5.6C also recorded in January
1981
Bari                -5.9  45.6
Palermo Observatory-0.5   44.6*    * a questioned 45.5C also recorded in
August 1885
Cagliari            -4.8  43.7
Catenanuova               48.5
Lampedusa Island     2.2  39.9
Plateau Rosa       -34.6  17.2
Mount Rose           -41  7.3*     * a record of 8.3C in August 2008 is
likely to be faulty
Livigno              -38  29
Gran Gioves          -42
Busa di Manna      -43.8*          * recorded in a frost hollow

Lowest temperature in L'Aquila region ~ -17 °C (255K)
```

Extracted from Maximiliano Herrera web-page [19]

As seen in an updated version of the Wikipedia encyclopaedia for "L'Aquila", the following climatic data for this region was observed. It has been said that the city enjoys each year eleven cold months and one cool one . This data was extracted on the 6th December 2008 by the Meteorological Station in L'Aquila, CETEMPS webpage.

Climate data for L'Aquila

Month	Jan	Feb	Mar	Apr	May	Jun	Jul	Aug	Sep	Oct	Nov	Dec
Record high °C (°F)	17.0 (63)	21.3 (70)	26.0 (79)	31.0 (88)	35.0 (95)	36.0 (97)	41.0 (106)	37.0 (99)	34.0 (93)	29.0 (84)	28.0 (82)	21.0 (70)
Average high °C (°F)	6.6 (44)	8.3 (47)	11.9 (53)	15.1 (59)	20.6 (69)	24.5 (76)	28.2 (83)	27.7 (82)	23.0 (73)	17.6 (64)	11.4 (53)	7.0 (45)
Daily mean °C (°F)	2.5 (37)	3.7 (39)	6.6 (44)	9.6 (49)	14.3 (58)	17.9 (64)	20.9 (70)	20.7 (69)	16.9 (62)	12.2 (54)	7.0 (45)	3.4 (38)
Average low °C (°F)	-1.6 (29)	-1.0 (30)	1.2 (34)	4.0 (39)	8.1 (47)	11.4 (53)	13.6 (56)	13.6 (56)	10.7 (51)	6.8 (44)	2.6 (37)	-0.3 (31)
Record low °C (°F)	-17.0 (1)	-15.0 (5)	-11.7 (11)	-7.3 (19)	-1.0 (30)	6.0 (43)	4.0 (39)	6.0 (43)	0.0 (32)	-3.0 (27)	-9.0 (16)	-17.0 (1)

Obtained from Wikipedia webpage [66]

Appendix E: Scripts

Python Script

- Stacking

```
# import standard modules
import os
import glob
import sys

# import image and array support
import Image
import numpy

# the envi2 module for writing ENVI format images
import envi2
import envi2.constants

# Here comes trouble!
import datetime

# define a generic time zone object
class UTC(datetime.tzinfo):
    def __init__(self, offset):
        self.offset = offset
    def utcoffset(self, dt):
        return datetime.timedelta(hours=self.offset)
    def dst(self, dt):
        return datetime.timedelta(0)
    def tzname(self, dt):
        return "UTC%+d" % (self.offset,)

# set time zone to UTC+0
tzUTC0 = UTC(0)

pattern = r'I:\copy_data_italy\italyLTS\LTS_2009\LST_2009*_IR_108.tif'
output = r'I:\copy_data_italy\italyLTS\LTS_2009\stack'

def to_linear_time(dt):
    ''' takes a datetime object
returns prolectic Gregorian ordinal (=days since 01-01-0001)
plus a fraction of the day
'''
    return dt.toordinal() +
(((dt.second/60.0)+dt.minute)/60.0+dt.hour)/24.0

def from_linear_time(lt):
    '''takes a prolectic Gregorian ordinal plus fraction of day
returns a datetime object
'''
    return datetime.datetime.fromordinal(int(lt)) +
datetime.timedelta(lt%1)
```

```
# test to read a TIFF

fnames = sorted(glob.glob(pattern))

bands = len(fnames)

print "Found %d files" % (bands,)

# open one image to get info
im = Image.open(fnames[0])

samples, lines = im.size

# assuming 16-bit data
if im.mode == 'I;16':
    data_type = 'H' # 'h' is signed, 'H' is unsigned 16 bit
else:
##    raise ValueError('Unsupported image mode')
    data_type = 'u1'
    print 'Assuming 8-bit data'

# figure out byte order of the machine
if sys.byteorder == 'little':
    byte_order = 0
else:
    byte_order = 1

# map info obtained from GeoTIFF tags (don't ask!)
try:
    map_info = ['Arbitrary', 1.0, 1.0, im.ifd[33922][3], im.ifd[33922][4],
                im.ifd[33550][0], im.ifd[33550][1], 0, 'units=Degrees']
except:
    map_info = None

print map_info

#raise IOError

del im

# loop over file names to get time stamps of images
wavelength = []
band_names = []
for fname in fnames:
##    print fname
    base = os.path.basename(fname)
##    t = base.split('_')[1]
    t = base.split('-')[-1][:12]
    band_names.append(t)
##    print t
    year, month, day, hour, minute = map(int, (t[:4], t[4:6], t[6:8],
t[8:10], t[10:]))
```

```
    dt = datetime.datetime(year, month, day, hour, minute, 0, 0,
tzinfo=tzUTC0)

    ltime = to_linear_time(dt)
##    print ltime
##    print from_linear_time(ltime)

    # add linear time to the list of 'wavelengths'
    wavelength.append(ltime)

# open the output image
im2 = envi2.New(output, file_type=envi2.constants.ENVI_Standard,
                data_type=data_type, interleave='bsq',
byte_order=byte_order,
                lines=lines, samples=samples, bands=bands,
                wavelength=wavelength, descripion=['GeoTIFF to ENVI
stacker'],
                wavelength_units='Gregorian day', z_plot_titles=['time',
'value'],
                map_info=map_info, band_names=band_names)

# and here we go...
band = 0
for fname in fnames:
##    print fname
#    fp = open(fname)
    try:
        im = Image.open(fname)
    except IOError:
        print band
        raise
    im.load()
##    im2[band] = numpy.asarray(im.getdata())
    # again, DON'T ASK!!!
    im2[band] = numpy.array(im.getdata()).reshape(im.size[::-1])
#    fp.close()
    del im
    band = band + 1

del im2
```

- Conversion of DN to Radiances to BT (comprises two scripts namely, calibration.py and meteosat.py)

(i) calibration.py:

```
from gregorian import *
from numpy import array

YEARS = [1999, 2000, 2001, 2002, 2003, 2004]

cname = 'Meteosat/IR_Calibration_info_'

mon2mon = {'Jan':1,
           'Feb':2,
           'Mar':3,
```

```
               'Apr':4,
               'May':5,
               'Jun':6,
               'Jul':7,
               'Aug':8,
               'Sep':9,
               'Oct':10,
               'Nov':11,
               'Dec':12}

def read_calibration(year, name):
    f = open(name)
    data = f.readlines()
    f.close()

    calib = []
    for line in data:
        dayofyear, daymonth, slot, coeff, spacecount =
line.strip().split()
        day, month = daymonth.split('-')
        day = int(day)
        month = mon2mon[month]
        hour = (int(slot)-1)/2.0    # does it include the slot or not?
        minute = int(hour%1 * 60)
        hour = int(hour)
        coeff = float(coeff)
        spacecount = float(spacecount)

        # Proleptic Gregorian time...
        ltime = to_linear_time(year, month, day, hour, minute)

        calib.append((ltime, year, month, day, hour, minute, coeff,
spacecount))
    return calib

calibration = []
for year in YEARS:
    name = cname + str(year) + '.txt'
    calibration.extend(read_calibration(year, name))

calibration_index = array([x[0] for x in calibration])

def get_coeffs(year, month, day, hour, minute):
    # Proleptic Gregorian time...
    ltime = to_linear_time(year, month, day, hour, minute)

    # add 4 minutes to be sure to fall inside a slot
    index = calibration_index.searchsorted(ltime+0.003)

    if index > 0:
        index = index - 1
    return calibration[index]


if __name__=='__main__':
```

```
    print get_coeffs(2003, 2, 1, 11, 0)
    #(731246.0625, 2003, 1, 31, 1, 30, 0.074721999999999997, 5.0)
```

(ii) meteosat.py

```
# import standard modules
import os
import glob
import sys

# import image and array support
import Image
import numpy

# the envi2 module for writing ENVI format images
import envi2
import envi2.constants

# local modules
import gregorian
import timestr
import calibration

def message(s):
    print s

def convert_meteosat(pattern, output, message=message):
    # figure out input files from the pattern

    fnames = sorted(glob.glob(pattern))

    bands = len(fnames)

    message("Found %d files" % (bands,))

    if not bands:
        return

    # open one image to get info
    im = Image.open(fnames[0])

    samples, lines = im.size

    # assuming 16-bit data
    if im.mode == 'I;16':
        data_type = 'H' # 'h' is signed, 'H' is unsigned 16 bit
        message("Data type: 2-byte")
        is_calibrated = True
    elif im.mode.startswith('F'):
        data_type = 'single'
        message("Data type: 4-byte single float")
        is_calibrated = True
    else:
        data_type = 'u1' # cross your fingers here...
        message("Data type: assuming 1-byte")
```

```
        is_calibrated = False
    ##    raise ValueError('Unsupported image mode')

    # figure out byte order of the machine
    if sys.byteorder == 'little':
        byte_order = 0
    else:
        byte_order = 1

    try:
        # map info obtained from GeoTIFF tags (don't ask!)
        map_info = ['Arbitrary', 1.0, 1.0, im.ifd[33922][3],
im.ifd[33922][4],
                    im.ifd[33550][0], im.ifd[33550][1], 0, 'units=Degrees']
    except KeyError:
        map_info = None

    message("Map info: %s" % (str(map_info),))

    del im

    # loop over file names to get time stamps of images
    wavelength = []
    band_names = []
    for fname in fnames:
        base = os.path.basename(fname)
        message("Inspecting '%s'" % (base,))

        year, month, day, hour, minute = timestr.time_from_string(base)
        band_names.append("%4d%02d%02d%02d%02d" % (year, month, day, hour,
minute))

        ltime = gregorian.to_linear_time(year, month, day, hour, minute)
        message("Linear time: %f" % (ltime,))
##        print gregorian.from_linear_time(ltime)

        # add linear time to the list of 'wavelengths'
        wavelength.append(ltime)

    # open the output image
    im2 = envi2.New(output, file_type=envi2.constants.ENVI_Standard,
                    data_type='single', interleave='bsq',
byte_order=byte_order,
                    lines=lines, samples=samples, bands=bands,
                    wavelength=wavelength, descripion=['GeoTIFF to ENVI
stacker'],
                    wavelength_units='Gregorian day',
z_plot_titles=['time', 'value'],
                    map_info=map_info, band_names=band_names)

    # and here we go...
    band = 0
    for fname in fnames:
        try:
            im = Image.open(fname)
```

```
        except IOError, errtext:
            raise IOError('%s on file %s band %d' % (errtext, fname, band))

        base = os.path.basename(fname)

        if is_calibrated:
            message("Convering: %s" % (base,))
            message('Calibration SKIPPED')

            im.load()
            # again, DON'T ASK!!!
            BT = numpy.array(im.getdata()).reshape(im.size[::-1])
        else:
            year, month, day, hour, minute = timestr.time_from_string(base)
            calib = calibration.get_coeffs(year, month, day, hour, minute)

            alpha = calib[-2]
            space_count = calib[-1]

            message("Calibrating: %s" % (base,))
            message('Calibration data: %f %f' % (alpha, space_count))

            im.load()
            # again, DON'T ASK!!!
            data = numpy.array(im.getdata()).reshape(im.size[::-1])

            # convert to radiance
            radiance = alpha * (data - space_count)

            # convert to brightness temperature
            A = 6.7348
            B = -1272.2
            BT = B / (numpy.log(radiance) - A)

        message("Average scene brightness temperature: %.1f Kelvin" %
(BT.mean()))

        im2[band] = BT

        del im
        band = band + 1

    del im2

if __name__=='__main__':
    pattern = r'/data/Data/Nadira/format1/*.tif'
    output = r'/data/Data/Nadira/format1/stack'

    convert_meteosat(pattern, output)
```

- Time Series for one pixel

```
import envi2
import timeutil
import gregorian

#### INPUT PARAMETERS

im = envi2.Open(r'K:\Bam_1999\images\stack1999')
#im = envi2.Open(r'K:\sample\italy\stack2006')

Y = 20
X = 20

#### ANALYSE DATA

# get the band names as strings (from envi2 they come out as longs)
band_names = [str(bn) for bn in im.band_names]

has_quarters = False
for band in range(im.bands):
    bname = band_names[band]
    year, month, day, hour, minute = timeutil.time_unpack(bname)
    # check if this data has quarters in it
    if minute==15 or minute==45:
        has_quarters = True
##    print "%s;%f;%f" % (bname, im.wavelength[band], series[band])

if has_quarters:
##    print "15 minute data"
    delta = 15
else:
##    print "30 minute data"
    delta = 30

#### REPLACE MISSING VALUES

# get the complete time range
timerange =
timeutil.time_pack_seq(timeutil.timerange(timeutil.time_unpack(band_names[0
]),
                               timeutil.time_unpack(band_names[-1]),
delta))
##print timerange

result = []
for t in timerange:
    # check if this time is in the data
    try:
        band = band_names.index(t)
        value = im[Y, X, band]
    # otherwise give it a NaN value
    except ValueError:
        value = float('nan')
```

```
    # append value to the result list
    result.append(value)

    # get the proleptic gregorian day
    gt = gregorian.to_linear_time(*timeutil.time_unpack(t))

    # print everything
    print "%s;%f;%f" % (t, gt, value)

### OR, print in 'yyyy-mm-dd hh:mm' format
##    year, month, day, hour, minute = timeutil.time_unpack(t)
##    print "%4d-%02d-%02d %02d:%02d;%f;%f" % (year, month, day, hour,
minute, gt, value)

### OR do something with the result list
##print result
```

PERL Script

- Cloud Masking

```
########################################################################
#Cloud removal algorithm. Will remove anything that is below min+(0.95*max-
min)-20 (abs min + range - allowed variation)
# applied per image. pxls per time are extracted from pxl files and
corrected before being written away in CLOUDREMOVED folder
sub CLOUD {

#$nr_images = 0;
$nr_pixels = 0;
$min_temp = 260;
$variation = 20;

# create array of files to be opened, can be called through indexing
open (PIXELS, "test.lst") || die "can't open file data.lst: $!"; # open
list with all files to be processed
while (defined (my $pixels = <PIXELS>)){ # go through list and open every
file in sequence
       $nr_pixels++;
       chomp ($pixels);
       push (@location, $pixels);
}
close (PIXELS);
print "nr of pixels is, $nr_pixels\n";

################################################################
############# LOOP 1
# create matrix of all files
for ($p=0; $p<=$nr_pixels-1; $p++) {
       open (PIXEL, "$location[$p]") || die "can't open file pixel file
$location[$i] : $!";
       print "opened file $location[$p]\n";
       $i=0;
```

```
	while (defined (my $pixel = <PIXEL>)){  # go through every file and
use counter p for location of value in matrix

#		my @pixel = split (/,/, $pixel);
		if ($i <= 4303){
			chomp ($pixel);
			$m_value[$p][$i] = $pixel;
		}
		$i++;
	}
	close (PIXEL);
}

$nr_images = 4304;
print "nr of images is, $nr_images\n";

#calculate min and max for each image and add treshold to matrix
for ($i=0; $i<=$nr_images-1; $i++) { #take every line from each file as
part of the image it belonged to.
	$min = 1000; $max = 0;

print "calculate min/max for image $i\n";

	for  ($p=0; $p<=$nr_pixels-1; $p++) { #loop over all pixels in image
		if ($m_value[$p][$i] > $max){$max = $m_value[$p][$i];}
		if ($m_value[$p][$i] < $min){$min = $m_value[$p][$i];}
	}
	# put treshold at last position of matrix for studied image
	$m_value[$nr_pixels][$i] = $min + (0.95*$max - $min) - $variation;
	print "for image $i min,max,treshold is: $min, $max,
$m_value[$nr_pixels][$i]\n";
}

#remove clouds based in treshold
for ($i=0; $i<=$nr_images-1; $i++) { #take every line from each file as
part of the image it belonged to.

print "calculate cloudremoval for image $i\n";

	for  ($p=0; $p<=$nr_pixels-1; $p++) {
		if ($m_value[$p][$i] < $m_value[$nr_pixels][$i] ||
$m_value[$p][$i] < $min_temp){
			print "pixel is $m_value[$p][$i], treshold is
$m_value[$nr_pixels][$i]\n";
			$m_value[$p][$i] = "NaN";
		}
	}
}

#write data back to file
print "write back to files started\n";
for ($p=0; $p<=$nr_pixels-1; $p++) {
	open (OUT, ">>$location[$p]_CR_20_$min_temp") || die "can't open file
pixel file $location[$i] : $!";
```

```
	for ($i=0; $i<=$nr_images-1; $i++) { #take every line from each file
as part of the image it belonged to.
#		print OUT "$m_time[$p][$i], $m_value[$p][$i]\n";
		print OUT "$m_value[$p][$i]\n";
	}
	close (OUT);
}


################################################################
########### LOOP 2
# create matrix of all files
for ($p=0; $p<=$nr_pixels-1; $p++) {
	open (PIXEL, "$location[$p]") || die "can't open file pixel file
$location[$i] : $!";
	print "opened file $location[$p]\n";
	$i=0;
	while (defined (my $pixel = <PIXEL>)){  # go through every file and
use counter p for location of value in matrix

#		my @pixel = split (/,/, $pixel);
		if ($i > 4303 && $i <=8607){
			$j= $i-4304;
			chomp ($pixel);
			$m_value[$p][$j] = $pixel;
		}

#		$m_time[$p][$i] = $pixel[0];
		$i++;
	}
	close (PIXEL);
}
$nr_images = 4304;
print "nr of images is, $nr_images\n";

#calculate min and max for each image and add treshold to matrix
for ($i=0; $i<=$nr_images-1; $i++) { #take every line from each file as
part of the image it belonged to.
	$min = 1000; $max = 0;

print "calculate min/max for image $i\n";

	for  ($p=0; $p<=$nr_pixels-1; $p++) { #loop over all pixels in image
		if ($m_value[$p][$i] > $max){$max = $m_value[$p][$i];}
		if ($m_value[$p][$i] < $min){$min = $m_value[$p][$i];}
	}
	# put treshold at last position of matrix for studied image
	$m_value[$nr_pixels][$i] = $min + (0.95*$max - $min) - $variation;
### ADJUST HERE YOUR ALLOWED VARIATION IN TEMP!!!!
	print "for image $i min,max,treshold is: $min, $max,
$m_value[$nr_pixels][$i]\n";
}

#remove clouds based in treshold
```

```
for ($i=0; $i<=$nr_images-1; $i++) { #take every line from each file as
part of the image it belonged to.

print "calculate cloudremoval for image $i\n";

	for  ($p=0; $p<=$nr_pixels-1; $p++) {
		if ($m_value[$p][$i] < $m_value[$nr_pixels][$i] ||
$m_value[$p][$i] < $min_temp){
#			print "pixel is $m_value[$p][$i], treshold is
$m_value[$nr_pixels][$i]\n";
			$m_value[$p][$i] = "NaN";
		}
	}
}

#write data back to file
print "write back to files started\n";
for ($p=0; $p<=$nr_pixels-1; $p++) {
	open (OUT, ">>$location[$p]_CR_20_$min_temp") || die "can't open file
pixel file $location[$i] : $!";
	for ($i=0; $i<=$nr_images-1; $i++) { #take every line from each file
as part of the image it belonged to.
#		print OUT "$m_time[$p][$i], $m_value[$p][$i]\n";
		print OUT "$m_value[$p][$i]\n";
	}
	close (OUT);
}



################################################################
########### LOOP 3
# create matrix of all files
for ($p=0; $p<=$nr_pixels-1; $p++) {
	open (PIXEL, "$location[$p]") || die "can't open file pixel file
$location[$i] : $!";
	print "opened file $location[$p]\n";
	$i=0;
	while (defined (my $pixel = <PIXEL>)){  # go through every file and
use counter p for location of value in matrix
#		my @pixel = split (/,/, $pixel);

		if ($i > 8607 && $i <= 12911){
			$j= $i-8608;
			chomp ($pixel);
			$m_value[$p][$j] = $pixel;
		}

#		$m_time[$p][$i] = $pixel[0];
		$i++;
	}
	close (PIXEL);
}
$nr_images = 4304;
print "nr of images is, $nr_images\n";
```

```
#calculate min and max for each image and add treshold to matrix
for ($i=0; $i<=$nr_images-1; $i++) { #take every line from each file as
part of the image it belonged to.
	$min = 1000; $max = 0;

print "calculate min/max for image $i\n";

	for  ($p=0; $p<=$nr_pixels-1; $p++) { #loop over all pixels in image
		if ($m_value[$p][$i] > $max){$max = $m_value[$p][$i];}
		if ($m_value[$p][$i] < $min){$min = $m_value[$p][$i];}
	}
	# put treshold at last position of matrix for studied image
	$m_value[$nr_pixels][$i] = $min + (0.95*$max - $min) - $variation;
### ADJUST HERE YOUR ALLOWED VARIATION IN TEMP!!!!
	print "for image $i min,max,treshold is: $min, $max,
$m_value[$nr_pixels][$i]\n";
}

#remove clouds based in treshold
for ($i=0; $i<=$nr_images-1; $i++) { #take every line from each file as
part of the image it belonged to.

print "calculate cloudremoval for image $i\n";

	for  ($p=0; $p<=$nr_pixels-1; $p++) {
		if ($m_value[$p][$i] < $m_value[$nr_pixels][$i] ||
$m_value[$p][$i] < $min_temp){
#			print "pixel is $m_value[$p][$i], treshold is
$m_value[$nr_pixels][$i]\n";
			$m_value[$p][$i] = "NaN";
		}
	}
}

#write data back to file
print "write back to files started\n";
for ($p=0; $p<=$nr_pixels-1; $p++) {
	open (OUT, ">>$location[$p]_CR_20_$min_temp") || die "can't open file
pixel file $location[$i] : $!";
	for ($i=0; $i<=$nr_images-1; $i++) { #take every line from each file
as part of the image it belonged to.
#		print OUT "$m_time[$p][$i], $m_value[$p][$i]\n";
		print OUT "$m_value[$p][$i]\n";
	}
	close (OUT);
}

################################################################
########### LOOP 4
# create matrix of all files
for ($p=0; $p<=$nr_pixels-1; $p++) {
	open (PIXEL, "$location[$p]") || die "can't open file pixel file
$location[$i] : $!";
	print "opened file $location[$p]\n";
```

```
	$i=0;
	while (defined (my $pixel = <PIXEL>)){  # go through every file and 
use counter p for location of value in matrix

#		my @pixel = split (/,/, $pixel);

		if ($i > 12911 && $i <= 17215){
			$j= $i-12912;
			chomp ($pixel);
			$m_value[$p][$j] = $pixel;
		}

#		$m_time[$p][$i] = $pixel[0];
		$i++;
	}
	close (PIXEL);
}
$nr_images = 4304;
print "nr of images is, $nr_images\n";

#calculate min and max for each image and add treshold to matrix
for ($i=0; $i<=$nr_images-1; $i++) { #take every line from each file as 
part of the image it belonged to.
	$min = 1000; $max = 0;

print "calculate min/max for image $i\n";

	for  ($p=0; $p<=$nr_pixels-1; $p++) { #loop over all pixels in image
		if ($m_value[$p][$i] > $max){$max = $m_value[$p][$i];}
		if ($m_value[$p][$i] < $min){$min = $m_value[$p][$i];}
	}
	# put treshold at last position of matrix for studied image
	$m_value[$nr_pixels][$i] = $min + (0.95*$max - $min) - $variation; 
### ADJUST HERE YOUR ALLOWED VARIATION IN TEMP!!!!
	print "for image $i min,max,treshold is: $min, $max, 
$m_value[$nr_pixels][$i]\n";
}

#remove clouds based in treshold
for ($i=0; $i<=$nr_images-1; $i++) { #take every line from each file as 
part of the image it belonged to.

print "calculate cloudremoval for image $i\n";

	for  ($p=0; $p<=$nr_pixels-1; $p++) {
		if ($m_value[$p][$i] < $m_value[$nr_pixels][$i] || 
$m_value[$p][$i] < $min_temp){
#			print "pixel is $m_value[$p][$i], treshold is 
$m_value[$nr_pixels][$i]\n";
			$m_value[$p][$i] = "NaN";
		}
	}
}

#write data back to file
```

```
print "write back to files started\n";
for ($p=0; $p<=$nr_pixels-1; $p++) {
	open (OUT, ">>$location[$p]_CR_20_$min_temp") || die "can't open file
pixel file $location[$i] : $!";
	for ($i=0; $i<=$nr_images-1; $i++) { #take every line from each file
as part of the image it belonged to.
#		print OUT "$m_time[$p][$i], $m_value[$p][$i]\n";
		print OUT "$m_value[$p][$i]\n";
	}
	close (OUT);
}

##############################################################
########### LOOP 5
# create matrix of all files
for ($p=0; $p<=$nr_pixels-1; $p++) {
	open (PIXEL, "$location[$p]") || die "can't open file pixel file
$location[$i] : $!";
	print "opened file $location[$p]\n";
	$i=0;
	while (defined (my $pixel = <PIXEL>)){  # go through every file and
use counter p for location of value in matrix

#		my @pixel = split (/,/, $pixel);

		if ($i > 17215 && $i <= 17226){
			$j= $i-17215;
			chomp ($pixel);
			$m_value[$p][$j] = $pixel;
		}

#		$m_time[$p][$i] = $pixel[0];
		$i++;
	}
	close (PIXEL);
}
$nr_images = 12;
print "nr of images is, $nr_images\n";

#calculate min and max for each image and add treshold to matrix
for ($i=0; $i<=$nr_images-1; $i++) { #take every line from each file as
part of the image it belonged to.
	$min = 1000; $max = 0;

print "calculate min/max for image $i\n";

	for  ($p=0; $p<=$nr_pixels-1; $p++) { #loop over all pixels in image
		if ($m_value[$p][$i] > $max){$max = $m_value[$p][$i];}
		if ($m_value[$p][$i] < $min){$min = $m_value[$p][$i];}
	}
	# put treshold at last position of matrix for studied image
	$m_value[$nr_pixels][$i] = $min + (0.95*$max - $min) - $variation;
### ADJUST HERE YOUR ALLOWED VARIATION IN TEMP!!!!
	print "for image $i min,max,treshold is: $min, $max,
$m_value[$nr_pixels][$i]\n";
```

```
}

#remove clouds based in treshold
for ($i=0; $i<=$nr_images-1; $i++) { #take every line from each file as
part of the image it belonged to.

print "calculate cloudremoval for image $i\n";

	for  ($p=0; $p<=$nr_pixels-1; $p++) {
		if ($m_value[$p][$i] < $m_value[$nr_pixels][$i] ||
$m_value[$p][$i] < $min_temp){
#			print "pixel is $m_value[$p][$i], treshold is
$m_value[$nr_pixels][$i]\n";
			$m_value[$p][$i] = "NaN";
		}
	}
}

#write data back to file
print "write back to files started\n";
for ($p=0; $p<=$nr_pixels-1; $p++) {
	open (OUT, ">>$location[$p]_CR_20_$min_temp") || die "can't open file
pixel file $location[$i] : $!";
	for ($i=0; $i<=$nr_images-1; $i++) { #take every line from each file
as part of the image it belonged to.
#		print OUT "$m_time[$p][$i], $m_value[$p][$i]\n";
		print OUT "$m_value[$p][$i]\n";
	}
	close (OUT);
}


} # end of subroutine
```

- Anomaly Detection

```
######################anomaly detection algorithm######################

sub ANOMALY {

$kernel = 10;
$nr_l = 80;
$nr_c = 73;

#$kernel = 1;
#$nr_l = 2;
#$nr_c = 2;

for ($l=1; $l <= $nr_l; $l++){
	for ($c=1; $c <= $nr_c; $c++){
		$i=0;

	#PIXEL COUNTER
```

```
            print " working on pixel $l,$c\n";

            open (OUT, ">ANOMALY/2001L$l\C$c\_CR_20_260_ANOM") || die
"can't open anomaly output file: $!";

            open (PIXEL, "DATA_TIME/2001L$l\C$c\_CR_20_260") || die "can't
open file pixel file: $!";
            $j=0;
            while (defined (my $pixel = <PIXEL>)){
      #add central pxl to matrix at (0,0)
                  chomp ($pixel);
                  my @pixel = split (/,/, $pixel);
                  $matrix[$i][$j] = $pixel[1];
                  $time[$j] = $pixel[0];
                  $j++;
            }
            $max_times = $j;
            close (PIXEL);

#upper part
            $l_k = $l - $kernel;                                          #
shift to upper line and check if exists
            if ($l_k >= 1) {
                  print "working on upper part\n";
                  $i++;

                  open (PIXEL, "DATA_TIME/2001L$l_k\C$c\_CR_20_260") ||
die "can't open file pixel file: $!";
                  $j=0;
                  while (defined (my $pixel = <PIXEL>)){
            #add central pxl to matrix at (0,0)
                        chomp ($pixel);
                        my @pixel = split (/,/, $pixel);
                        $matrix[$i][$j] = $pixel[1];
                        $j++;
                  }
                  close (PIXEL);

                        # if line exists, shift columns and check if
exists
                  for ($k=1; $k <= $kernel; $k++){

                        $c_k = $c - $k;
                        if ($c_k >= 1) {
                              $i++;
                              open (PIXEL,
"DATA_TIME/2001L$l_k\C$c_k\_CR_20_260") || die "can't open file pixel file:
$!";  #CHECK IF NAME WILL WORK
                              $j=0;
                              while (defined (my $pixel = <PIXEL>)){

                                    chomp ($pixel);
                                    my @pixel = split (/,/, $pixel);
                                    $matrix[$i][$j] = $pixel[1];
                                    $j++;
```

```
                                }
                                close (PIXEL);
                        }

                        $c_k = $c + $k;
                        if ($c_k <= $nr_c) {
                                $i++;
                                open (PIXEL,
"DATA_TIME/2001L$l_k\C$c_k\_CR_20_260") || die "can't open file pixel file:
$!";  #CHECK IF NAME WILL WORK
                                $j=0;
                                while (defined (my $pixel = <PIXEL>)){

                                        chomp ($pixel);
                                        my @pixel = split (/,/, $pixel);
                                        $matrix[$i][$j] = $pixel[1];
                                        $j++;
                                }
                                close (PIXEL);
                        }
                }
        }


#lower part
        $l_k = $l + $kernel;                                            #
shift to upper line and check if exists
        if ($l_k <= $nr_l) {
                $i++;
                print "working on lower part\n";

                open (PIXEL, "DATA_TIME/2001L$l_k\C$c\_CR_20_260") ||
die "can't open file pixel file: $!";
                $j=0;
                while (defined (my $pixel = <PIXEL>)){
        #add central pxl to matrix at (0,0)
                        chomp ($pixel);
                        my @pixel = split (/,/, $pixel);
                        $matrix[$i][$j] = $pixel[1];
                        $j++;
                }
                close (PIXEL);

                        # if line exists, shift columns and check if
exists
                for ($k=1; $k <= $kernel; $k++){

                        $c_k = $c - $k;
                        if ($c_k >= 1) {
                                $i++;
                                open (PIXEL,
"DATA_TIME/2001L$l_k\C$c_k\_CR_20_260") || die "can't open file pixel file:
$!";  #CHECK IF NAME WILL WORK
                                $j=0;
```

```
                                while (defined (my $pixel = <PIXEL>)){

                                        chomp ($pixel);
                                        my @pixel = split (/,/, $pixel);
                                        $matrix[$i][$j] = $pixel[1];
                                        $j++;
                                }
                                close (PIXEL);
                        }

                        $c_k = $c + $k;
                        if ($c_k <= $nr_c) {
                                $i++;
                                open (PIXEL,
"DATA_TIME/2001L$l_k\C$c_k\_CR_20_260") || die "can't open file pixel file:
$!";  #CHECK IF NAME WILL WORK
                                $j=0;
                                while (defined (my $pixel = <PIXEL>)){

                                        chomp ($pixel);
                                        my @pixel = split (/,/, $pixel);
                                        $matrix[$i][$j] = $pixel[1];
                                        $j++;
                                }
                                close (PIXEL);
                        }
                }
        }

#left part
        $c_k = $c - $kernel;                                            #
shift to upper line and check if exists
        if ($c_k >= 1) {
                print "working on left part\n";
                $i++;

                open (PIXEL, "DATA_TIME/2001L$l\C$c_k\_CR_20_260") ||
die "can't open file pixel file: $!";
                $j=0;
                while (defined (my $pixel = <PIXEL>)){
        #add central pxl to matrix at (0,0)
                        chomp ($pixel);
                        my @pixel = split (/,/, $pixel);
                        $matrix[$i][$j] = $pixel[1];
                        $j++;
                }
                close (PIXEL);

                        # if line exists, shift columns and check if
exists
                for ($k=1; $k <= $kernel-1; $k++){

                        $l_k = $l - $k;
                        if ($l_k >= 1) {
                                $i++;
```

```
                                open (PIXEL,
"DATA_TIME/2001L$l_k\C$c_k\_CR_20_260") || die "can't open file pixel file:
$!";  #CHECK IF NAME WILL WORK
                                $j=0;
                                while (defined (my $pixel = <PIXEL>)){

                                        chomp ($pixel);
                                        my @pixel = split (/,/, $pixel);
                                        $matrix[$i][$j] = $pixel[1];
                                        $j++;
                                }
                                close (PIXEL);
                        }

                        $l_k = $l + $k;
                        if ($l_k <= $nr_l) {
                                $i++;
                                open (PIXEL,
"DATA_TIME/2001L$l_k\C$c_k\_CR_20_260") || die "can't open file pixel file:
$!";  #CHECK IF NAME WILL WORK
                                $j=0;
                                while (defined (my $pixel = <PIXEL>)){

                                        chomp ($pixel);
                                        my @pixel = split (/,/, $pixel);
                                        $matrix[$i][$j] = $pixel[1];
                                        $j++;
                                }
                                close (PIXEL);
                        }
                }
        }

#right part
        $c_k = $c + $kernel;                                            #
shift to upper line and check if exists
        if ($c_k <= $nr_c) {
                print "working on right part\n";
                $i++;

                open (PIXEL, "DATA_TIME/2001L$l\C$c_k\_CR_20_260") ||
die "can't open file pixel file: $!";
                $j=0;
                while (defined (my $pixel = <PIXEL>)){
        #add central pxl to matrix at (0,0)
                        chomp ($pixel);
                        my @pixel = split (/,/, $pixel);
                        $matrix[$i][$j] = $pixel[1];
                        $j++;
                }
                close (PIXEL);

                        # if line exists, shift columns and check if
exists
                for ($k=1; $k <= $kernel-1; $k++){
```

```
                              $l_k = $l - $k;
                              if ($l_k >= 1) {
                                     $i++;
                                     open (PIXEL,
"DATA_TIME/2001L$l_k\C$c_k\_CR_20_260") || die "can't open file pixel file:
$!";  #CHECK IF NAME WILL WORK
                                     $j=0;
                                     while (defined (my $pixel = <PIXEL>)){

                                            chomp ($pixel);
                                            my @pixel = split (/,/, $pixel);
                                            $matrix[$i][$j] = $pixel[1];
                                            $j++;
                                     }
                                     close (PIXEL);
                              }

                                     $l_k = $l + $k;
                              if ($l_k <= $nr_l) {
                                     $i++;
                                     open (PIXEL,
"DATA_TIME/2001L$l_k\C$c_k\_CR_20_260") || die "can't open file pixel file:
$!";  #CHECK IF NAME WILL WORK
                                     $j=0;
                                     while (defined (my $pixel = <PIXEL>)){

                                            chomp ($pixel);
                                            my @pixel = split (/,/, $pixel);
                                            $matrix[$i][$j] = $pixel[1];
                                            $j++;
                                     }
                                     close (PIXEL);
                              }
                       }
               }
               $max_images = $i;

               print "used $max_images pixels for background with $max_times
timestamps each\n";

### ANOMALY CALCULATION
               for ($j = 0; $j <= $max_times-1; $j++) {
                       $sum = 0; $image_used = 0;
                       for ($i = 1; $i <= $max_images; $i++) {
#                             print "matrix value = $matrix[$i][$j]\n";
                              if ($matrix[$i][$j] != NaN) {
                                     $image_used++;
                                     $sum = $sum + $matrix[$i][$j];
                              }
                       }
#                      print "sum is $sum for $image_used images used\n";
                       if ($sum == NaN) {
                              $anomaly = "NaN";
                       } else {
```

```
#                           $background  = $sum/$image_used;
                            $anomaly = ($matrix[0][$j] / $sum) * $image_used;
                    #replace original value with anomaly
                    }
                    print OUT "$time[$j], $anomaly\n";
             }
             close (OUT);
      }
}

} # end of subroutine
```

Appendix F: HANTS cloud removal

Procedure taken in HANTS to obtain cloud free images

(1) Meteosat-5 TIR images are of data type, floating point. This data type needs to be converted into an integer type [fix((b1-273.15)*100)] to be used in HANTS.

(2) Processing of time series imagery in HANTS is executed on a single-interleaved image file (BIL). Input of Meteosat-5 are in band sequential format(BSQ) so a conversion from BSQ to BIL is needed (NB: The header files were edited, so for an image of Sample 73, Line 80 and Bands 17078, the new header information contains Sample 5840, Line 17078 and Bands 1).

(3) Output is a single image file in BIL without cloud contaminated observations.

(4) This final image was converted back into a BSQ format (Sample 73, Line 80 and Bands 17520). The number of bands in this output took into account those missing images.

(5) The BSQ image was then converted into the original datatype, floating point using the following formula: [float((b1/100)+273.15)].

Appendix G: Earthquake Definitions

Diagram and Terminologies for Earthquake events

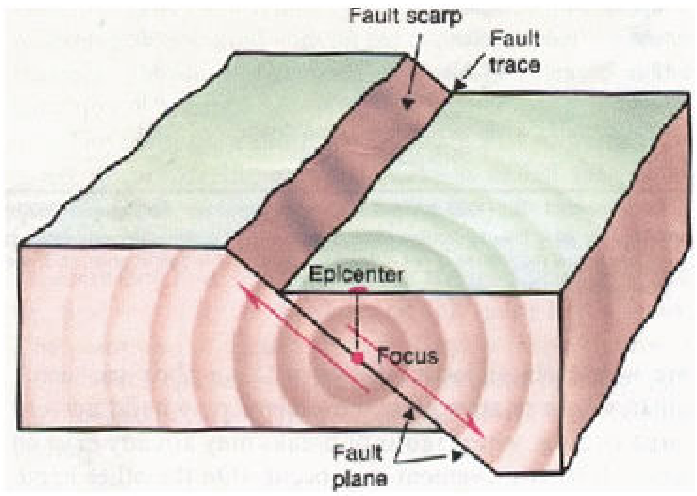

Figure 5-2: Diagram showing the features involved in an earthquake event [59].

Focus/hypocenter: is the point within the earth where an earthquake rupture starts.

Epicentre: is the point on the earth's surface directly above the hypocenter at the surface of the earth.

Fault plane: is the planar (flat) surface along which there is slip during an earthquake.

Fault trace: is the intersection of a fault with the ground surface.

Fault scarp: is the feature on the surface of the earth that looks like a step caused by slip on the fault.

Appendix H: Earthquake scales and NEIC results

Earthquake Scales and Brief Description for NEIC Earthquake Search Results

Scale	*T* (sec)	λ_{max} (km)	*Related scales*
$\mathbf{M_L}$	0.1 ~ 3	10	m_{bLg}
$\mathbf{M_S}$	~ 20	70	M_{GR}, M_R, M_D, M_Z, M_V, M_{JMA}
$\mathbf{m_B}$	0.5 ~ 12	70	
$\mathbf{m_b}$	~ 1	10	m_{bLg}
Moment magnitude ($\mathbf{M_W}$)	10 ~ ∝	∝	M_M, M_W, M_E, M_t
$\mathbf{M_C}$	-	-	
$\mathbf{M_I}$	-	-	M_K

Table 5-3: Different Magnitude Scales [20].

where
T Period
λ_{MAX} Maximum wavelength
M_L Local magnitude, Richter (1935)
M_S Surface-wave magnitude, Gutenberg (1945a)
m_B Body-wave magnitude, Gutenberg (1945b), Gutenberg and Richter (1956)
m_b Short-period body-wave magnitude reported in “Earthquake Data Reports” and “Bulletin of International Seismological Center”
m_{bLg} Lg-wave magnitude, e.g., Nuttli (1973)
M_{GR} Magnitude used in Gutenberg and Richter (1954)
M_R Magnitude used in and Richter (1958)
M_D Magnitude used in and Duda (1965)
M_Z Surface-wave magnitude determined from the vertical-component seismograms (e.g. Earthquake Data Reports)
M_V Surface-wave magnitude defined by Vanêk et al. (1962)
M_{JMA} Magnitude scale used by the Japan Meteorological Agency
M_M Moment magnitude by Brune and Engen (1969)
M_W Kanamori (1977)
M_E Purcaru and Berckhemer (1978)
M_t Tsunami magnitude regressed against MW, Abe (1979)
M_C Coda (or duration magnitude), e.g., Bisztricsány (1959), Tsumura (1967), Real and Teng (1973)
M_I Magnitude determined from intensity data and macro-seismic data, e.g., Nuttli and Zollweg (1974), Nuttli et al., (1979), Utsu (1979)
M_K Kawasumi (1951) [20]

Surface-wave magnitude M_S: although this scale suffers from the saturation at $M_S \geq 8$, it can be determined very easily, and is a useful scale for most events larger than M_S =5. Surface waves are analogous to water waves and travel along the Earth’s surface [20]. They travel slower than body waves. Because of their low fequency, long duration and large amplitude, they can be the most destructive type of seismic wave. There are two types of surface waves: Rayleigh waves and Love waves. This scale can be used for moderate to large earthquake and for shallow earthquakes wih depths less than 70 km. Also it is suitable to detect earthquakes a distance greater than 1000km from the epicenter.

Body-wave magnitude m_B: the body-wave magnitude which is determined from the maximum amplitude of various body-wave phases, here denoted by m_B. is useful to represent the source spectrum at a period from 1 to 10 seconds. Many recent studies on the amplitude attenuation curves and their regional variations will hopefully make inter-regional comparisons of m_B more meaningful than in the past [20]. Body waves travel through the interior of the Earth. They follow raypaths refracted by the varying density and modulus (stiffness) of the Earth's interior. The density and modulus, in turn, vary according to temperature, composition and phase.

Body-wave magnitude m_b: this scale, which is determined from the first few seconds of short-period P waves, represents the size of an earthquake at its beginning. Because of this, for earthquakes with a large fault dimension and complex rupture mechanism, the usefulness if this scale is limited. However, for relatively small events (e.g., $m_b \leq 5.5$), this scale approximately represents the source spectrum at the period of 1 second and is useful for quantification of earthquakes at short periods [20]. It is ideal to locat earthquakes up to a distance of 5° geographical coordinates away from the epicenter.

Moment magnitude: the moment magnitude is made (longer than 100 seconds for very large events) more directly than the conventional scales. If the energy-moment relation is correct, the moment magnitude can be determined from the seismic moment by using the formula [M_W = (log M_O -16.1)/1.5] for both shallow and deep earthquakes. Since the determination of the seismic moment is becoming a relatively routine practice, the moment magnitude is a very useful parameter for earthquake quantification [20].

Local and regional scales: local magnitude M_L, the JMA magnitude M_{JMA}, Lg magnitude m_{bLg}, the coda (duration) magnitude M_C and the intensity magnitude M_I. Since the types of the data used in these scales are very different from region to region, it is often difficult to relate one scale to another [20]. This magnitude sclae systems were developed for shallow and local earthquakes.

The problem of the magnitude scale became very complex as many different scales were introduced to accomodate different situations such as use of teleseismic surface and body waves, extension of the scale to intermediate and deep earthquakes, change in the seismic instrumentation, extension of the scale to very small and very large earthquakes and introduction of new seismological concepts.

Most magnitude scales currently in use are empirical[1]. Usually a magnitude M is determined from the amplitude A and the period T of a certain type of seismic waves through a formula which contains several constants. These constants are determined in such a way that the magnitudes on the new scale agree with those of an existing one, at least over a certain magnitude range. In some case, the duration of seismogram, macro-seismic data (e.g., intensity, tsunami source area) and geodetic data are used for the determination of magnitude. In this case too, the new scale is regressed against existing ones.

Earthquakes can be quantified with respect to various physical parameters such as the fault length, fault area, fault displacement, particle velocity and acceleration of fault motion and a combination of these. It is impossible to represent all of these parameters by a single number, the magnitude. Obviously there is a limitation in the use of the magnitude scale for quantification of earthquakes. The main purpose of the magnitude scale is to provide a parameter which can be used for the first-cut reconnaissance analysis of earthquake data (catalogue) for various geophysical and engineering investigations; special caution should be exercised in using the magnitude beyond the reconnaissance purposes [20].

[1] Empirical denotes information gained by means of observation, experience, or experiment. A certain concept in science and the scientific method is that all evidence must be empirical that is dependent on evidence or consequences that are observable by the senses. It refers to the use of working hypotheses that are testable using observation or experiment [65].

NEIC EARTHQUAKE RESULTS FOR BAM as extracted from USGS for Pixel 35,44

NEIC: Earthquake Search Results

U. S. GEOLOGICAL SURVEY

EARTHQUAKE DATA BASE

FILE CREATED: Sat Mar 13 21:01:55 2010
Circle Search Earthquakes= 96
Circle Center Point Latitude: 28.840N Longitude: 58.240E
Radius: 200.000 km
Catalog Used: PDE
Date Range: 1999 to 2004
Magnitude Range: 4.0 - 9.0
Data Selection: Historical & Preliminary Data

CAT	YEAR	MO	DA	ORIG TIME	LAT	LONG	DEP	MAGNITUDE	IEM NFO TF	DTSVNWG	DIST km
PDE	1999	01	02	032802.29	30.28	57.44	33	4.4 mbGS	...	....	177
PDE	1999	01	14	221249.22	29.15	56.35	33	5.0 MwHRV	..M	....	186
PDE	1999	01	25	005451.08	28.21	57.42	33	4.2 mbGS	...	....	106
PDE	1999	03	04	053826.52	28.34	57.19	33	6.6 MwHRV	.CM	....	116
PDE	1999	03	04	054749.91	28.32	57.15	33	5.6 mbGS	...	....	121
PDE	1999	03	04	055028.33	28.41	57.10	33	5.1 mbGS	...	....	121
PDE	1999	03	04	062151.24	28.34	57.09	33	4.6 mbGS	...	....	125
PDE	1999	03	04	071636.23	28.50	57.08	33	5.0 mbGS	...	....	119
PDE	1999	03	04	071918.24	28.13	57.11	33	5.3 mbGS	...	....	135
PDE	1999	03	04	072604.41	28.47	56.94	33	5.2 mbGS	...	....	133
PDE	1999	03	04	091936.30	28.48	57.01	33	4.5 mbGS	...	....	126
PDE	1999	03	04	095203.02	28.51	57.21	33	5.3 mbGS	...	....	106
PDE	1999	03	04	111259.11	28.41	57.09	33	4.9 mbGS	...	....	122
PDE	1999	03	04	192554.58	28.33	56.95	33	4.9 mbGS	...	....	137
PDE	1999	03	05	010254.73	28.55	57.12	33	4.6 mbGS	...	....	114
PDE	1999	03	09	120808.35	28.77	56.58	81	4.5 mbGS	...	....	161
PDE	1999	03	10	074543.47	28.87	56.60	84	4.8 mbGS	...	....	160
PDE	1999	03	12	075932.34	27.89	57.40	33	4.4 mbGS	...	....	133
PDE	1999	03	19	153054.93	28.55	56.99	33	4.0 mbGS	...	....	126
PDE	1999	04	02	005458.46	28.28	57.11	33	4.2 mbGS	...	....	126
PDE	1999	04	11	065256.54	28.39	57.17	61	4.5 mbGS	...	....	115
PDE	1999	05	25	111728.88	28.46	57.65	33	4.7 mbGS	...	....	71
PDE	1999	05	28	113729.67	28.31	57.67	33	4.1 mbGS	...	....	81
PDE	1999	08	16	222136.04	28.15	56.69	33	4.3 mbGS	...	....	169
PDE	1999	08	29	205631.53	28.15	56.46	33	4.4 mbGS	...	....	190
PDE	1999	10	19	130228.04	30.08	57.61	33	4.7 mbGS	...	....	150
PDE	2000	02	25	045519.39	30.45	57.61	33	4.0 mbGS	...	....	187
PDE	2000	02	29	171607.90	28.25	57.14	120	4.5 mbGS	...	....	126
PDE	2000	03	05	094006.06	27.95	56.47	33	5.4 MwHRV	..M	....	199
PDE	2000	07	26	224338.04	28.10	57.00	33	4.3 mbGS	...	....	146

PDE	2000	08	20	222020.08	28.09	57.22	33	4.5	mbGS	... .	130
PDE	2000	08	27	204455.24	28.06	57.17	33	4.1	mbGS	... .	136
PDE	2000	11	07	184426.41	28.20	56.93	33	4.0	mbGS	... .	146
PDE	2000	11	11	181602.63	28.32	57.63	33	4.5	mbGS	... .	82
PDE	2000	11	24	091820.38	28.15	57.64	82	4.4	mbGS	... .	96
PDE	2001	02	13	034240.21	28.32	56.34	33	4.6	mbGS	... .	194
PDE	2001	05	09	234815.03	27.92	58.21	33	4.2	mbGS	... .	101
PDE	2001	08	12	110329.01	27.62	57.69	33	4.6	mbGS	... .	145
PDE	2001	08	25	232922.11	30.43	57.45	33	4.4	mbGS	... .	191
PDE	2001	11	01	195436.98	28.24	57.47	33	4.6	mbGS	... .	101
PDE	2001	11	22	170002.61	27.81	57.52	33	4.4	mbGS	... .	133
PDE	2001	11	23	171947.89	28.35	57.44	33	4.1	mbGS	... .	95
PDE	2001	11	25	213054.35	28.32	57.27	40	5.0	MwHRV	.FM	110
PDE	2001	12	15	141838.38	28.10	56.37	33	4.6	mbGS	... .	199
PDE	2002	01	04	090618.32	28.41	57.24	33	4.0	mbGS	... .	108
PDE	2002	04	11	060548.63	27.70	56.67	33	4.8	mbGS	... .	198
PDE	2002	04	17	084722.85	27.66	56.75	33	5.3	MwGS	..M	195
PDE	2002	05	27	011629.16	27.79	56.71	33	4.2	mbGS	... .	189
PDE	2002	05	28	190532.09	27.72	56.74	50	4.7	mbGS	... .	192
PDE	2002	06	02	200822.66	27.92	57.67	29	4.7	mbGS	... .	116
PDE	2002	06	02	201725.62	27.90	57.73	33	4.4	mbGS	... .	115
PDE	2002	12	13	003620.59	28.98	57.45	93	4.2	mbGS	... .	78
PDE	2003	02	14	102858.93	28.05	56.82	37	5.6	MwHRV	.FM	164
PDE	2003	03	01	184554.81	28.75	57.42	33	4.5	mbGS	... .	80
PDE	2003	03	08	092803.78	27.98	56.76	33	4.7	mbGS	... .	173
PDE	2003	04	16	110605.06	30.20	57.42	33	4.5	mbGS	... .	170
PDE	2003	06	13	025544.46	27.99	57.85	33	4.0	mbGS	... .	101
PDE	2003	07	06	160420.62	28.09	57.74	33	5.0	MwHRV	.FM	96
PDE	2003	08	04	032819.76	29.08	59.74	33	5.6	MwHRV	.FM	148
PDE	2003	08	05	204851.76	28.29	57.24	33	4.2	mbGS	... .	115
PDE	2003	08	21	040209.17	29.05	59.77	20	5.9	MwGS	.DM	151
PDE	2003	09	12	073417.93	28.38	59.22	33	4.6	mbGS	... .	108
PDE	2003	10	01	071403.27	28.28	57.30	33	4.8	mbGS	... .	111
PDE	2003	12	03	072706.78	28.08	56.99	33	4.3	mbGS	... .	148
PDE	2003	12	26	015652.44	29.00	58.31	10	6.6	MwHRV	9CM F.....S	18
PDE	2003	12	26	030613.64	28.93	58.33	10	5.1	mbGS	... .	13
PDE	2003	12	26	035325.18	28.79	58.12	10	4.5	mbGS	... .	13
PDE	2003	12	26	091635.34	29.01	58.28	10	4.0	mbGS	... .	18
PDE	2003	12	26	095958.98	29.01	58.32	10	4.0	mbGS	... .	19
PDE	2003	12	26	140816.02	29.08	58.20	10	4.6	mbGS	... .	26
PDE	2003	12	28	092422.92	29.21	58.55	10	4.1	mbGS	... .	50
PDE	2003	12	28	150212.01	29.01	58.39	10	4.2	mbGS	... .	24
PDE	2004	01	11	050604.75	29.19	58.55	10	4.1	mbGS	... .	48
PDE	2004	01	21	132336.33	29.17	58.24	10	4.3	mbGS	... .	36
PDE	2004	01	28	172931.57	29.01	58.33	10	4.1	mbGS	... .	20
PDE	2004	01	31	095912.01	28.61	57.81	55	4.1	mbGS	... .	49
PDE	2004	03	18	132120.74	28.41	56.97	50	4.5	mbGS	... .	132
PDE	2004	04	08	142304.03	28.97	58.20	10	4.0	mbGS	... .	14
PDE	2004	04	11	072730.60	28.98	57.84	25	4.5	mbGS	... .	41
PDE	2004	04	21	144522.25	28.49	57.14	55	4.6	mbGS	... .	114
PDE	2004	05	29	023348.27	29.11	58.35	10	4.2	mbGS	... .	31
PDE	2004	07	03	222222.16	28.38	56.50	90	4.2	mbGS	... .	177
PDE	2004	07	13	055005.35	29.23	57.09	25	4.2	mbGS	... .	119
PDE	2004	07	22	045136.01	29.11	58.31	10	4.8	MwHRV	.FM	31
PDE	2004	08	05	162521.27	28.86	57.22	10	4.1	mbGS	... .	99
PDE	2004	08	10	023103.90	28.49	57.07	24	5.0	mbGS	... .	121
PDE	2004	10	06	111434.03	28.84	57.93	72	5.2	MwHRV	.FM	30
PDE	2004	10	07	071711.10	28.80	57.84	104	4.5	mbGS	... .	39
PDE	2004	10	07	125501.04	28.33	57.31	56	5.0	MwHRV	..M	106
PDE	2004	10	09	060826.43	28.30	57.13	63	4.5	mbGS	... .	123
PDE	2004	10	10	162750.15	28.22	57.27	21	4.7	mbGS	... .	117
PDE	2004	11	11	203644.30	28.47	56.96	59	4.6	mbGS	... .	131
PDE	2004	11	12	003034.56	28.60	56.81	96	4.3	mbGS	... .	141
PDE	2004	12	08	100412.92	27.92	57.49	77	5.0	MwHRV	..M	125
PDE	2004	12	11	033555.44	27.77	57.57	20	4.6	mbGS	... .	134
PDE	2004	12	23	110110.14	28.14	57.19	35	4.5	mbGS	... .	128

NEIC EARTHQUAKE RESULTS FOR L'AQUILA

NEIC: Earthquake Search Results

U. S. G E O L O G I C A L S U R V E Y

E A R T H Q U A K E D A T A B A S E

FILE CREATED: Thu Feb 18 16:26:59 2010
Circle Search Earthquakes= 532
Circle Center Point Latitude: 42.423N Longitude: 13.395E
Radius: 250.000 km
Catalog Used: PDE
Date Range: 2005 to 2010
Data Selection: Historical & Preliminary Data

CAT	YEAR	MO	DA	ORIG TIME	LAT	LONG	DEP	MAGNITUDE	IEM NFO TF	DTSVNWG	DIST km
PDE	2005	01	08	234538.16	43.18	15.16	10		...	....	167
PDE	2005	01	08	235310.56	43.04	15.36	10		...	....	174
PDE	2005	01	09	034912.30	43.08	15.36	10	3.1 MLLDG	...	....	176
PDE	2005	01	13	071538.89	43.15	15.30	10	3.8 MLZAMG	...	....	175
PDE	2005	01	22	033418.87	43.15	15.29	10	3.0 MLLDG	...	....	174
PDE	2005	02	02	020619.40	42.82	13.36	25	2.5 MDROM	...	....	44
PDE	2005	02	02	020916	43.16	15.43	10	4.2 MLZAMG	...	....	185
PDE	2005	02	03	053309.80	43.45	15.85	10	3.5 MLGRF	...	....	230
PDE	2005	02	03	201757.50	42.57	13.24	10	2.6 MDROM	...	....	20
PDE	2005	02	03	231717.50	42.36	13.22	16	2.6 MDROM	...	....	16
PDE	2005	02	04	053011.90	44.22	11.82	4	2.5 MDROM	...	....	236
PDE	2005	02	06	235117	42.35	13.22	10	2.8 MDROM	...	....	16
PDE	2005	02	07	224315	43.17	15.17	10	3.5 MLZAMG	...	....	166
PDE	2005	02	08	022316	43.18	12.61	10	2.5 MDROM	...	....	105
PDE	2005	02	08	113602.50	41.29	15.99	4	2.6 MDROM	...	....	249
PDE	2005	02	11	162310.10	43.32	13.27	10	2.5 MDROM	...	....	100
PDE	2005	02	11	234228.60	41.47	14.63	6	2.6 MDROM	...	....	147
PDE	2005	02	13	110926.80	41.67	14.82	13	2.7 MDROM	...	....	144
PDE	2005	02	13	111534.20	41.67	14.82	10	3.1 MDROM	...	....	144
PDE	2005	02	13	215727.50	43.90	11.93	7	2.9 MDROM	...	....	202
PDE	2005	02	16	023638.50	43.23	15.16	10	3.3 MLZAMG	...	....	170
PDE	2005	02	16	044522.80	41.72	13.68	8	3.0 MDROM	...	....	81
PDE	2005	02	16	125442.20	41.71	13.68	3	2.5 MDROM	...	....	82
PDE	2005	02	16	144948.10	41.73	13.70	8	2.7 MDROM	...	....	80
PDE	2005	02	17	170930.40	41.76	15.19	5	2.5 MDROM	...	....	166
PDE	2005	02	17	200525.47	43.15	15.40	10	3.2 MLZAMG	...	....	183
PDE	2005	02	22	112151.10	43.65	13.48	5	2.7 MDROM	...	....	136
PDE	2005	02	22	164320.10	43.11	12.89	69	2.6 MDROM	...	....	86
PDE	2005	02	24	041457	43.12	14.99	10	3.6 MLZAMG	...	....	151
PDE	2005	02	27	031633.90	41.66	14.84	12	2.9 MDROM	...	....	146
PDE	2005	02	27	180338	41.84	15.71	14	2.7 MDROM	...	....	202

PDE	2005	03	01	054137.40	41.67	14.87	9	3.4	MDROM	...	....	148
PDE	2005	03	02	005407.20	43.17	13.62	3	2.6	MDROM	...	....	84
PDE	2005	03	02	100643.60	42.53	13.01	10	2.6	MDROM	...	....	33
PDE	2005	03	03	025039.90	41.78	14.82	9	3.1	MDROM	...	....	138
PDE	2005	03	03	225357.50	42.24	13.90	16	2.5	MDROM	...	....	46
PDE	2005	03	12	033549.20	42.42	12.34	7	2.8	MDROM	...	....	86
PDE	2005	03	13	174815.50	42.52	13.28	10	3.6	MDPDG	...	....	14
PDE	2005	03	15	000303.60	41.94	15.85	28	3.1	MDROM	...	....	209
PDE	2005	03	17	113427.60	43.06	13.51	10	2.5	MDROM	...	....	71
PDE	2005	03	21	004147.70	41.57	14.35	19	2.7	MDROM	...	....	123
PDE	2005	03	22	020023.30	41.87	15.62	3	3.1	MDROM	...	....	193
PDE	2005	03	22	160929.30	41.76	12.57	15	2.6	MDROM	...	....	100
PDE	2005	03	24	044848.10	43.07	13.48	10	2.7	MDROM	...	....	72
PDE	2005	03	24	165522.60	43.02	10.92	9	2.5	MDROM	...	....	213
PDE	2005	03	25	163155.80	42.64	13.06	10	2.6	MDROM	...	....	36
PDE	2005	03	25	164420.70	42.64	13.06	14	2.6	MDROM	...	....	36
PDE	2005	03	26	041502	42.41	12.33	5	3.4	MDROM	...	....	87
PDE	2005	03	26	042149.30	42.41	12.32	5	2.5	MDROM	...	....	88
PDE	2005	03	26	134207.20	42.44	12.33	5	3.0	MDROM	...	....	87
PDE	2005	03	27	003806	42.15	12.95	13	2.7	MDROM	...	....	47
PDE	2005	03	28	010500.10	41.70	14.86	7	2.5	MDROM	...	....	145
PDE	2005	03	28	102414.20	42.50	12.68	9	2.6	MDROM	...	....	59
PDE	2005	03	28	120617.80	42.97	10.91	9	2.7	MLLDG	...	....	212
PDE	2005	03	28	201108	43.87	11.36	10	2.6	MDROM	...	....	230
PDE	2005	03	30	071437.10	41.76	15.79	16	2.6	MDROM	...	....	211
PDE	2005	04	02	110511.50	44.19	11.55	10	2.7	MLLDG	...	....	246
PDE	2005	04	02	212922.30	44.18	11.81	5	2.6	MDROM	...	....	233
PDE	2005	04	02	232943	41.03	14.55	5	3.0	MDROM	...	....	181
PDE	2005	04	04	222136.10	41.83	13.57	10	3.1	MDROM	...	....	67
PDE	2005	04	05	024954.80	43.89	12.51	33	2.5	MDROM	...	....	178
PDE	2005	04	05	133827.70	42.33	12.66	10	2.8	MDROM	...	....	61
PDE	2005	04	06	033119.20	40.75	14.66	10	2.6	MDROM	...	....	213
PDE	2005	04	06	231158.40	42.14	13.35	9	2.7	MDROM	...	....	31
PDE	2005	04	07	200155	43.19	11.07	4	2.6	MDROM	...	....	207
PDE	2005	04	07	214424.80	42.68	11.77	5	2.8	MDROM	...	....	136
PDE	2005	04	08	090443.80	43.09	13.35	10	2.6	MDROM	...	....	73
PDE	2005	04	09	003147.50	43.08	13.34	4	3.3	MDROM	...	....	72
PDE	2005	04	09	010754.20	43.74	12.03	2	2.7	MDROM	...	....	184
PDE	2005	04	09	035426.20	43.72	12.00	4	2.5	MDROM	...	....	182
PDE	2005	04	09	201718.10	42.98	10.87	6	2.5	MLLDG	...	....	215
PDE	2005	04	09	205904.80	42.95	10.94	8	3.2	MLLDG	...	....	209
PDE	2005	04	09	215957.20	42.95	10.94	7	3.1	MLLDG	...	....	209
PDE	2005	04	11	013218.10	44.36	12.33	5	2.7	MDROM	...	....	232
PDE	2005	04	11	220814.30	42.33	12.65	14	2.5	MDROM	...	....	61
PDE	2005	04	12	003151.60	43.09	13.38	4	3.5	MDROM	...	....	74
PDE	2005	04	13	054846	41.51	13.77	10	2.6	MDROM	...	....	106
PDE	2005	04	14	194123.40	43.06	13.98	5	2.5	MDROM	...	....	85
PDE	2005	04	22	234728.79	44.15	11.75	10	3.4	MLZAMG	...	....	233
PDE	2005	04	26	201522.35	43.08	13.23	10	2.9	MLZAMG	...	....	74
PDE	2005	04	27	130810.47	43.27	12.73	10	3.8	MLZAMG	...	....	108
PDE	2005	05	03	224004.80	43.85	11.92	10	2.9	MLLDG	...	....	198
PDE	2005	05	05	132123.62	41.92	13.64	10	2.9	MLLDG	...	....	58
PDE	2005	05	21	195520.70	41.03	14.38	15	3.6	MDPDG	.F.	....	175
PDE	2005	05	22	114019.66	44.18	11.76	4	2.7	MLLDG	...	....	235
PDE	2005	06	06	220305.83	43.28	12.89	10	2.7	MLLDG	...	....	103
PDE	2005	06	12	092147.80	41.63	16.06	9	2.7	MDROM	...	....	237
PDE	2005	06	12	155949.50	44.01	12.97	14	2.7	MDROM	...	....	180
PDE	2005	06	13	013338.10	41.56	14.72	17	2.7	MDROM	...	....	145
PDE	2005	06	13	223334	41.71	15.82	27	2.7	MLROM	...	....	215
PDE	2005	06	18	025609.20	40.86	15.13	14	2.5	MLROM	...	....	226

PDE	2005	06	21	000636.10	43.02	13.28	6	2.9	MLROM	...	....	67
PDE	2005	06	21	193959.60	43.02	13.01	16	2.5	MDROM	...	....	72
PDE	2005	06	23	025519.60	43.89	11.73	10	2.8	MLZAMG	...	....	211
PDE	2005	06	27	024306.40	42.69	12.55	10	2.8	MLROM	.F.	....	75
PDE	2005	07	11	070541.30	44.00	11.66	28	2.8	MLROM	...	....	224
PDE	2005	07	15	150924	44.20	12.09	19	3.0	MLZAMG	...	....	224
PDE	2005	07	15	151718	44.21	12.12	22	4.2	mbGS	.F.	....	223
PDE	2005	07	15	152347.30	44.22	12.10	22	4.0	MLZAMG	...	....	225
PDE	2005	07	15	171901.50	44.20	12.09	21	3.0	MLZAMG	...	....	224
PDE	2005	07	30	005628.60	43.73	12.70	39	3.0	MDLDG	...	....	156
PDE	2005	07	30	010728.60	43.38	12.56	8	2.5	MDROM	...	....	126
PDE	2005	07	31	225337.50	44.06	13.52	30	2.8	MLLDG	...	....	182
PDE	2005	08	02	201349.53	44.25	12.11	10	3.0	MLZAMG	...	....	228
PDE	2005	08	03	063156.52	40.72	13.55	392	4.0	mbGS	...	....	189
PDE	2005	08	06	093148.01	42.06	13.26	10	3.0	MLLDG	...	....	41
PDE	2005	08	13	213223.50	42.46	13.02	22	2.5	MDROM	...	....	31
PDE	2005	08	17	025409.04	43.42	12.85	10	3.5	MLSTR	...	....	119
PDE	2005	08	22	120208.60	41.47	12.53	10	4.8	MwHRV	4FM	....	127
PDE	2005	08	31	150444.96	44.34	12.19	10	3.2	MLZAMG	...	....	233
PDE	2005	09	03	123043.70	41.53	14.52	12	2.5	MDROM	...	....	136
PDE	2005	09	11	032554.60	43.46	12.75	44	2.5	MDROM	...	....	126
PDE	2005	09	13	190318.80	43.08	13.37	8	2.8	MDROM	...	....	73
PDE	2005	09	15	084750.20	43.06	12.91	20	2.9	MLROM	...	....	81
PDE	2005	09	18	152701.50	43.79	12.43	15	2.9	MLROM	...	....	171
PDE	2005	09	18	215420.90	43.80	12.43	19	3.1	MLROM	...	....	171
PDE	2005	09	20	074638.68	42.43	13.10	10	3.3	MLLDG	...	....	24
PDE	2005	09	20	095009.30	43.80	12.43	20	2.5	MLROM	...	....	171
PDE	2005	09	20	100101.50	42.50	13.19	14	2.8	MLROM	...	....	18
PDE	2005	09	22	134720.80	41.97	12.76	19	2.9	MLROM	...	....	72
PDE	2005	09	22	135139.50	41.96	12.77	18	2.5	MLROM	...	....	72
PDE	2005	09	22	141222.50	41.97	12.76	20	2.9	MLROM	...	....	73
PDE	2005	09	24	010034.90	43.81	13.39	9	2.9	MDROM	...	....	153
PDE	2005	09	25	125155.60	43.80	12.44	21	2.5	MDROM	...	....	171
PDE	2005	09	29	224508	44.08	11.49	9	2.5	MDROM	...	....	240
PDE	2005	09	30	211901.55	43.85	12.43	10	3.6	MLGRF	...	....	176
PDE	2005	10	02	013252	43.81	12.43	17	2.5	MDROM	...	....	173
PDE	2005	10	02	190911.40	41.88	15.67	19	2.8	MLROM	...	....	197
PDE	2005	10	03	090051.40	41.60	14.34	19	2.8	MLROM	...	....	119
PDE	2005	10	04	070517	41.66	12.95	9	2.6	MLROM	...	....	92
PDE	2005	10	07	164754.30	43.79	12.43	7	3.2	MLROM	...	....	171
PDE	2005	10	07	175209.10	43.81	12.43	8	2.7	MDROM	...	....	172
PDE	2005	10	07	175740.70	43.08	13.46	9	2.6	MDROM	...	....	72
PDE	2005	10	08	123419.50	42.85	13.15	16	2.5	MDROM	...	....	51
PDE	2005	10	09	014256.40	43.80	12.43	16	2.9	MLLDG	...	....	172
PDE	2005	10	09	134841.30	42.57	13.19	3	3.1	MLROM	...	....	23
PDE	2005	10	14	034158	42.69	13.53	21	2.6	MLROM	...	....	31
PDE	2005	10	15	065901	42.93	13.09	16	2.7	MLROM	...	....	61
PDE	2005	10	30	162329.50	43.21	13.67	1	2.7	MLLDG	...	....	89
PDE	2005	11	04	095011.70	42.04	13.81	9	2.7	MLROM	...	....	54
PDE	2005	11	08	211026.50	44.15	12.25	19	3.9	MLGRF	...	....	213
PDE	2005	11	09	034934.20	44.16	12.25	21	2.8	MLLDG	...	....	214
PDE	2005	11	10	132628	44.17	12.23	21	3.0	MLLDG	...	....	215
PDE	2005	11	11	031408.70	44.21	12.20	12	2.8	MLLDG	...	....	221
PDE	2005	11	15	050704.40	42.74	13.20	13	3.1	MLROM	...	....	38
PDE	2005	11	26	140715.70	41.10	15.35	18	2.7	MLROM	...	....	219
PDE	2005	12	03	132442.10	43.08	11.01	9	2.6	MLLDG	...	....	208
PDE	2005	12	09	200432	43.15	15.52	12	3.6	MLFUR	...	....	191
PDE	2005	12	11	015121.80	42.75	12.77	7	2.6	MLROM	...	....	63
PDE	2005	12	13	071212.80	42.75	12.76	10	3.0	MLROM	...	....	63
PDE	2005	12	13	122335.50	42.69	13.18	9	2.6	MLROM	...	....	34

PDE	2005	12	15	060032.80	42.75	12.77	19	3.3	MLROM	...	....	62
PDE	2005	12	15	132839.50	42.74	12.76	18	4.3	mbGS	...	....	62
PDE	2005	12	15	175714.20	42.75	12.78	21	2.6	MLROM	...	....	61
PDE	2005	12	16	201238.78	42.66	12.70	10	3.4	MLLDG	...	....	62
PDE	2005	12	17	040340.50	42.74	12.76	7	2.6	MDROM	...	....	63
PDE	2005	12	18	080648.30	42.74	12.75	9	3.6	MLLDG	...	....	63
PDE	2005	12	21	170708.46	43.21	11.38	10	2.6	MLROM	...	....	187
PDE	2005	12	23	042510.40	41.90	15.30	23	2.7	MLROM	...	....	167
PDE	2005	12	23	213821.20	41.98	15.31	12	2.9	MLROM	...	....	165
PDE	2005	12	24	211644.80	42.98	12.89	17	2.8	MLROM	...	....	74
PDE	2006	01	05	173039.80	42.76	12.88	10	3.8	MDPDG	...	....	56
PDE	2006	01	08	004859.70	42.74	12.77	6	2.7	MDROM	...	....	62
PDE	2006	01	09	011844	43.80	12.00	7	2.9	MLLDG	...	....	190
PDE	2006	01	13	102010.50	42.47	13.28	9	3.4	MLLDG	...	....	10
PDE	2006	01	15	094718.90	43.04	13.33	6	2.5	MDROM	...	....	68
PDE	2006	01	17	193930.90	43.39	13.53	20	3.1	MLLDG	...	....	108
PDE	2006	01	22	161858.40	40.54	13.34	10	2.5	MLROM	...	....	209
PDE	2006	02	02	104757.70	43.94	11.91	7	2.7	MLROM	...	....	207
PDE	2006	02	02	145554.20	42.52	13.23	10	2.5	MLROM	...	....	17
PDE	2006	02	02	190822.50	42.28	13.26	10	2.6	MLROM	...	....	19
PDE	2006	02	05	170259.50	40.79	15.22	10	3.2	MLROM	...	....	236
PDE	2006	02	06	211553.80	42.06	15.71	10	3.0	MLROM	...	....	195
PDE	2006	02	09	0101	42.77	12.78	8	3.1	MLROM	...	....	63
PDE	2006	02	09	055548.30	42.76	12.80	7	2.9	MLROM	...	....	61
PDE	2006	02	13	230307.30	42.60	13.26	5	3.0	MLROM	...	....	22
PDE	2006	02	14	165054.30	43.77	13.03	34	2.5	MLROM	...	....	152
PDE	2006	02	19	034348.10	42.45	13.31	9	2.9	MLROM	...	....	7
PDE	2006	02	19	061804.70	42.46	13.31	10	2.5	MLROM	...	....	7
PDE	2006	02	19	065727.90	42.45	13.32	10	2.5	MDROM	...	....	7
PDE	2006	02	24	004804.10	42.73	12.76	5	2.5	MLROM	...	....	62
PDE	2006	02	26	110727.80	42.60	13.06	10	2.9	MLROM	...	....	33
PDE	2006	02	27	200207.10	41.77	15.93	24	2.7	MLROM	...	....	221
PDE	2006	03	02	144753.30	43.21	15.60	10	2.8	MLROM	...	....	200
PDE	2006	03	06	010251.10	41.65	12.88	9	3.0	MLROM	...	....	96
PDE	2006	03	14	031503.60	40.80	15.32	8	2.7	MLROM	...	....	241
PDE	2006	03	14	133343	40.79	15.32	8	2.5	MLROM	...	....	242
PDE	2006	03	25	052244.60	41.73	13.90	10	3.1	MLROM	...	....	87
PDE	2006	03	31	224808	42.74	12.77	4	3.2	MLLDG	...	....	62
PDE	2006	04	04	023644.80	43.02	12.91	4	3.3	MLROM	...	....	77
PDE	2006	04	10	190336.60	43.40	13.49	33	4.1	mbGS	5F.	....	108
PDE	2006	04	12	001137.70	42.04	15.49	5	2.5	MDROM	...	....	177
PDE	2006	04	13	030254.90	42.40	15.95	10	2.7	MLROM	...	....	210
PDE	2006	04	14	012159.40	41.71	16.02	29	3.3	MLROM	...	....	231
PDE	2006	04	16	211502.70	43.96	11.80	27	4.2	mbGS	5F.	....	214
PDE	2006	04	24	234858.20	42.62	12.56	5	2.5	MLROM	...	....	72
PDE	2006	04	27	185318.40	43.07	12.63	6	2.2	MLROM	.F.	....	95
PDE	2006	04	30	210757.10	41.47	15.70	6	3.3	MDPDG	...	....	218
PDE	2006	05	01	155914.80	42.62	12.56	10	2.9	MLLDG	...	....	72
PDE	2006	05	03	162024.50	41.72	14.78	21	2.7	MLROM	...	....	138
PDE	2006	05	05	085909.30	42.73	12.56	10	2.5	MDROM	...	....	76
PDE	2006	05	05	135031.20	42.32	15.96	10	2.5	MLROM	...	....	211
PDE	2006	05	06	224235.60	43.04	12.57	5	3.2	MLROM	...	....	96
PDE	2006	05	06	225044.50	43.06	12.56	4	3.0	MLROM	...	....	97
PDE	2006	05	06	231438.10	43.05	12.58	6	2.7	MDROM	...	....	96
PDE	2006	05	06	235724.20	42.62	12.57	7	2.8	MDROM	...	....	71
PDE	2006	05	08	010807.40	41.85	15.63	5	2.7	MDROM	...	....	195
PDE	2006	05	11	125422.20	43.36	12.57	2	2.7	MLROM	...	....	123
PDE	2006	05	13	162056.50	44.14	12.06	2	2.8	MLLDG	...	....	219
PDE	2006	05	13	162218	44.13	12.04	1	3.9	MLSTR	...	....	219
PDE	2006	05	15	020817.50	43.06	12.56	7	2.5	MDROM	...	....	97

PDE	2006	05	15	021953	43.09	13.48	4	2.6	MDROM	...	....	73
PDE	2006	05	16	210252.61	42.59	12.56	10	3.6	MLROM	.F.	....	71
PDE	2006	05	20	070928.60	42.89	13.12	9	2.6	MLROM	...	....	55
PDE	2006	05	20	091908.90	43.70	12.62	40	2.8	MDROM	...	....	154
PDE	2006	05	20	111917.80	40.76	15.26	8	2.6	MDROM	...	....	241
PDE	2006	05	23	092657.40	43.08	13.47	3	2.5	MLROM	...	....	72
PDE	2006	05	24	020355.60	42.15	15.83	9	2.9	MLROM	...	....	203
PDE	2006	05	26	002641.20	43.74	11.92	8	3.6	MLSTR	...	....	189
PDE	2006	05	27	214848.60	41.87	13.02	8	2.6	MDROM	...	....	68
PDE	2006	05	29	022006.20	41.80	15.90	31	4.7	MwHRV	.FM	....	218
PDE	2006	05	29	024235.20	41.78	15.87	18	2.8	MDROM	...	....	217
PDE	2006	05	29	054433.70	41.84	15.86	22	2.5	MDROM	...	....	213
PDE	2006	05	30	232647.20	41.81	15.83	23	2.6	MLROM	...	....	212
PDE	2006	05	31	124835.10	42.90	16.27	10	3.2	MDPDG	...	....	241
PDE	2006	05	31	125126.70	42.91	16.04	10	3.5	MLLDG	...	....	223
PDE	2006	06	01	024336	42.97	16.15	10	2.8	MLROM	...	....	233
PDE	2006	06	01	062932.90	43.80	11.96	5	2.9	MLROM	...	....	192
PDE	2006	06	03	102650.90	43.11	12.54	7	2.9	MLLDG	...	....	103
PDE	2006	06	03	184433.60	41.82	15.88	25	2.7	MLROM	...	....	216
PDE	2006	06	04	155036.60	41.81	15.86	24	2.5	MLROM	...	....	214
PDE	2006	06	05	000750.20	41.82	13.88	9	2.7	MLROM	...	....	78
PDE	2006	06	05	203759.80	43.19	13.82	26	2.5	MLROM	...	....	91
PDE	2006	06	08	194606.40	41.81	15.90	28	2.8	MLROM	...	....	218
PDE	2006	06	10	142539.30	42.84	16.33	10	2.7	MLROM	...	....	245
PDE	2006	06	10	143824.60	42.95	16.32	10	2.9	MLROM	...	....	246
PDE	2006	06	11	020918.50	42.95	16.28	10	2.5	MLROM	...	....	243
PDE	2006	06	11	060829.40	43.13	15.31	10	2.5	MLROM	...	....	175
PDE	2006	06	12	211835.50	41.89	15.69	5	2.6	MLROM	...	....	198
PDE	2006	06	17	002142.60	43.38	12.57	2	2.6	MDROM	...	....	125
PDE	2006	06	22	003200.29	42.62	12.56	4	3.0	MLROM	...	....	72
PDE	2006	06	22	074442.10	44.23	13.33	9	3.4	MLLDG	...	....	200
PDE	2006	06	23	192137.50	42.63	12.55	2	2.8	MLROM	...	....	72
PDE	2006	06	24	063504.50	42.62	12.55	2	3.2	MLROM	4F.	....	72
PDE	2006	06	24	071636.30	42.60	12.58	10	3.1	MLROM	...	....	69
PDE	2006	07	04	215112.33	42.83	15.98	0	3.3	MDPDG	...	....	216
PDE	2006	07	05	030254.40	42.97	16.14	10	2.7	MLROM	...	....	232
PDE	2006	07	06	214731.60	42.65	12.06	3	3.2	MLROM	5F.	....	112
PDE	2006	07	06	215516.30	42.65	12.05	5	2.7	MLROM	...	....	113
PDE	2006	07	08	022724.20	42.61	12.57	8	2.8	MLROM	...	....	70
PDE	2006	07	08	125529.60	42.98	12.93	16	2.5	MLROM	...	....	72
PDE	2006	07	09	012628	41.64	13.98	19	2.5	MDROM	...	....	99
PDE	2006	07	13	184101	43.66	11.83	9	3.1	MLROM	...	....	187
PDE	2006	08	06	193330.85	41.89	15.34	10	4.0	MLPDG	...	....	171
PDE	2006	08	08	194830	43.47	12.47	10	2.7	MLLDG	...	....	138
PDE	2006	08	17	034656	43.26	13.38	5	2.8	MLLDG	4F.	....	93
PDE	2006	08	19	073330.20	42.45	13.24	10	2.5	MLROM	...	....	12
PDE	2006	08	22	165948.60	43.14	12.75	59	2.9	MDROM	...	....	95
PDE	2006	08	24	035601.20	42.78	13.35	4	2.8	MLROM	...	....	39
PDE	2006	08	29	211610.80	43.76	12.14	4	2.5	MLROM	...	....	180
PDE	2006	08	29	225403.70	43.76	12.15	5	3.1	MLLDG	...	....	180
PDE	2006	08	29	233031.70	43.77	12.16	3	2.7	MLLDG	...	....	180
PDE	2006	08	30	080745.40	43.76	12.15	5	2.5	MLROM	...	....	179
PDE	2006	08	30	100151.40	43.76	12.15	4	3.9	MDPDG	4F.	....	179
PDE	2006	08	30	112047.60	43.73	12.09	19	2.6	MLROM	...	....	179
PDE	2006	08	31	011221.10	41.92	15.39	5	2.5	MLROM	...	....	174
PDE	2006	09	01	014322.40	43.62	12.04	10	2.7	MLLDG	...	....	172
PDE	2006	09	01	151241	42.24	13.29	10	3.0	MLLDG	...	....	21
PDE	2006	09	03	190925.80	43.88	12.05	6	2.6	MLROM	...	....	195
PDE	2006	09	03	215438	43.88	12.04	2	2.5	MLLDG	...	....	195
PDE	2006	09	08	073151.60	41.80	15.89	24	3.0	MLROM	...	....	217

PDE	2006	09	11	110624	43.43	12.50	2	2.5	MDROM	...	....	133
PDE	2006	09	11	110815.50	42.09	13.34	6	2.8	MLROM	...	....	37
PDE	2006	09	14	113114.20	43.04	13.51	11	2.7	MLROM	...	....	69
PDE	2006	09	25	191312.30	42.14	15.93	5	3.5	MLROM	...	....	211
PDE	2006	09	26	223435.20	42.44	13.29	6	2.9	MLROM	...	....	9
PDE	2006	10	02	033607.60	41.83	13.74	12	2.6	MDROM	...	....	71
PDE	2006	10	02	161138.40	43.08	13.33	22	2.7	MLROM	...	....	73
PDE	2006	10	04	173420.50	42.07	15.75	36	4.9	MLTHE	...	....	197
PDE	2006	10	08	192158.30	42.85	13.40	23	2.6	MLROM	...	....	47
PDE	2006	10	09	113654.30	41.77	15.87	27	3.0	MLROM	...	....	216
PDE	2006	10	12	183001.30	43.01	13.26	20	3.2	MLROM	...	....	65
PDE	2006	10	14	151546.90	40.68	12.93	10	2.7	MLROM	...	....	197
PDE	2006	10	14	161315.50	40.65	12.91	10	2.8	MLROM	...	....	200
PDE	2006	10	14	161536.80	40.73	12.94	10	2.8	MLROM	...	....	191
PDE	2006	10	16	202001.80	43.05	13.50	11	2.5	MLROM	...	....	70
PDE	2006	10	17	212231.58	42.39	12.94	10	2.9	MLROM	...	....	37
PDE	2006	10	21	070410.60	43.65	13.00	36	4.0	mbGS	...	....	139
PDE	2006	10	21	085517.70	43.60	12.96	32	3.8	MLSTR	...	....	135
PDE	2006	10	21	142219.30	42.26	12.95	11	3.0	MLROM	...	....	41
PDE	2006	10	22	110602.40	42.27	12.94	9	2.6	MDROM	...	....	41
PDE	2006	10	24	055457.80	43.30	10.91	4	2.5	MDROM	...	....	225
PDE	2006	10	25	133414.20	41.55	13.79	8	3.5	MDPDG	...	....	102
PDE	2006	10	27	090913.10	43.05	13.55	32	2.6	MLROM	...	....	70
PDE	2006	10	27	145836.90	43.06	13.55	33	2.5	MLROM	...	....	71
PDE	2006	10	27	150946	43.06	13.54	34	2.5	MLROM	...	....	71
PDE	2006	10	29	031615.20	43.06	13.52	22	2.9	MLLDG	...	....	71
PDE	2006	11	01	071824.30	42.60	13.07	6	3.0	MLROM	...	....	32
PDE	2006	11	01	145353.90	42.59	13.08	5	2.7	MLROM	...	....	31
PDE	2006	11	02	112738.30	42.74	12.76	10	2.6	MLROM	...	....	62
PDE	2006	11	04	100417.60	41.98	13.06	7	2.6	MDROM	...	....	56
PDE	2006	11	05	165735.10	42.74	12.76	3	2.6	MLROM	...	....	62
PDE	2006	11	13	233347	43.88	12.30	22	2.8	MLROM	...	....	184
PDE	2006	11	14	155356.20	43.10	12.64	5	2.5	MLROM	...	....	97
PDE	2006	12	05	062017	41.08	15.27	15	2.5	MLROM	...	....	215
PDE	2006	12	05	080734.80	43.44	12.65	56	2.5	MDROM	...	....	128
PDE	2006	12	09	221512	42.64	12.01	7	2.7	MLROM	...	....	116
PDE	2006	12	10	110342	41.94	16.20	35	4.6	mbGS	...	....	237
PDE	2006	12	16	143519.40	43.36	12.37	63	2.9	MDROM	...	....	133
PDE	2006	12	22	175036.30	41.94	14.13	8	2.8	MLROM	...	....	81
PDE	2006	12	27	221341.60	41.31	14.21	10	3.7	MDPDG	3F.	....	140
PDE	2006	12	28	013053.80	41.32	14.20	10	2.7	MLROM	...	....	139
PDE	2006	12	29	021401.10	44.22	13.55	10	3.4	MLGRF	...	....	199
PDE	2006	12	29	062331.60	41.78	15.50	3	2.8	MLROM	...	....	188
PDE	2006	12	29	070727.80	41.19	14.76	9	2.6	MDROM	...	....	177
PDE	2006	12	30	010908.60	42.77	12.76	10	2.5	MDROM	...	....	64
PDE	2007	01	05	014328.70	42.91	10.57	10	2.5	MLLDG	...	....	237
PDE	2007	01	05	160548	43.04	13.11	56	3.0	UKROM	...	....	72
PDE	2007	01	12	073802.20	42.78	12.75	9	2.6	MDROM	...	....	66
PDE	2007	01	16	103308.80	42.08	15.64	7	2.6	MLROM	...	....	189
PDE	2007	01	21	032636.40	41.89	12.78	8	2.5	MLROM	...	....	77
PDE	2007	01	22	065955.10	42.88	12.66	6	2.6	MDROM	...	....	78
PDE	2007	01	23	235828.60	43.12	13.41	23	2.5	MLROM	...	....	77
PDE	2007	01	24	220131.30	41.89	12.80	8	2.5	MLROM	...	....	76
PDE	2007	01	25	213609.56	43.58	13.53	10	3.8	MLLDG	...	....	128
PDE	2007	02	05	131028.50	43.05	13.52	10	3.2	MLLDG	...	....	70
PDE	2007	02	08	012626.39	42.80	13.21	6	3.2	MLROM	...	....	44
PDE	2007	02	08	013256.50	42.79	13.18	10	4.2	mbGS	...	....	44
PDE	2007	02	08	014724.40	42.79	13.21	9	2.5	MLROM	...	....	43
PDE	2007	02	09	003607.80	41.92	15.64	3	2.7	MLROM	...	....	194
PDE	2007	02	09	175109	43.76	13.26	10	2.6	MLROM	...	....	149

PDE	2007	02	11	152346.90	41.86	15.60	1	2.5	MLROM	...	....	192
PDE	2007	02	13	054840.60	41.79	13.94	8	2.5	MLROM	...	....	83
PDE	2007	02	14	231054.20	44.31	12.03	17	3.7	MLLDG	4F.	....	236
PDE	2007	02	17	193539.70	42.48	13.32	11	2.5	MLROM	...	....	8
PDE	2007	02	20	102749.20	40.81	15.25	11	2.5	MLROM	...	....	236
PDE	2007	02	24	111638.40	43.14	15.34	10	2.6	MLROM	...	....	177
PDE	2007	02	25	145859	41.80	15.91	26	3.1	MLROM	...	....	219
PDE	2007	02	28	134235.20	41.67	14.83	18	2.6	MLROM	...	....	145
PDE	2007	03	04	143940.80	43.78	11.97	5	2.5	MLLDG	...	....	190
PDE	2007	03	11	001251.70	41.79	13.93	7	2.7	MLROM	...	....	83
PDE	2007	03	11	053731.30	42.51	13.30	11	2.9	MLROM	...	....	12
PDE	2007	03	11	143603.80	41.78	13.93	7	2.5	MLROM	...	....	83
PDE	2007	03	15	084814.60	42.12	15.91	4	2.7	MLROM	...	....	210
PDE	2007	03	24	103152.35	40.59	15.09	309	3.3	UKROM	...	....	247
PDE	2007	03	29	043729.80	42.83	13.20	4	4.0	MLPDG	...	....	47
PDE	2007	04	16	235338	41.91	15.48	10	2.9	MLROM	...	....	181
PDE	2007	04	20	090332.60	43.66	13.36	5	2.6	MLROM	...	....	137
PDE	2007	04	23	170122.18	43.06	15.63	10	3.1	MLROM	...	....	196
PDE	2007	04	27	011930.80	42.92	13.63	14	3.3	MLLDG	...	....	58
PDE	2007	05	05	140355	42.74	13.56	8	3.4	MLLDG	...	....	37
PDE	2007	05	11	162055	44.33	12.23	30	2.7	MLZAG	...	....	231
PDE	2007	05	14	212926.80	41.80	15.92	23	2.5	MLROM	...	....	219
PDE	2007	05	17	233513.10	44.09	12.23	3	3.7	MLSTR	...	....	208
PDE	2007	05	17	233946	44.07	12.22	4	2.5	MLLDG	...	....	206
PDE	2007	05	17	235012	44.08	12.22	3	2.6	MLLDG	...	....	207
PDE	2007	05	18	013814.80	44.06	12.22	2	3.0	MLLDG	...	....	205
PDE	2007	05	18	041115.60	44.07	12.23	3	2.8	MLLDG	...	....	206
PDE	2007	05	18	052126.30	44.11	12.24	4	3.2	MLLDG	...	....	209
PDE	2007	05	22	214140	44.08	12.22	10	3.1	MLLDG	...	....	207
PDE	2007	05	23	205551.60	43.20	12.60	7	2.7	MLLDG	...	....	108
PDE	2007	05	24	173214.10	41.69	14.81	14	2.6	MLROM	...	....	142
PDE	2007	05	27	125538	42.11	15.06	5	2.6	MLROM	...	....	141
PDE	2007	06	02	123859.20	41.75	16.10	24	3.0	MLROM	...	....	235
PDE	2007	06	13	061015.90	43.19	12.63	4	2.7	MLROM	...	....	105
PDE	2007	06	22	160425	43.41	10.85	7	2.9	MLLDG	3F.	....	234
PDE	2007	07	18	105411.60	43.74	15.17	3	4.7	MLPDG	.F.	....	205
PDE	2007	07	18	143300.18	43.78	15.19	5	3.5	MLLDG	...	....	209
PDE	2007	07	20	015625.20	43.80	15.40	5	3.1	MLZAG	...	....	223
PDE	2007	07	22	172603	41.91	13.67	17	3.6	MLPDG	4F.	....	61
PDE	2007	07	22	205737.90	43.80	15.40	0	3.3	MLLDG	...	....	223
PDE	2007	07	28	004124	43.72	13.39	5	3.2	MLROM	4F.	....	144
PDE	2007	08	01	121725	43.66	13.34	3	3.1	MLLDG	3F.	....	137
PDE	2007	08	12	015211	42.74	13.04	11	3.8	MLGRF	4F.	....	45
PDE	2007	08	16	002942	42.82	13.12	10	3.6	MLLDG	4F.	....	49
PDE	2007	08	16	042549	42.82	13.12	7	2.8	MLROM	.F.	....	49
PDE	2007	08	16	204604	41.49	13.77	10	3.5	MLROM	4F.	....	108
PDE	2007	08	20	141958.80	41.88	15.62	2	2.9	MLROM	...	....	193
PDE	2007	08	22	070708.30	41.44	15.79	2	2.8	MLROM	...	....	226
PDE	2007	08	23	091509.20	43.15	13.40	25	2.6	MDROM	...	....	81
PDE	2007	08	23	093119.90	43.13	13.43	3	2.6	MLROM	...	....	79
PDE	2007	08	23	233847.80	42.82	13.17	7	2.5	MLROM	...	....	47
PDE	2007	08	24	100003.30	43.15	13.40	29	2.5	MLROM	...	....	81
PDE	2007	08	26	153658.30	43.65	12.00	50	2.5	MDROM	...	....	177
PDE	2007	08	30	144246.20	42.68	12.73	10	2.7	MLROM	...	....	61
PDE	2007	09	08	175612.40	43.99	12.44	35	2.7	MLLDG	...	....	190
PDE	2007	09	14	171924.50	42.72	13.14	1	2.5	MLROM	...	....	38
PDE	2007	09	28	065923.37	43.11	15.13	10	4.1	mbGS	...	....	161
PDE	2007	10	07	063623	43.19	13.02	48	3.4	UKROM	...	....	90
PDE	2007	10	18	232545.01	41.67	14.69	10	4.0	MLROM	...	....	135
PDE	2007	10	21	035536.40	42.41	13.07	10	4.3	mbGS	...	....	26

PDE	2007	10	25	073618.60	42.38	12.99	8	2.8	MLROM	...	....	33
PDE	2007	10	25	073858	42.39	12.99	9	2.9	MLROM	...	....	33
PDE	2007	10	25	091547.70	42.39	12.99	7	2.9	MLROM	...	....	33
PDE	2007	11	01	144846.40	43.95	11.89	7	2.8	MLROM	...	....	208
PDE	2007	11	03	002557.20	41.38	12.25	7	2.5	MLROM	...	....	149
PDE	2007	11	03	220840.70	43.28	10.87	5	3.2	MLLDG	...	....	227
PDE	2007	11	05	155313.20	42.79	13.41	9	2.8	MLROM	...	....	40
PDE	2007	11	09	092701	43.19	11.02	11	2.6	MLROM	...	....	211
PDE	2007	11	11	090724.30	42.64	12.71	10	2.5	MLROM	...	....	61
PDE	2007	11	16	123626.20	42.00	13.71	17	2.7	MLROM	...	....	54
PDE	2007	11	25	060722.10	41.88	12.93	8	2.5	MLROM	...	....	72
PDE	2007	12	04	135432	41.49	14.25	10	2.5	MLROM	...	....	125
PDE	2007	12	06	212526.30	40.85	15.18	10	2.8	MLROM	...	....	228
PDE	2007	12	17	131404.98	44.02	14.90	10	3.8	MLPDG	.F.	....	215
PDE	2007	12	20	175705.19	43.59	15.67	29	3.3	MLZAG	...	....	226
PDE	2007	12	24	015846	41.88	15.38	7	2.9	MLROM	...	....	174
PDE	2008	01	02	090447	42.38	12.88	8	2.9	MLROM	...	....	42
PDE	2008	01	08	195245.10	43.49	12.56	54	2.6	MDROM	...	....	136
PDE	2008	01	12	233948.50	41.39	14.50	5	2.8	MLROM	...	....	146
PDE	2008	01	18	091031.90	41.87	12.93	8	2.7	MLROM	...	....	72
PDE	2008	01	19	151145.50	41.76	16.26	24	3.2	MLROM	...	....	247
PDE	2008	01	22	113045.79	42.83	13.59	15	3.1	MLROM	...	....	48
PDE	2008	01	23	110426.50	42.83	13.62	23	2.8	MLROM	...	....	49
PDE	2008	01	24	131138.80	42.84	13.61	22	2.5	MLROM	...	....	49
PDE	2008	01	24	144302.60	41.49	14.60	12	2.7	MLROM	...	....	144
PDE	2008	01	24	204857	42.50	13.42	16	2.6	MLROM	...	....	9
PDE	2008	01	25	053320.50	44.12	12.15	10	2.7	MLLDG	...	....	213
PDE	2008	01	29	082921.30	41.59	13.77	8	2.9	MLROM	...	....	97
PDE	2008	02	06	052812.70	43.10	10.77	8	2.6	MLLDG	...	....	227
PDE	2008	02	06	183417.99	41.29	13.96	10	3.1	MLROM	...	....	133
PDE	2008	02	11	130536	41.71	14.94	16	2.6	MLROM	...	....	150
PDE	2008	02	16	221216.80	43.11	10.77	16	3.1	MLLDG	4F.	....	228
PDE	2008	02	19	215849	43.51	13.00	34	2.8	MLLDG	...	....	124
PDE	2008	02	20	080619.10	41.58	13.78	8	4.6	mbGS	4F.	....	98
PDE	2008	02	20	201242.10	43.42	12.67	64	2.6	MDROM	...	....	126
PDE	2008	02	24	121658	42.07	14.10	10	2.6	MLROM	...	....	70
PDE	2008	02	26	033715.20	41.75	15.20	17	3.3	MLPDG	3F.	....	167
PDE	2008	02	26	062931.80	41.77	15.19	14	2.5	MLROM	...	....	165
PDE	2008	02	27	110740.60	44.09	11.70	29	3.0	MLLDG	...	....	230
PDE	2008	03	07	190434.50	42.65	13.25	7	2.6	MLROM	...	....	27
PDE	2008	03	15	042844.40	43.76	15.37	10	3.7	MLGRF	...	....	218
PDE	2008	03	18	090118.60	41.37	15.70	3	2.7	MLROM	...	....	224
PDE	2008	03	19	143857.70	41.90	15.86	31	4.3	mbGS	4F.	....	211
PDE	2008	03	19	170219.30	41.89	15.74	16	2.6	MLROM	...	....	202
PDE	2008	03	20	175029.60	41.59	15.78	8	2.5	MLROM	...	....	218
PDE	2008	03	24	170426.10	43.16	15.35	10	3.0	MLZAG	...	....	179
PDE	2008	03	25	055138.20	44.02	11.74	8	3.0	MLLDG	...	....	223
PDE	2008	03	25	160714	44.03	11.73	6	2.5	MLROM	...	....	224
PDE	2008	03	29	144942	44.13	12.34	7	3.3	MLLDG	4F.	....	208
PDE	2008	04	09	195753.60	41.91	15.90	32	2.7	MLROM	...	....	214
PDE	2008	04	12	054442.20	41.78	12.58	14	3.7	MLROM	4F.	....	97
PDE	2008	04	12	0558	41.80	12.58	10	2.2	MLROM	.F.	....	96
PDE	2008	04	12	062056	44.53	12.91	27	2.5	MLROM	...	....	237
PDE	2008	04	14	080606.80	43.71	15.37	10	2.6	MLROM	...	....	215
PDE	2008	04	21	101733.20	41.68	15.76	23	2.8	MLROM	...	....	212
PDE	2008	04	22	040716.98	44.10	15.21	10	2.6	MLZAG	...	....	237
PDE	2008	04	22	095536	42.12	12.68	9	2.8	MLROM	4F.	....	67
PDE	2008	04	23	104824.70	41.81	16.00	22	2.7	MLROM	...	....	226
PDE	2008	04	27	074627.90	43.89	12.01	7	2.7	MLLDG	...	....	198
PDE	2008	05	04	232821	43.11	13.42	3	3.3	MLLDG	...	....	76

PDE	2008	05	05	181351.81	42.80	16.30	2	3.7	MLZAG	... .	241
PDE	2008	05	20	080811	41.65	14.86	18	2.8	MLROM	... .	148
PDE	2008	05	26	002453.30	43.20	13.47	1	2.8	MLLDG	.F.	86
PDE	2008	05	27	161933.50	40.76	15.32	8	2.7	MLROM	... .	244
PDE	2008	05	30	160413.60	41.95	13.28	7	2.6	MLROM	... .	53
PDE	2008	05	30	172253.79	40.57	14.88	309	4.4	mbGS	... .	240
PDE	2008	06	01	121855.20	43.49	12.70	36	2.6	MDROM	... .	130
PDE	2008	06	01	122433.40	43.49	12.71	36	2.8	MDROM	... .	130
PDE	2008	06	01	123023.10	43.49	12.69	36	3.6	MLLDG	.F.	131
PDE	2008	06	01	131245.50	43.50	12.72	38	2.8	MDROM	... .	131
PDE	2008	06	08	172326.30	41.04	11.90	5	2.8	MLLDG	... .	197
PDE	2008	06	10	193812.60	42.37	13.10	10	2.6	MLROM	... .	25
PDE	2008	06	11	164808.60	41.69	15.74	1	2.5	MLROM	... .	210
PDE	2008	06	29	084707.20	44.15	12.64	10	2.6	MLLDG	... .	201
PDE	2008	07	08	213538	43.22	15.52	10	3.0	MLROM	... .	195
PDE	2008	07	09	094720.60	42.51	13.27	10	3.1	MLROM	... .	13
PDE	2008	07	29	031121	42.48	13.36	9	3.2	MLROM	... .	7
PDE	2008	09	21	222554.86	43.20	10.80	8	2.6	MLLDG	... .	229
PDE	2008	10	01	224737.20	42.59	13.29	15	3.1	MLROM	... .	20
PDE	2008	10	09	031010.90	41.86	15.79	7	2.5	MLROM	... .	207
PDE	2008	10	11	114235.30	41.99	13.72	11	2.6	MLROM	... .	55
PDE	2008	10	11	125830.20	41.97	14.03	13	3.3	MLROM	... .	72
PDE	2008	10	11	185541.30	42.74	12.56	4	2.7	MLROM	... .	76
PDE	2008	10	12	065847.50	42.74	12.57	7	2.6	MLROM	... .	76
PDE	2008	10	13	181627.30	43.20	10.77	17	2.5	MLLDG	... .	230
PDE	2008	11	09	093003	43.18	13.37	31	3.1	MLLDG	... .	83
PDE	2008	11	18	170631	44.27	12.05	10	2.9	MLLDG	... .	232
PDE	2008	11	18	225003	44.15	11.96	9	3.0	MLLDG	... .	224
PDE	2008	11	20	153943.27	43.26	14.69	10	3.5	MLLDG	... .	141
PDE	2008	11	23	081158.60	44.27	12.06	10	2.7	MLLDG	... .	231
PDE	2008	12	02	0315	43.64	13.36	10	3.2	MLROM	4F.	135
PDE	2008	12	07	225750	42.57	12.70	7	2.7	MLROM	4F.	59
PDE	2008	12	23	190703.34	44.51	13.65	10	3.6	MLZAMG	... .	232
PDE	2009	03	29	084309.02	42.04	13.92	10	4.0	MLPDG	4F.	61
PDE	2009	03	30	133839.72	42.36	13.35	5	4.3	mbGS	5FM	7
PDE-W	2009	04	05	202053	44.24	12.00	28	4.6	mbGS	5FM	231
PDE-W	2009	04	05	204854	42.33	13.37	8	4.0	mbGS	4FM	10
PDE-W	2009	04	06	013239	42.33	13.33	8	6.3	MwUCMT	7CM ......S	11
PDE-W	2009	04	06	013630.46	42.41	13.22	5	4.8	mbGS	... .	14
PDE-W	2009	04	06	022746	42.37	13.34	10	4.2	mbGS	3F.	6
PDE-W	2009	04	06	023704	42.37	13.34	10	4.9	MwRMT	7FM	7
PDE-W	2009	04	06	035645	42.34	13.39	10	4.4	mbGS	3FM	9
PDE-W	2009	04	06	044753	42.35	13.35	9	4.0	MLPDG	2F.	8
PDE-W	2009	04	06	071710	42.35	13.37	9	4.3	mbGS	4FM	7
PDE-W	2009	04	06	163809	42.36	13.33	10	4.3	mbGS	.FM	8
PDE-W	2009	04	06	215653	42.40	13.32	9	4.1	mbGS	3F.	6
PDE-W	2009	04	06	224713	42.35	13.29	11	4.1	MLSTR	3F.	11
PDE-W	2009	04	06	231537	42.45	13.36	8	4.9	MwRMT	.FM	4
PDE-W	2009	04	07	092628	42.34	13.39	10	4.8	MwRMT	5FM	9
PDE-W	2009	04	07	174737	42.28	13.46	15	5.5	MwUCMT	6CM	17
PDE-W	2009	04	07	213429	42.38	13.38	7	4.6	mbGS	3FM	5
PDE-W	2009	04	08	042741	42.31	13.47	10	4.1	mbGS	.F.	14
PDE-W	2009	04	08	225650	42.51	13.36	10	4.1	mbGS	4FM	9
PDE-W	2009	04	09	005259	42.48	13.34	15	5.3	MwGS	5FM	8
PDE-W	2009	04	09	031452	42.34	13.44	18	4.3	mbGS	3FM	10
PDE-W	2009	04	09	043244	42.44	13.42	8	4.2	mbGS	2FM	3
PDE-W	2009	04	09	044309	42.51	13.37	9	4.0	MLZAMG	2F.	9
PDE-W	2009	04	09	131934.29	42.37	13.19	4	4.0	MLPDG	3FM	18
PDE-W	2009	04	09	193817.36	42.51	13.33	2	5.2	MwGCMT	6FM	11
PDE-W	2009	04	09	224006	42.48	13.30	10	3.6	MLROM	3F.	10
PDE-W	2009	04	10	032222	42.47	13.42	9	4.0	mbGS	3FM	5
PDE-W	2009	04	13	211424	42.50	13.36	7	4.9	mbGS	5FM	9
PDE-W	2009	04	14	135621	42.54	13.31	10	3.9	MLROM	3F.	14
PDE-W	2009	04	14	201727	42.53	13.29	10	4.1	MLZAMG	4FM	14
PDE-W	2009	04	15	225307	42.51	13.31	8			3FM	11
PDE-W	2009	04	16	174930	42.54	13.29	10	3.8	MLROM	3F.	15
PDE-W	2009	04	18	090556	42.44	13.36	14	3.8	MLROM	4F.	3
PDE-W	2009	04	23	151408	42.25	13.49	9	4.1	MLPDG	4FM	21
PDE-W	2009	04	23	2149	42.23	13.48	9	4.2	mbGS	.FM	22
PDE-W	2009	04	24	225129	42.27	13.51	11	3.0	MLROM	.F.	19
PDE-W	2009	05	01	051251	42.28	13.47	9	3.8	MLROM	.F.	17
PDE-W	2009	06	22	205840	42.45	13.36	14	4.7	mbGS	6FM	4
PDE-W	2009	06	23	004156.02	42.44	13.31	4	4.0	mbGS	4F.	7
PDE-W	2009	06	30	003810	42.57	13.20	10	3.4	MLROM	3F.	22
PDE-W	2009	07	03	110307	42.41	13.39	8	4.1	MLROM	... .	1
PDE-W	2009	07	12	083851	42.34	13.38	10	4.1	mbGS	.FM	9
PDE-W	2009	07	12	221424.88	42.33	13.34	5	3.6	MLROM	4F.	11
PDE-W	2009	08	06	153646.46	41.66	13.60	20	4.4	mbGS	... .	86
PDE-W	2009	09	20	035017	43.41	13.39	37	4.3	mbGS	5FM	109
PDE-Q	2010	01	12	082510	43.12	13.41	25	4.5	mbGS	... .	77
PDE-Q	2010	01	12	133547.06	43.26	13.47	31	4.6	mbGS	... .	92

Appendix I: Time series profiles of points analysed

Topography and Slope Aspects of points on Google map with Elevation Exaggeration of 3

Shade, slope, aspect and cloudiness play a dominant part in the spatial distribution of solar energy at a given elevation, to the extent that solar energy input can easily vary by a factor of 100 from a permanently shaded valley bottom to a well exposed slope [16]. Aspect controls solar radiation to hill-slopes: north facing slopes are more shaded in the northern hemisphere, while south facing slopes are not. South facing slopes are more directed to the sunlight, winds and snow becoming warmer and dryer (due to higher levels of evapotranspiration) than a north-facing slope. The aspect of a slope can make very significant influences on its local climate. The sun illumination also plays a significant role as it describes how much radiation an object will get throughout the day. For example, because the sun's rays are in the west at the hottest time of day in the afternoon, in most cases a west-facing slope will be warmer than a sheltered east-facing slope [64].

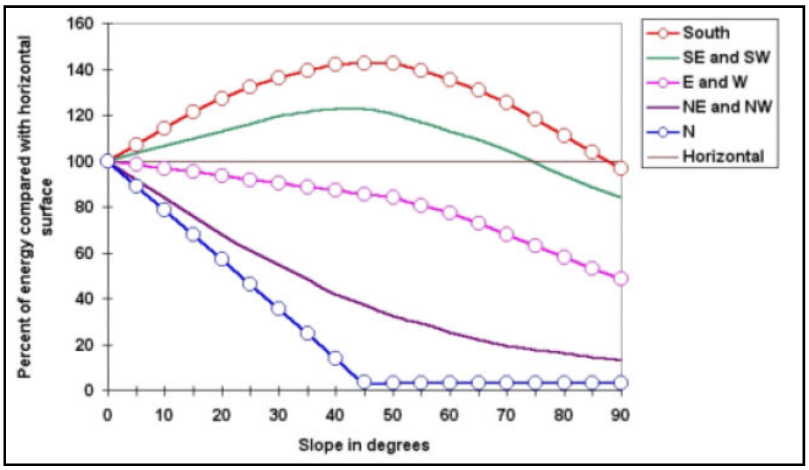

Figure 5-3: Amount of energy received by a sloping surface compared with a horizontal surface (Northern Hemisphere, 45º latitude). The abscissa indicates the slope in degrees, varying from 0º (horizontal) to 90º (vertical), while the different curves show the effect of aspect, i.e. the direction in which a perpendicular to the surface points, e.g. East and West indicates the energy received by surfaces that face the East and those that face the West [16].

As seen in Figure 5-3, the amount of energy received by sloping surfaces in the Northern hemisphere is illustrated so if a pixel in the image is located on a south facing slope it receives most energy. In the Southern Hemisphere, the N and S sky directions are inverted, i.e. the curve standing for North becomes South, South-East and South-West becomes North-East and North-West, etc... Also note that the curves go through a maximum at the slope that corresponds to the latitude, i.e. the closer the station is to the equator, the "flatter" the curves get: near the equator, steep slopes receive relatively less energy than gentle slopes.

BAM EARTHQUAKE: Located in the Northern Hemisphere

Condition (i): Pixel 37,40- which is the epicentre is oriented on a gently facing North-Eastern slope which is relatively flat in the region.

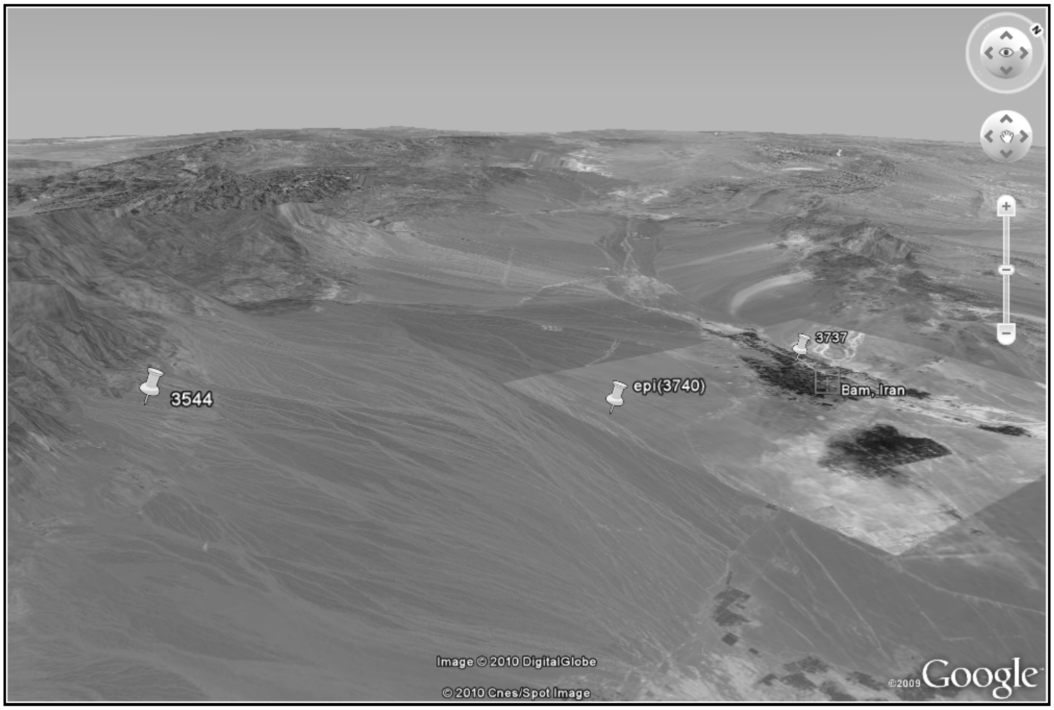

Condition (ii): Pixel 35,44- oriented on a North-Eastern slope and is in a close proximity to the epicentre is explained within this study.

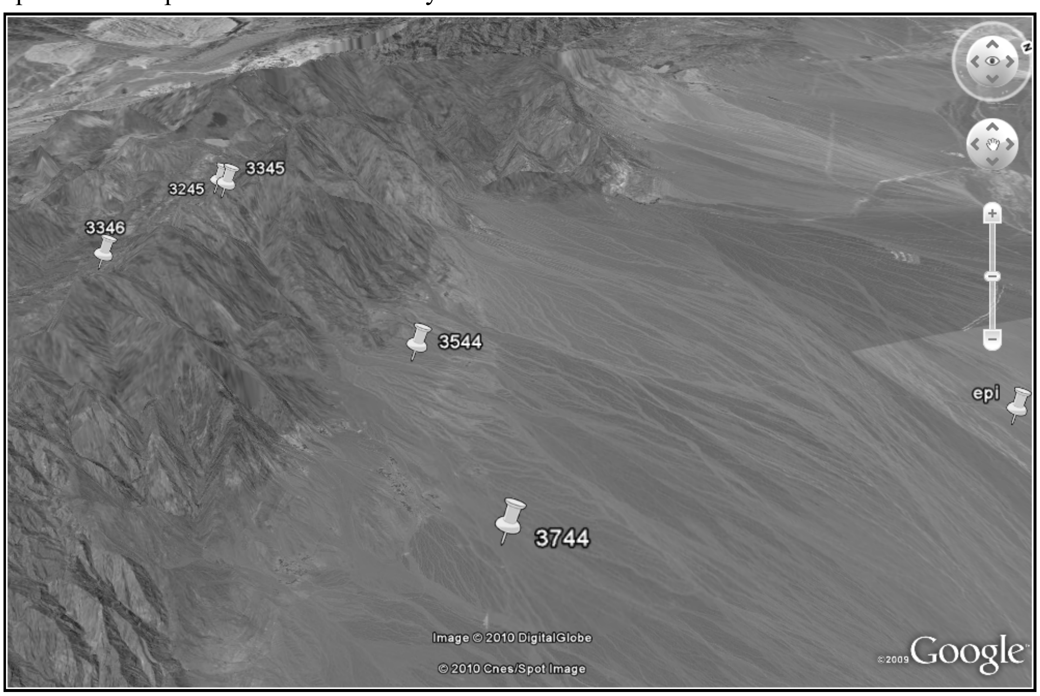

Condition (iii): Pixel 20,15- oriented on an Eastern slope and is far from the epicentral region.

Condition (iv): Pixel 32,45- oriented on a South-Western slope.

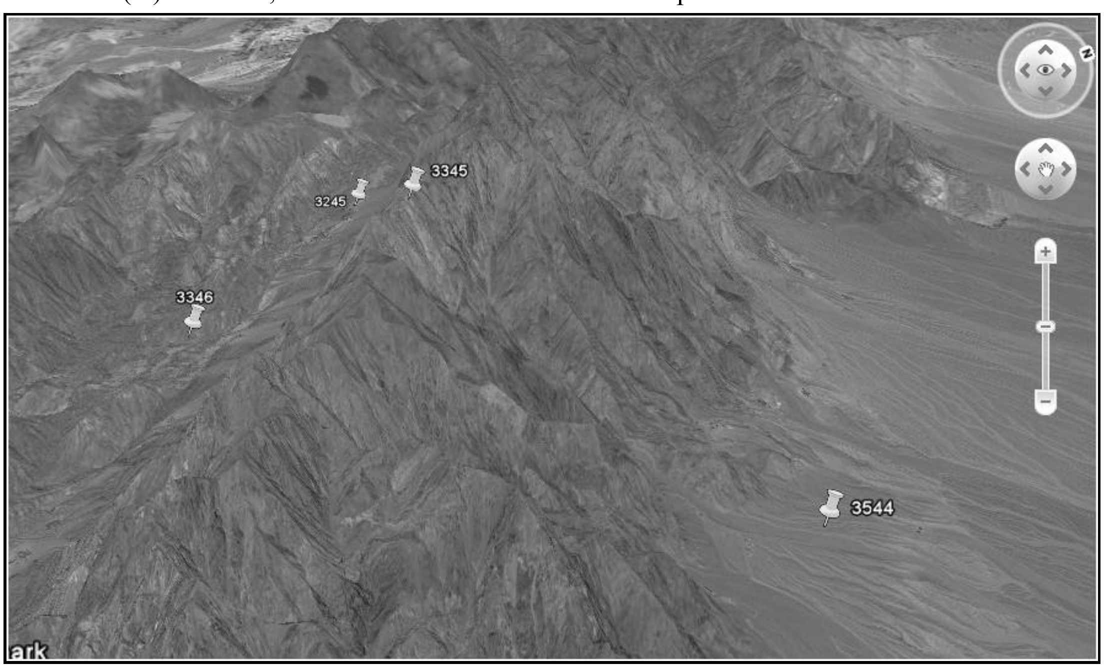

Condition (i) for the epicentre.

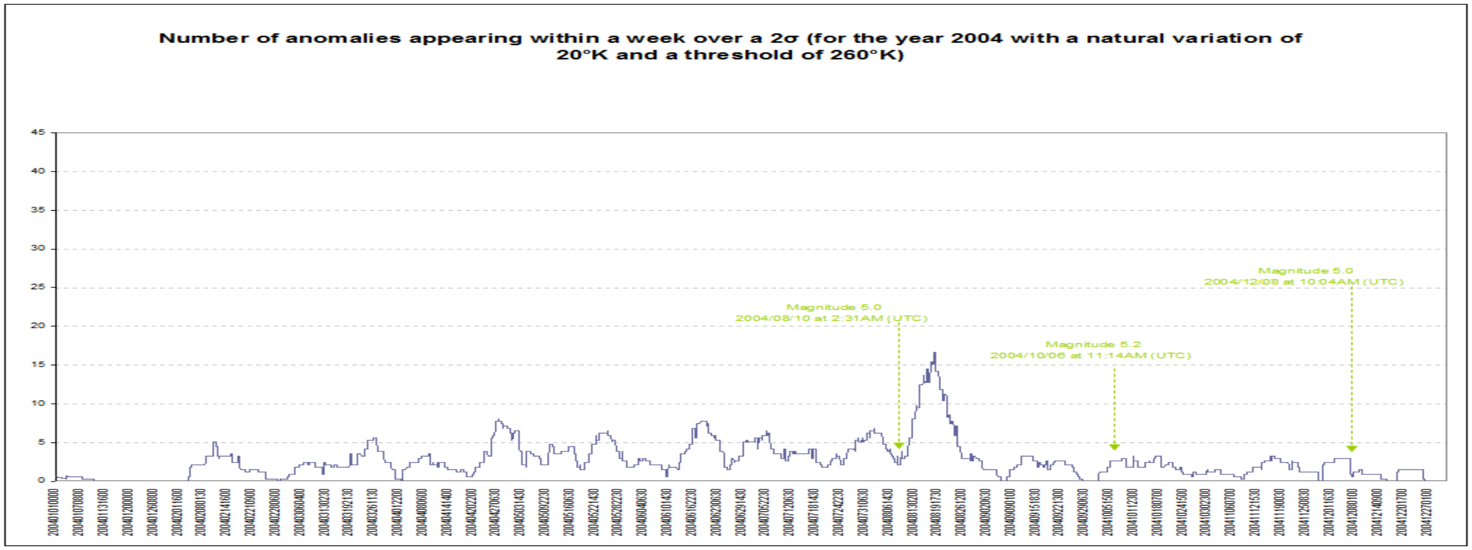

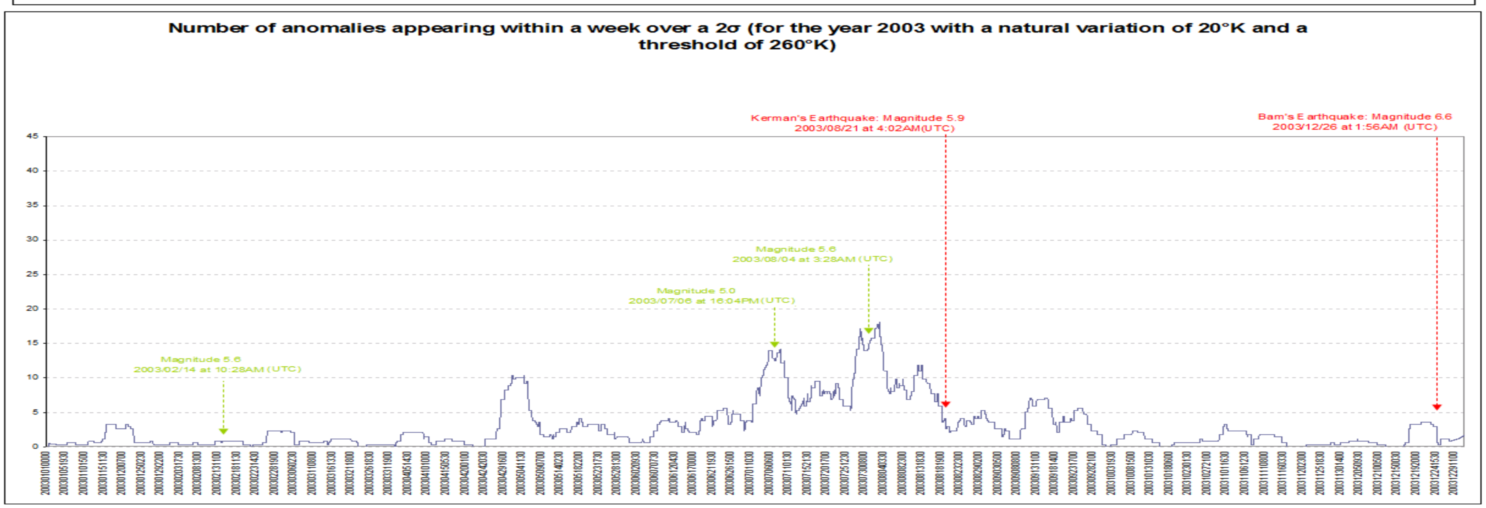

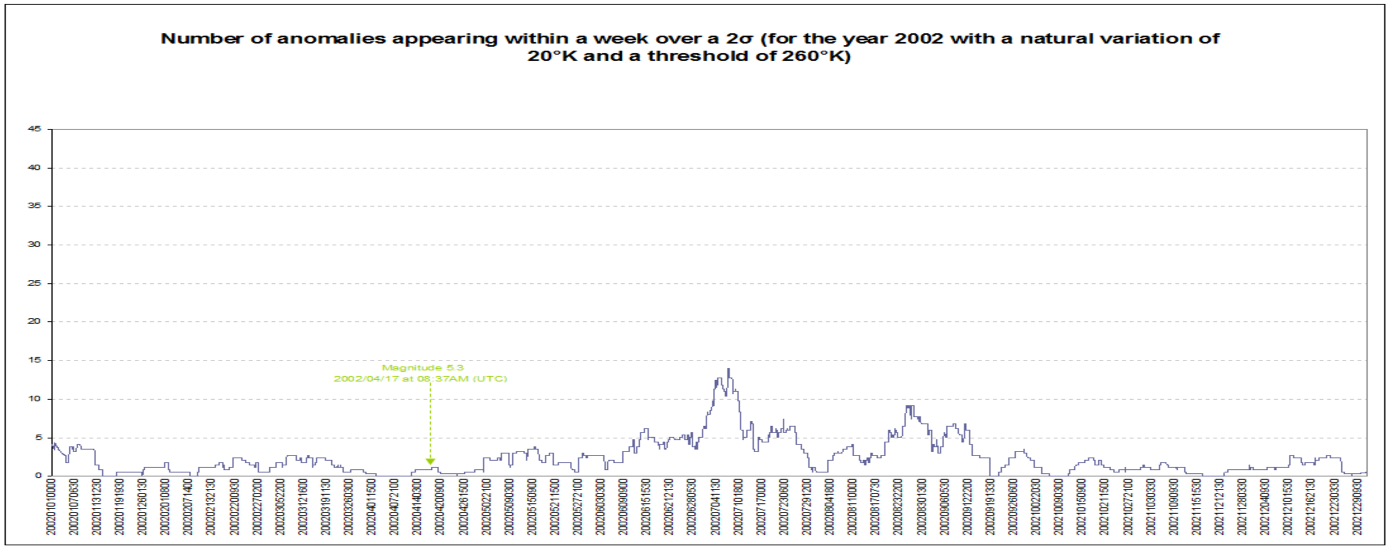
Number of anomalies appearing within a week over a 2σ (for the year 2002 with a natural variation of 20°K and a threshold of 260°K)
Magnitude 5.3
2002/04/17 at 08:37AM (UTC)

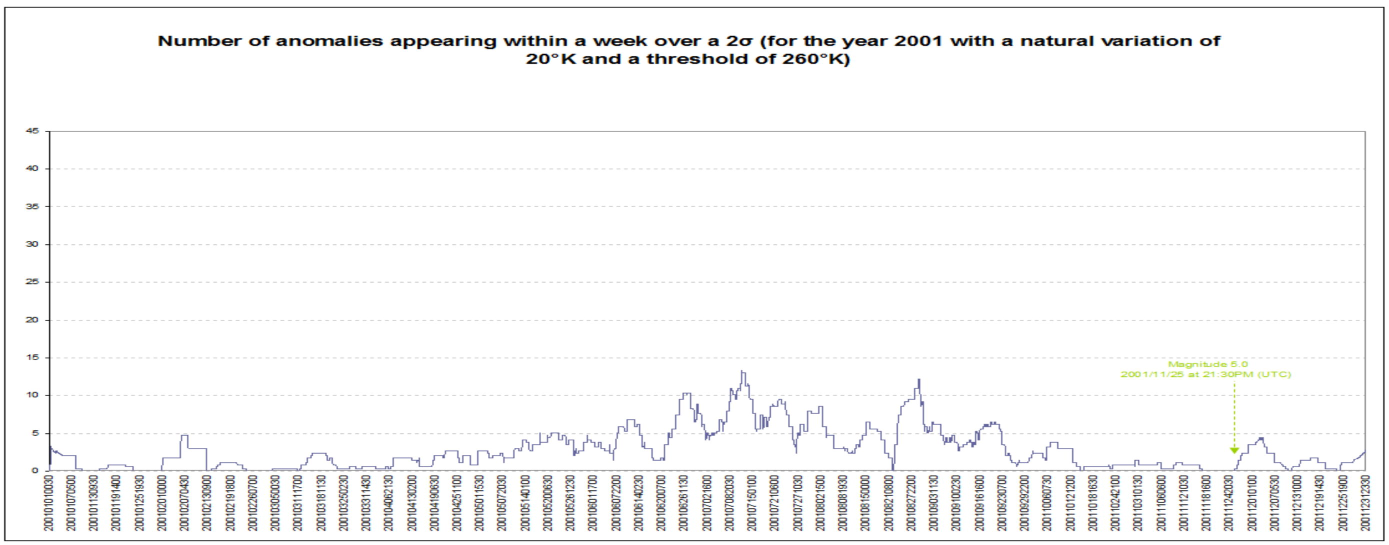
Number of anomalies appearing within a week over a 2σ (for the year 2001 with a natural variation of 20°K and a threshold of 260°K)
Magnitude 5.0
2001/11/25 at 21:30PM (UTC)

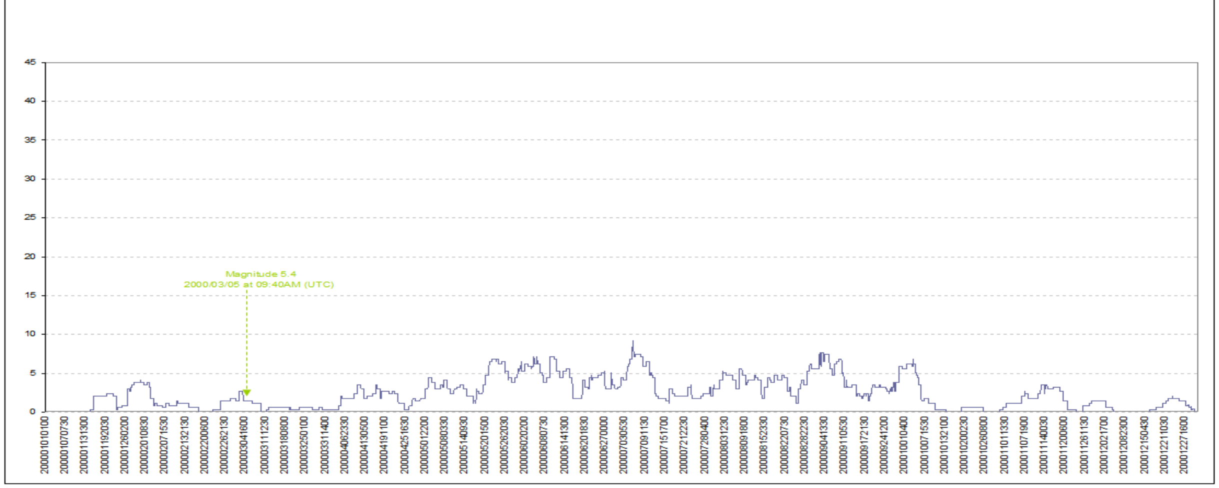

Number of anomalies appearing within a week over a 2σ (for the year 2000 with a natural variation of 20°K and a threshold of 260°K)

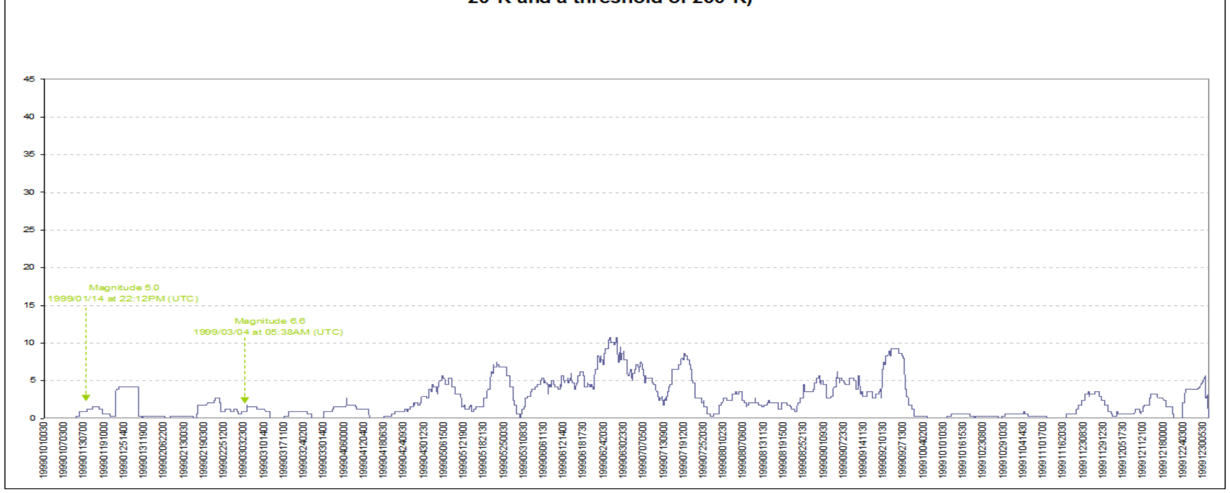

Number of anomalies appearing within a week over a 2σ (for the year 1999 with a natural variation of 20°K and a threshold of 260°K)

As seen from the 2003 profile, there is no significant earthquake-related anomaly generated for a month period before and a week after the Bam's earthquake event. Anomalies appear in summer whereby an approximate 20% count of anomalies last for a week period. This may be a result of another earthquake occurring in the summer period of the same year called Kerman's earthquake on August 21st 2003 with a lower magnitude of 5.9. This may lead us to understand that perhaps sporadic release of energy from stressed rocks leads to a reduction on magnitude of the main shock. Also, there was a 10% count of anomalies appearing in April which is regarded as a false positive since no earthquake (above magnitude 5.0) was recorded. This is half the number of anomalies appearing before the Kerman's earthquake which offers much uncertainty for the developed method. When analysed visually it was seen that there were still clouds affecting some of the background pixels within the ring. This uncertainty can be limited by the long time series dataset, as patterns can be used to draw conclusions about the anomalous behaviour. In comparison with other years, many of the false positives from 2003 appeared in other years. For instance, observing the Kerman's earthquake for a one month period prior to the event, it will suggest that the anomaly is a result of the earthquake. However, a distinct pattern or trend is still evident within each profile for the summer period (July-August months) suggesting that the anomaly within 2003 is not an earthquake-related anomaly but an anomaly caused by some other factor. Likewise, for the Bam earthquake in December, there was no sign of any anomalous activity for all the years including that of 2003.

Condition (iv) for 2003:

To assess topography and aspect, a different facing slope from condition (ii) is studied. By just observing 2003, there was a relatively significant earthquake-related anomaly of 25% in December. Early January of that same year, a smaller anomaly was seen and had a relation of 10% to an earthquake occurrence. This was regarded as a false positive within the series. There was no evidence which supported that an earthquake anomaly was apparent before the Kerman's earthquake, in this profile. In the year 2000, the maximum chance for an earthquake-related anomaly was 20% in November. Even though this value was decreasing, this anomalous behaviour lasted beyond November into December. Likewise, in 1999, a dual peak is prominent with maximum amplitudes of approximately 27% and 18%. Whilst comparing the other years, it was found that several false positives (especially in the month of January) as well as false negatives are within the profiles. This profile is comparable to that of the profiles in condition (ii). Watching these profiles not much can be said about the time the anomalies were detected. The time of day plays a significant role in the amount of heat transferred to an object. The original outputs from the anomaly detection algorithm were used which provided the times the anomaly was most prevalent within a 1σ, 2σ and 3σ profile. They were found to be common at the evening-night-time period.

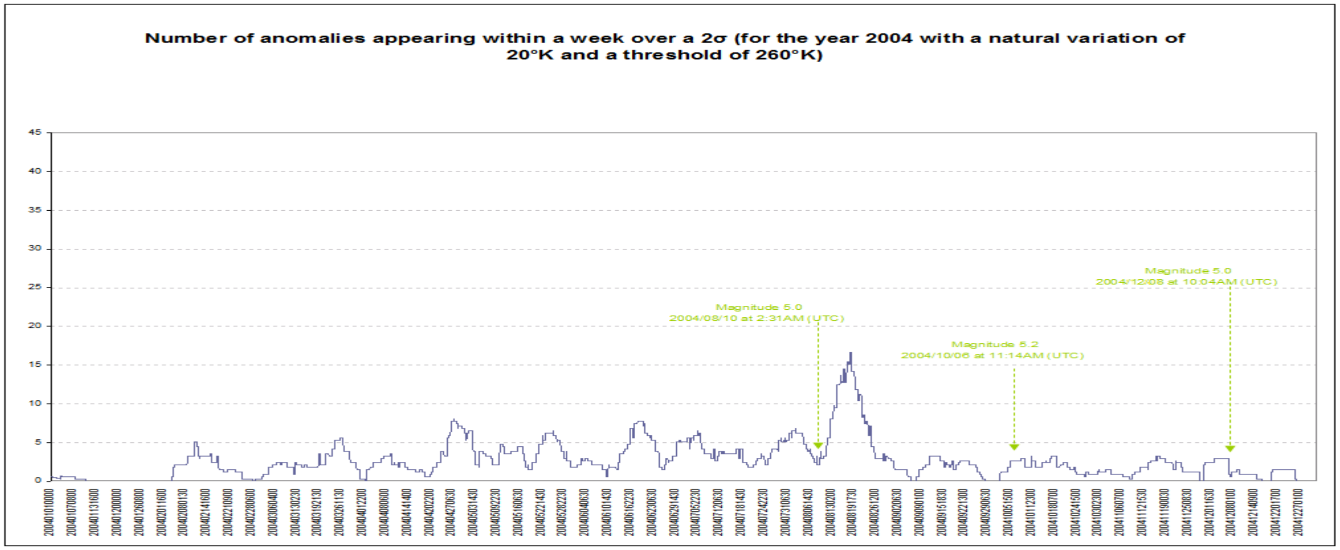
Number of anomalies appearing within a week over a 2σ (for the year 2004 with a natural variation of 20°K and a threshold of 260°K)
Magnitude 5.0
2004/08/10 at 2:31AM (UTC)
Magnitude 5.2
2004/10/06 at 11:14AM (UTC)
Magnitude 5.0
2004/12/08 at 10:04AM (UTC)

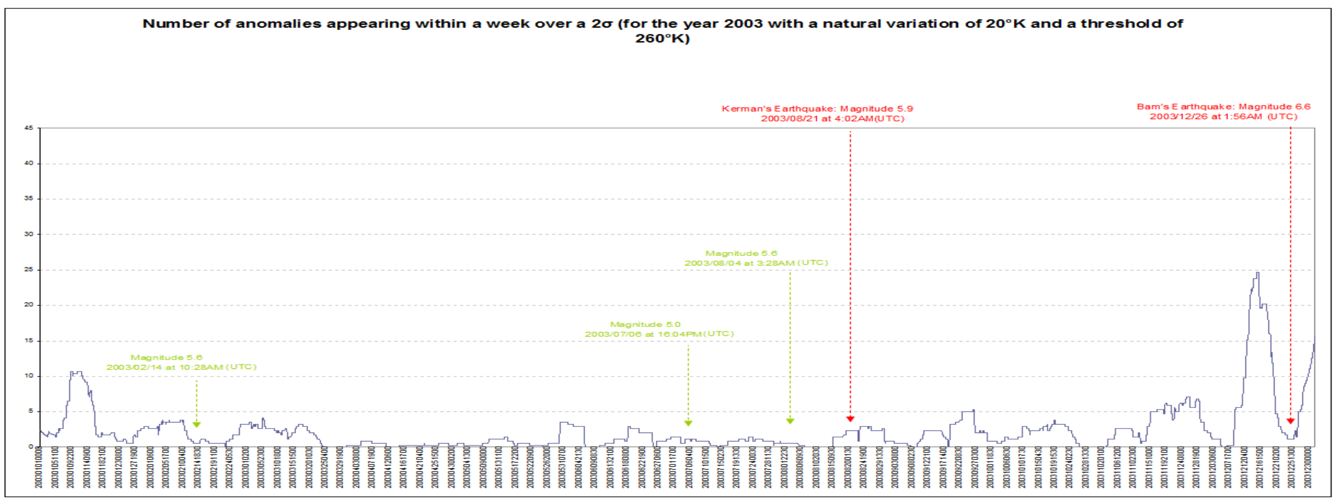
Number of anomalies appearing within a week over a 2σ (for the year 2003 with a natural variation of 20°K and a threshold of 260°K)
Magnitude 5.6
2003/02/14 at 10:28AM (UTC)
Magnitude 5.0
2003/07/06 at 16:04PM (UTC)
Magnitude 5.6
2003/08/04 at 3:28AM (UTC)
Kerman's Earthquake: Magnitude 5.9
2003/08/21 at 4:02AM(UTC)
Bam's Earthquake: Magnitude 6.6
2003/12/26 at 1:56AM (UTC)

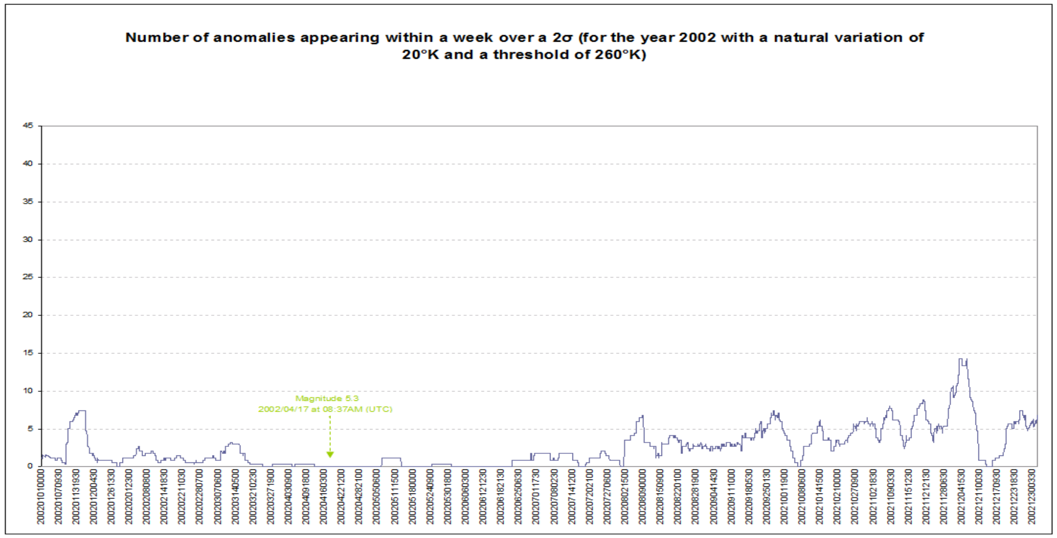
Number of anomalies appearing within a week over a 2σ (for the year 2002 with a natural variation of 20°K and a threshold of 260°K)
Magnitude 5.3
2002/04/17 at 08:37AM (UTC)

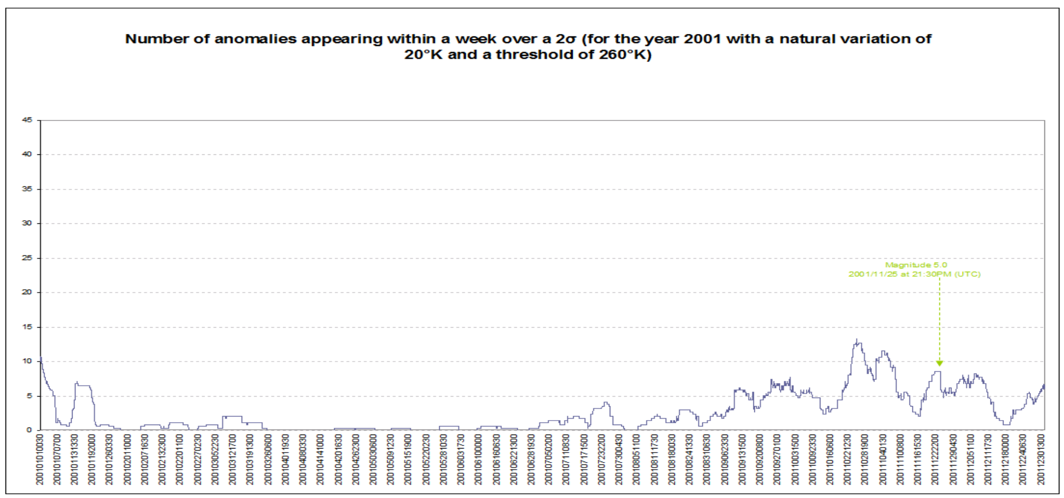
Number of anomalies appearing within a week over a 2σ (for the year 2001 with a natural variation of 20°K and a threshold of 260°K)
Magnitude 5.0
2001/11/25 at 21:30PM (UTC)

Number of anomalies appearing within a week over a 2σ (for the year 2000 with a natural variation of 20°K and a threshold of 260°K)

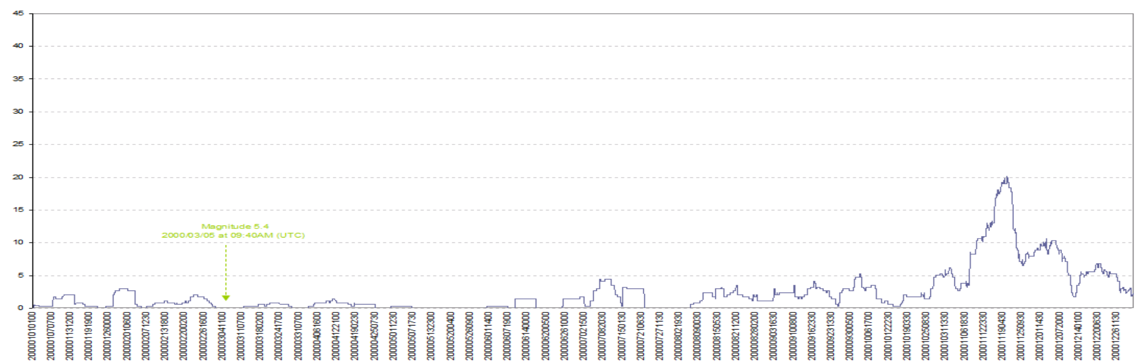

Number of anomalies appearing within a week over a 2σ (for the year 1999 with a natural variation of 20°K and a threshold of 260°K)

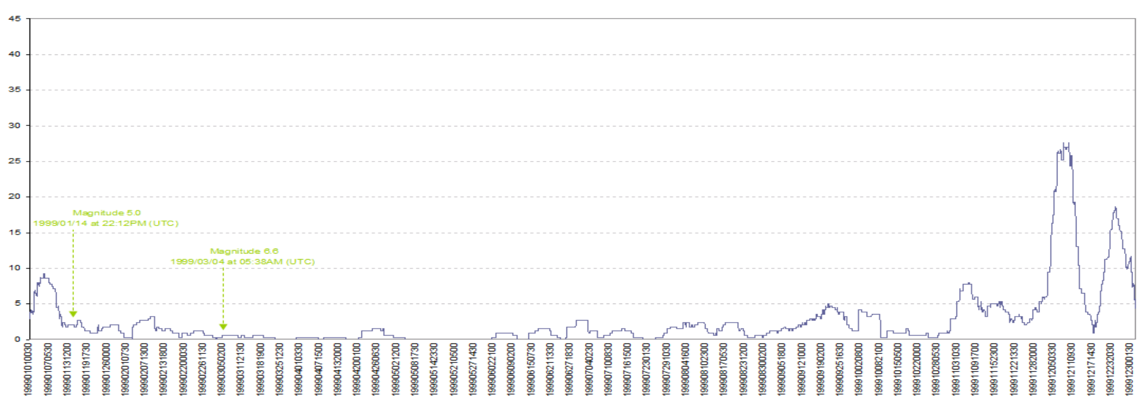

Condition (iii) which is a pixel (20,15) located far from the epicentre. This pixel is oriented on an eastern slope. In Section 4.1.2, describes the evnt taking place in the year of the earthquake occurrence as observed in this pixel. The other years are shown in figures below.

As suggested, pixels occurring far from the epicentre should not be influenced by the thermal anomalies and have a greater chance of not being related to the impending earthquake event. For 2003, there were no earthquake-related anomalies for Bam neither for Kerman. All the anomalies within this year were relatively insignificant as they were all under a 5% chance of being related to the earthquake phenomena. As compared to other years, the maximum relation for any sort of an earthquake anomaly was 10%. In 2001, a magnitude 5.0 earthquake produced an approximate 10% chance of being earthquake-related. Even though there was an earthquake in 2001, a similar pattern in 2002 appeared suggesting that, this cannot be caused by the earthquake but by another component such as seasonality within the dataset. False positives continuously emerge within the dataset.

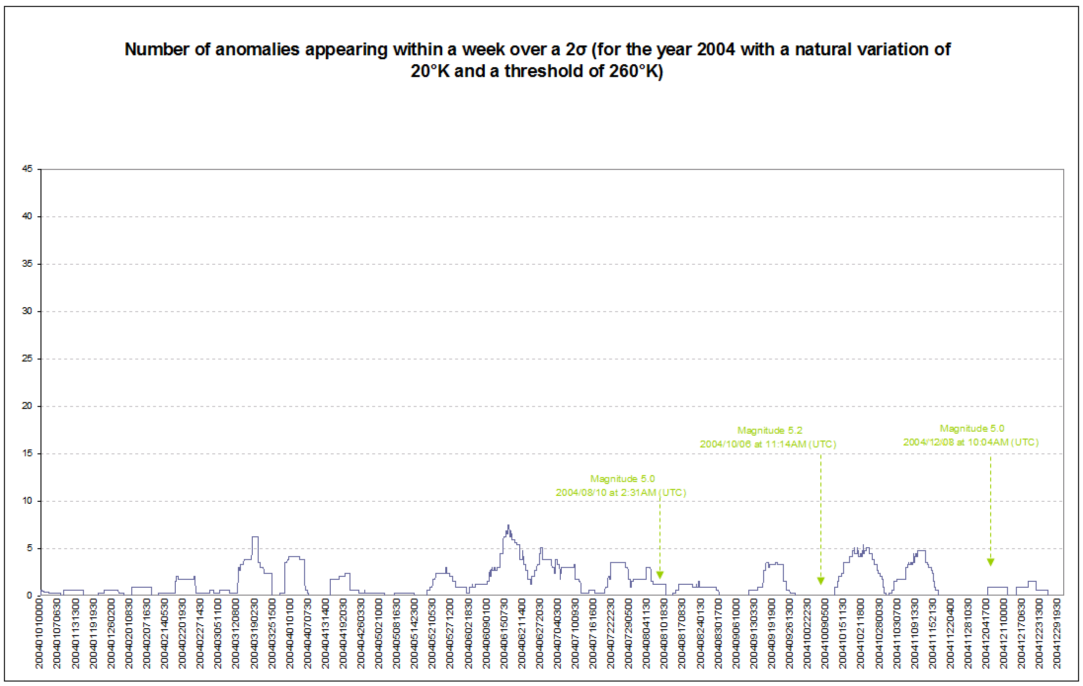

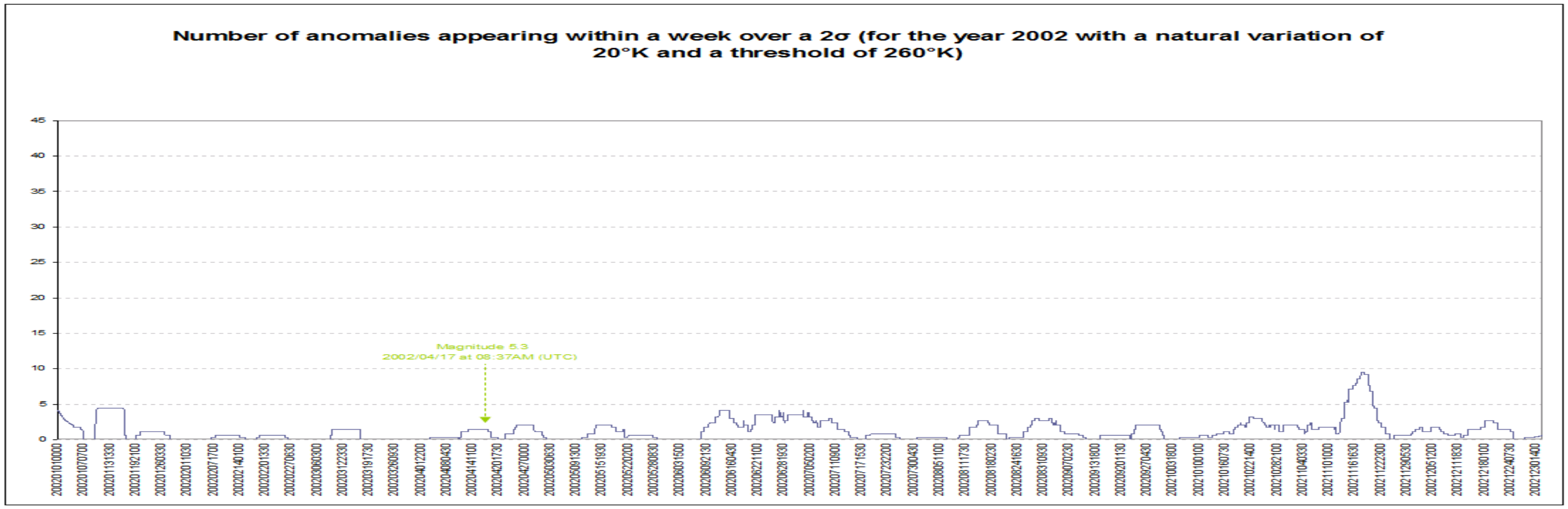
Number of anomalies appearing within a week over a 2σ (for the year 2002 with a natural variation of 20°K and a threshold of 260°K)
Magnitude 5.3
2002/04/17 at 08:37AM (UTC)

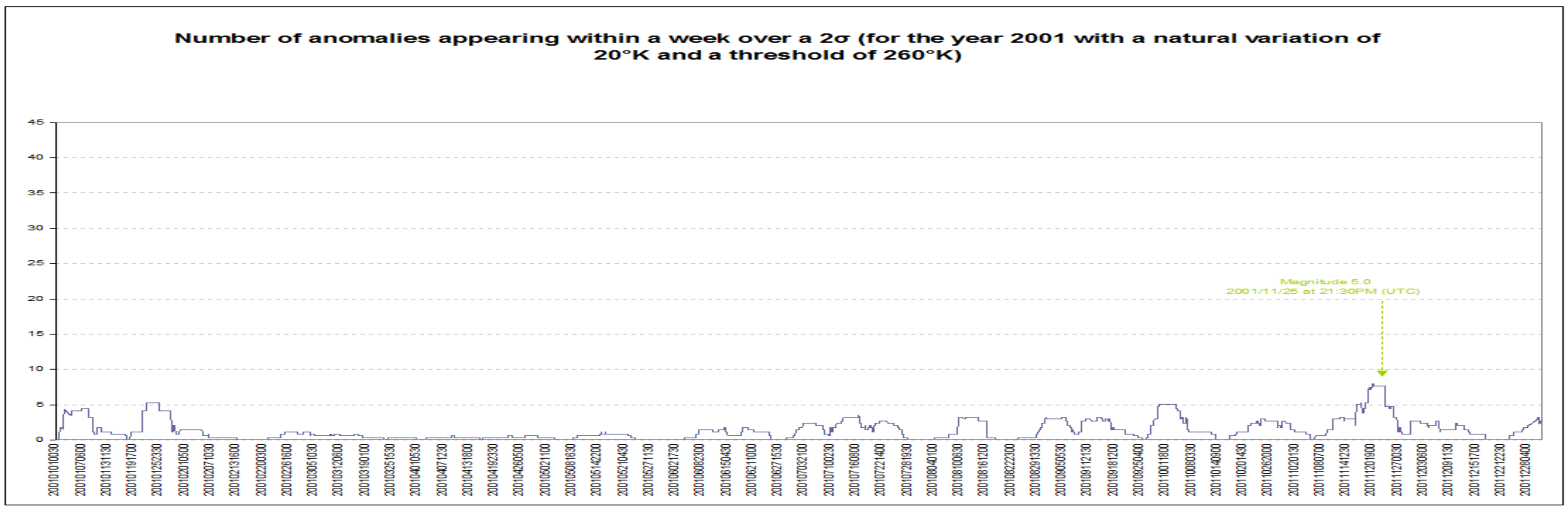
Number of anomalies appearing within a week over a 2σ (for the year 2001 with a natural variation of 20°K and a threshold of 260°K)
Magnitude 5.0
2001/11/25 at 21:30PM (UTC)

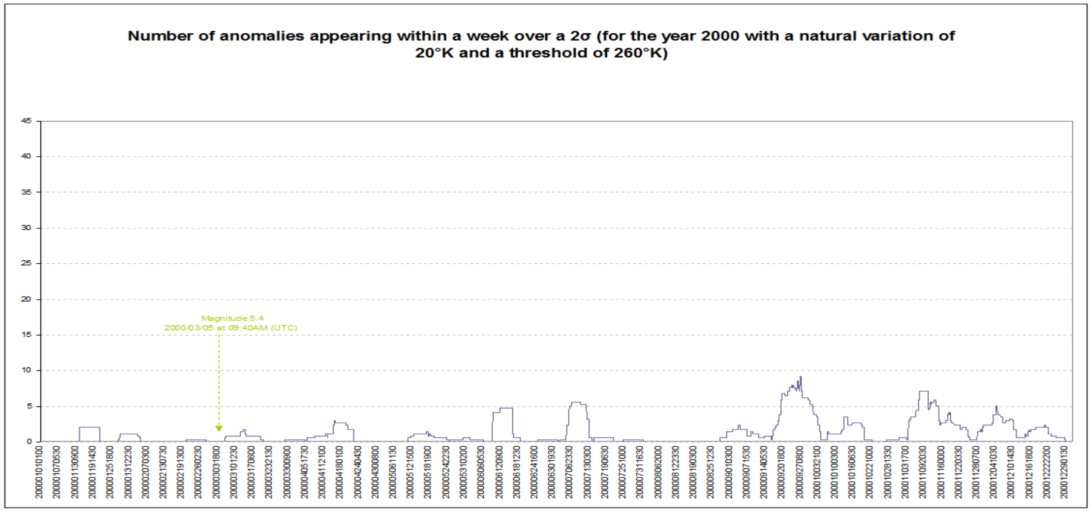
Number of anomalies appearing within a week over a 2σ (for the year 2000 with a natural variation of 20°K and a threshold of 260°K)
Magnitude 5.4
2000/03/05 at 09:40AM (UTC)

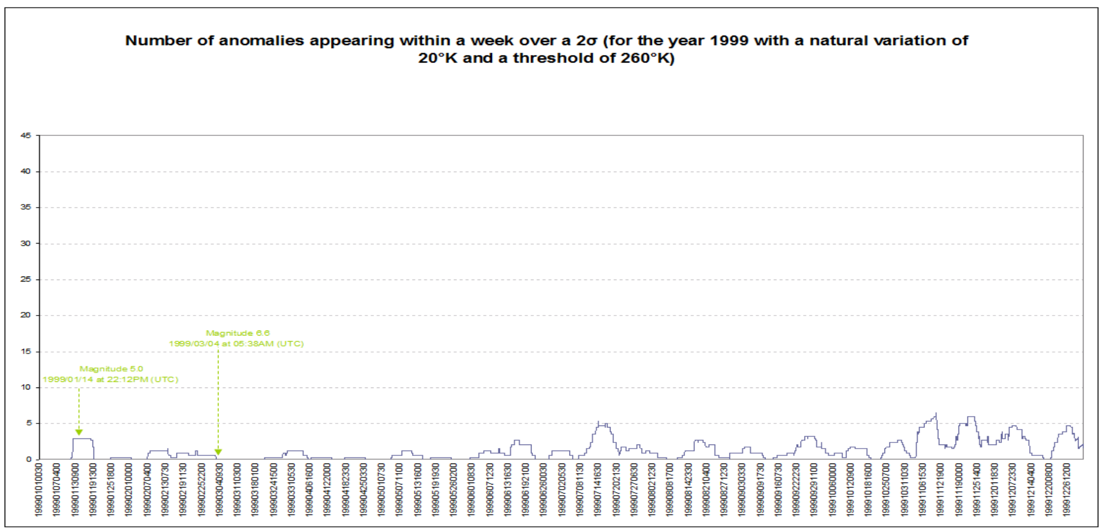
Number of anomalies appearing within a week over a 2σ (for the year 1999 with a natural variation of 20°K and a threshold of 260°K)
Magnitude 6.6
1999/03/04 at 05:38AM (UTC)
Magnitude 5.0
1999/01/14 at 22:12PM (UTC)

L'AQUILA EARTHQUAKE: Also located in the Northern Hemisphere

Condition (i): Pixel 58,55- which is the epicentre and is oriented on a steep South slope.

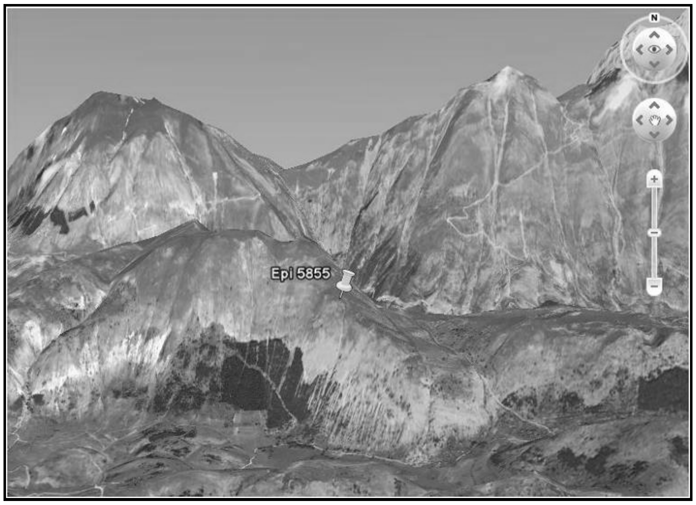

Condition (ii): Pixel 43,25- oriented on a gently facing south slope

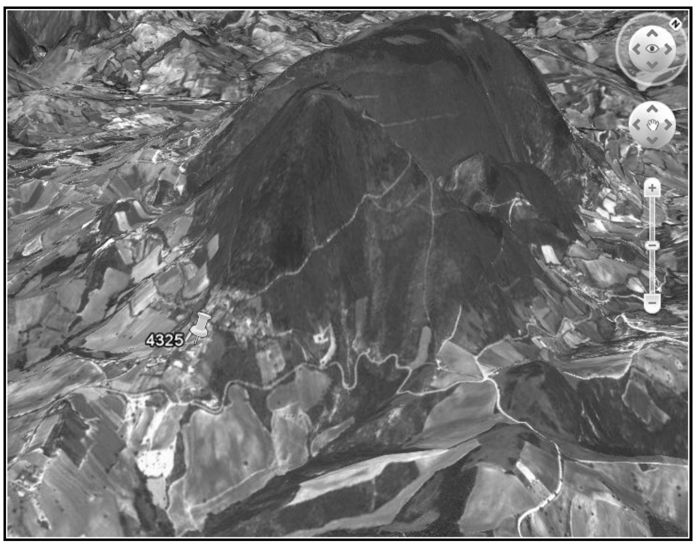

Condition (iii): Pixel 21, 32- which is oriented on a west-facing slope.

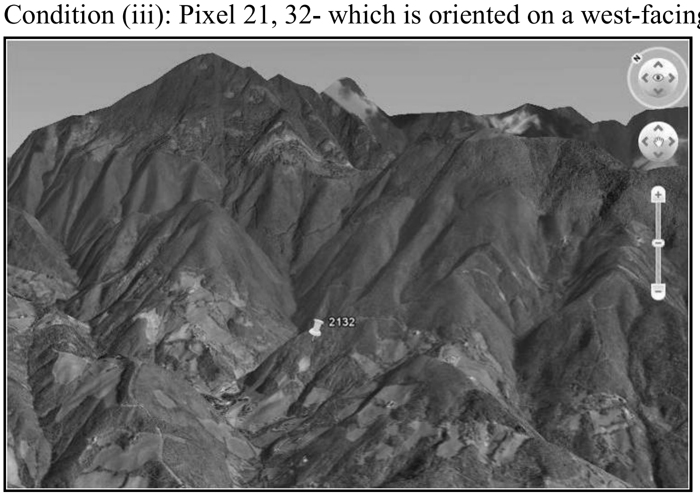

Condition (iv): Pixel 55, 62- which is oriented on a south-western slope.

Condition (v): Pixel 60,49 and Pixel 60,50 - which is oriented on a north-eastern slope and on an eastern slope respectively.

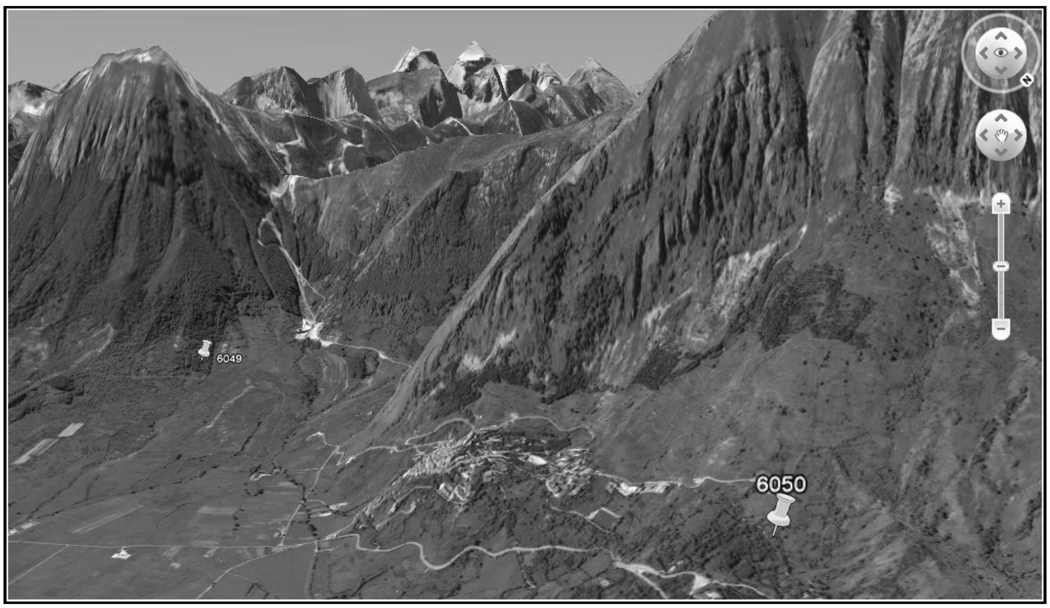

Condition (vi): Pixel 54,66- which is oriented on a south-eastern slope.

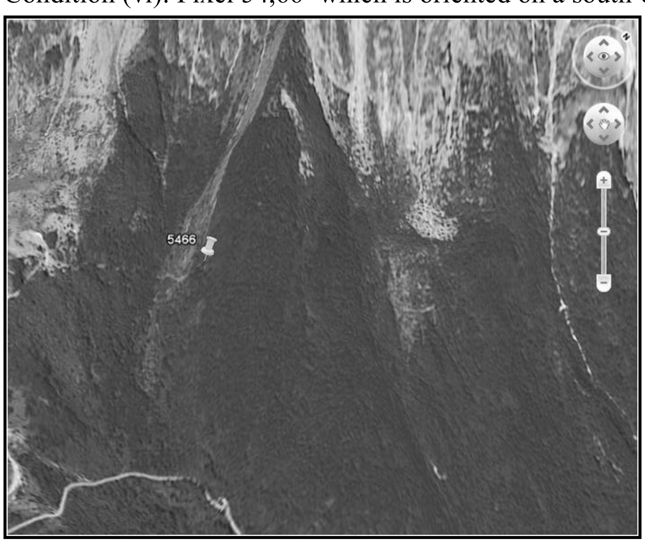

Condition (vii): Pixel 55,64- which is oriented on a north-western slope.

Condition (viii): Pixel 15,59- which is located in a waterbody.

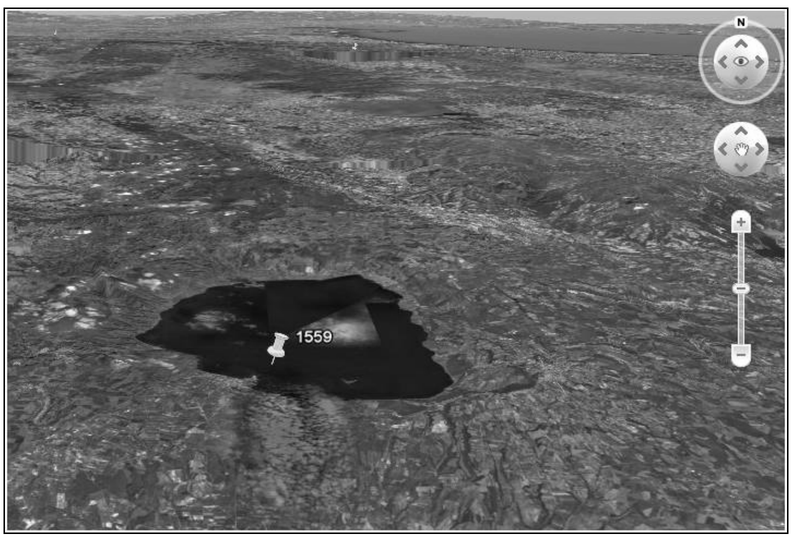

Condition (i) at epicentre (Pixel 58,55) and is oriented on a steep South slope. There was a significant anomaly in December with an approximation of 55% being related to an earthquake. However, NEIC results showed that this peak cannot be caused by any earthquake, since no earthquake was recorded at this time. Throughout the year, anomalous activity was seen but it was not significant to be regarded as an earthquake-related thermal anomaly.

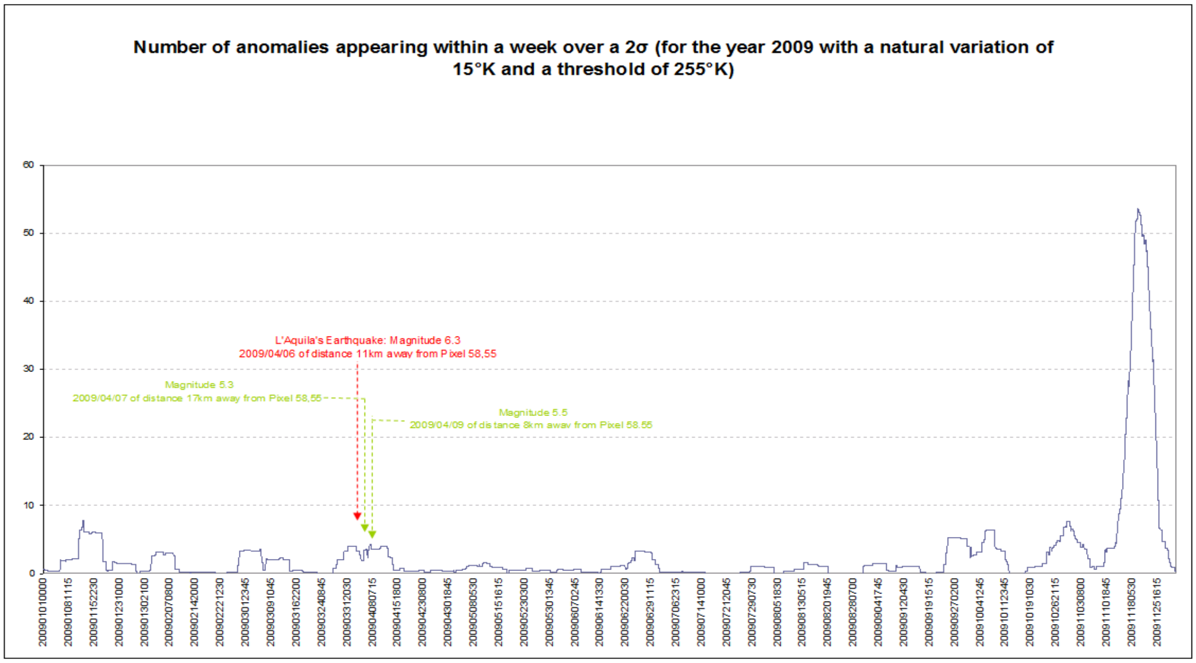

Condition (ii) at Pixel 43,25 and is oriented on a gently facing south slope. The topography also influences the amount of anomalies manifesting itself in an area. On a steep slope, which is open to the direct solar radiation will be heated faster and will take a long time for the temperatures to be reduced as compared to a gentle facing slope. The intensity of anomalies appearing on a steep slope will be greater than that of a gentle slope but even this is subjected to the time of the day. If the sun is positioned over a gentle slope, the temperature will be higher than those on a steep elevated slope. This is probably one reason which explains the 15% anomalies in September.

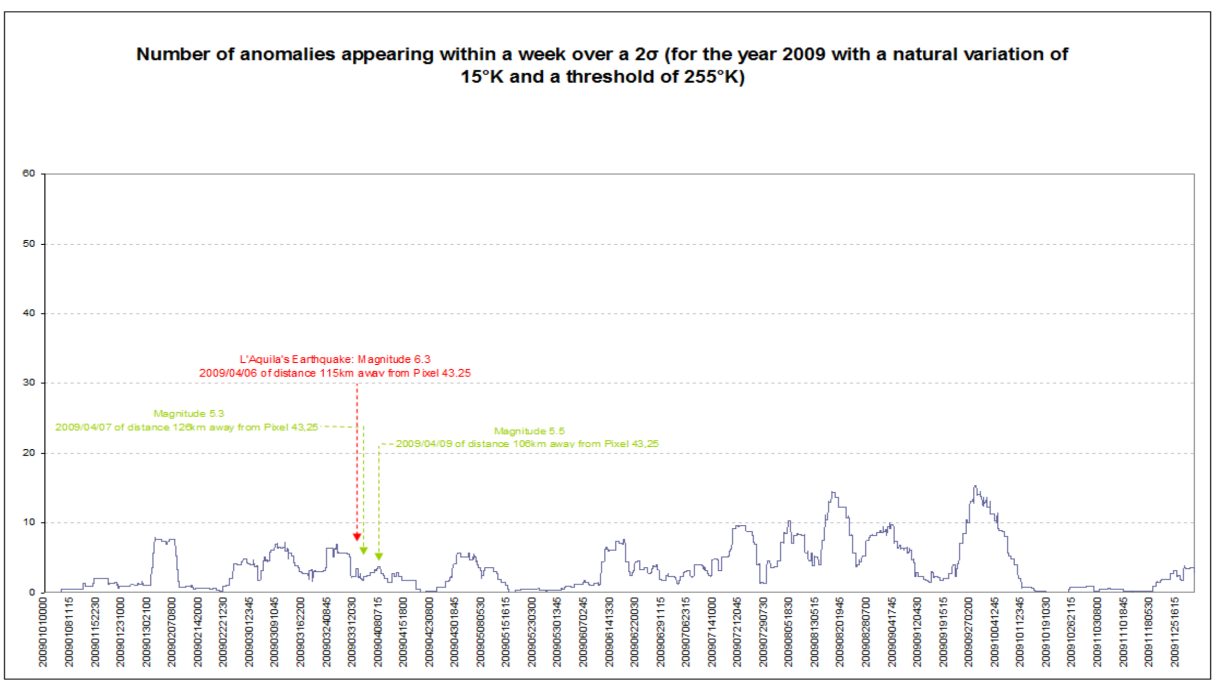

Condition (iii) at Pixel 21,32 and is oriented on a west-facing slope. All anomalies on this slope are relatively insignificant.

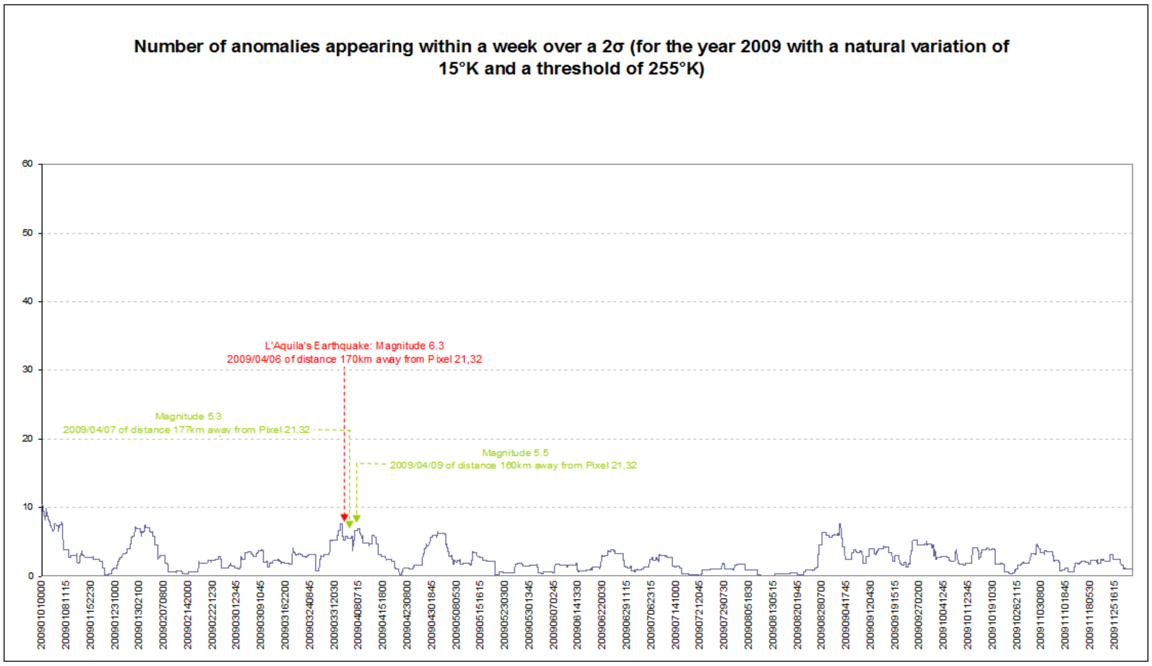

Condition (iv) at Pixel 55,62 and is oriented on a south-western slope.

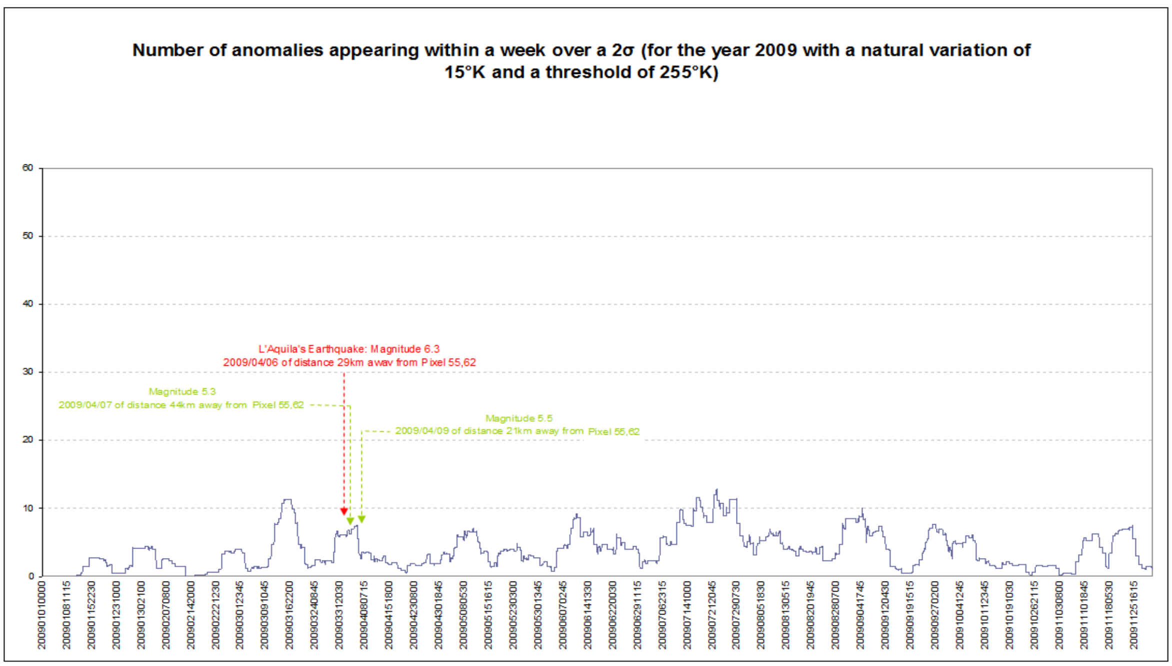

Condition (vi) at Pixel 60,50 and is oriented on an eastern slope.

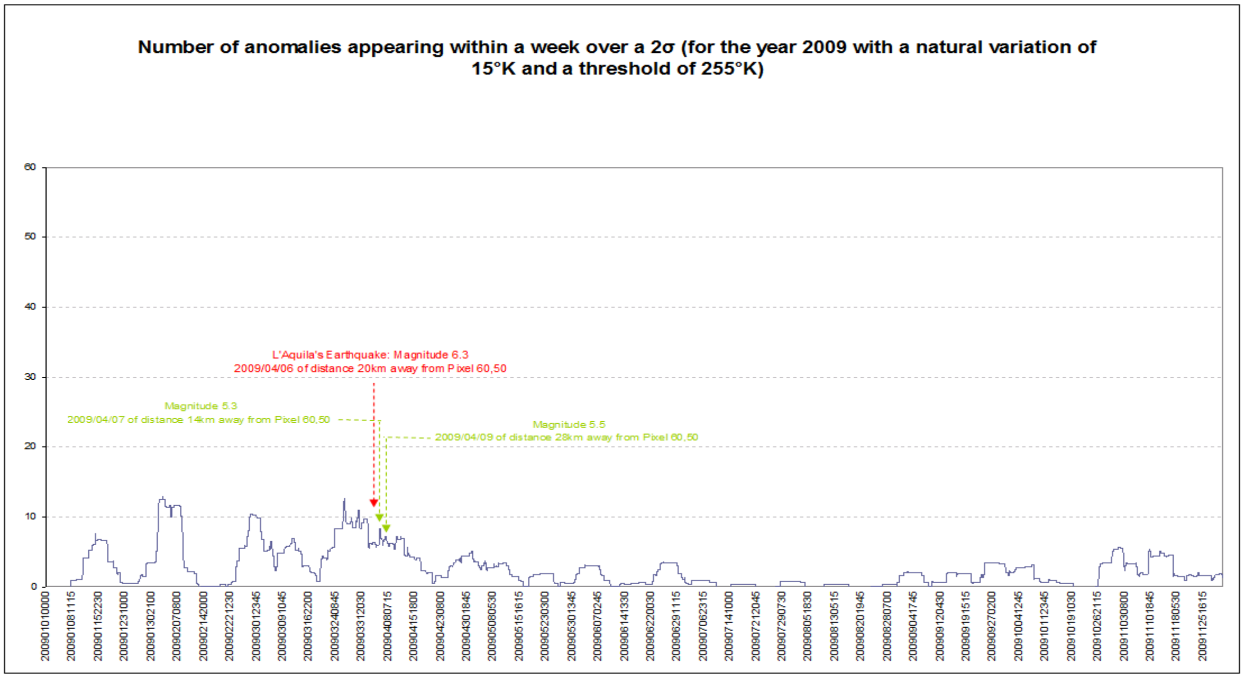

Condition (vii) at Pixel 54,66 and is oriented on a south-eastern slope

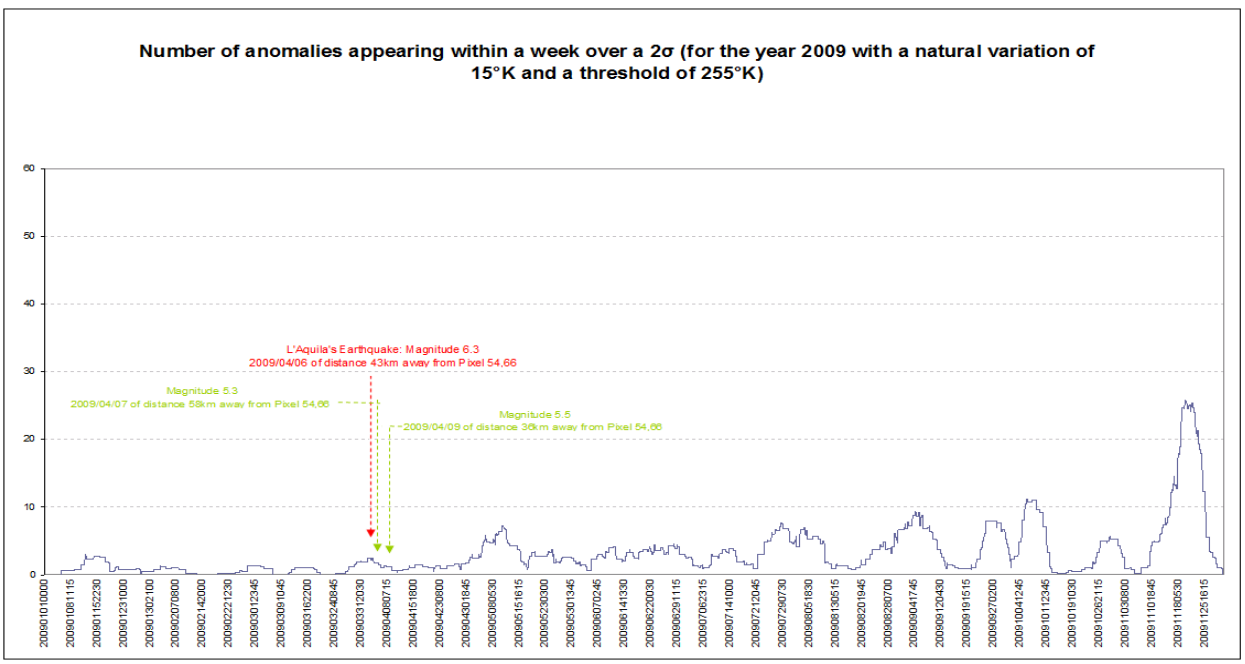

Condition (viii) at Pixel 55,64 and is oriented on a north-western slope.

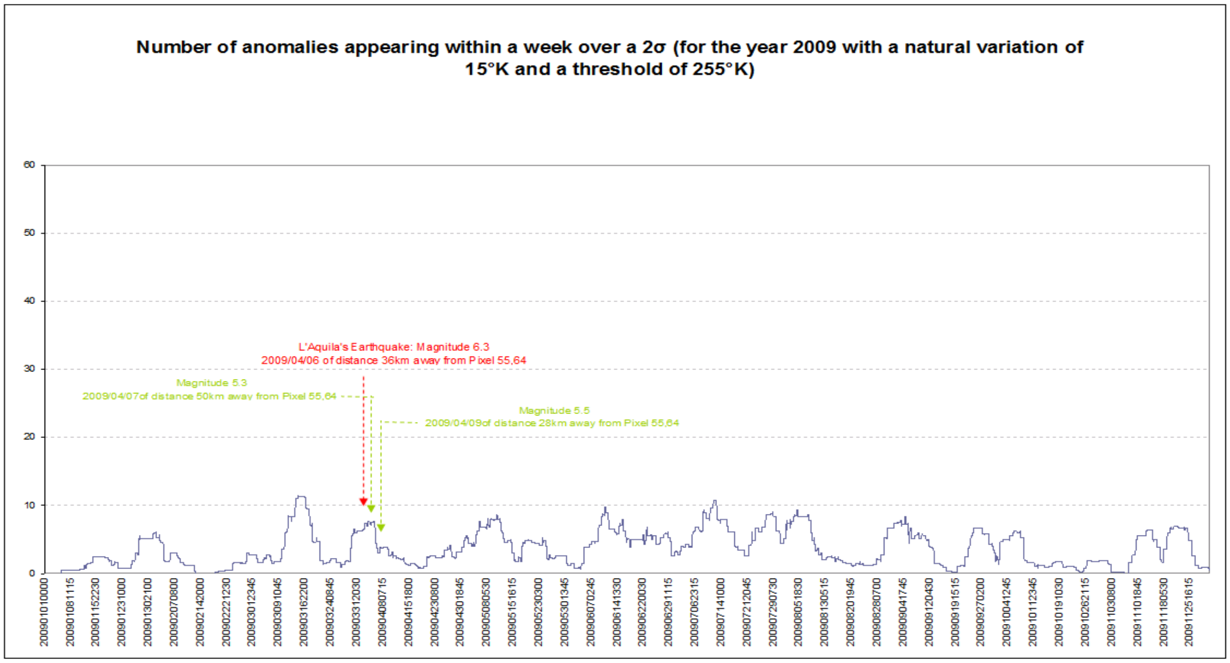

Appendix J: Frequency of Earthquakes

Average frequency of occurrence of earthquakes

Earthquakes are classified in categories ranging from imperceptible to great, depending on their magnitude. The earthquakes under study fell within the description of large earthquake events.

DESCRIPTION	MAGNITUDE	OCCURRENCE/year	AVERAGE/day
Great	8.0 +	1	
Major	7.0-7.9	18	
Large (destructive)	6.0-6.9	120	0.5
Moderate (damaging)	5.0-5.9	1000	4
Minor (damage slight)	4.0-4.9	6000	36
Generally felt	3.0-3.9	49000	360 (every 4 minutes)
Potentially perceptible	2.0-2.9	300000	3600 (every 24 seconds)
Imperceptible	less than 2.0	600000+	> 3600 (every 24 seconds)

Extracted from SEVGİ [47].